Università degli Studi del Piemonte Orientale

“Amedeo Avogadro”

Dipartimento di Scienze e Innovazione Tecnologica

Dottorato di Ricerca in Chemistry&Biology

Curriculum: Energy, environmental and food sciences

XXIX ciclo a.a. 2016-2017

SSD: CHIM/01

Elemental profiling as a chemical investigation approach: application to health studies and food authentication

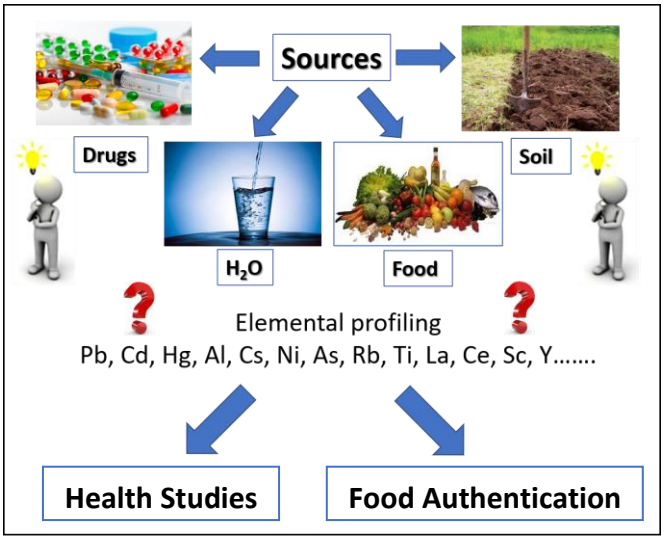

Fabio Quasso

Supervised by Prof. Emilio Marengo

Co-Supervised by Prof.ssa Elisa Robotti

PhD program co-ordinator Prof. Domenico Osella

Università degli Studi del Piemonte Orientale
"Amedeo Avogadro"

Dipartimento di Scienze e Innovazione Tecnologica
Dottorato di Ricerca in Chemistry&Biology
Curriculum: Energy, environmental and food sciences
XXIX ciclo a.a. 2016-2017
SSD: CHIM/01

Elemental profiling as a chemical investigation approach: application to health studies and food authentication

Fabio Quasso

Supervised by Prof. Emilio Marengo
Co-Supervised by Prof.ssa Elisa Robotti

PhD program co-ordinator Prof. Domenico Osella

Contents

CHAPTER 1

1.1 Introduction

Since the ancient times philosophers and thinkers have been questioning the structure of material. The ancient Greeks elaborated the concept of "elements" as fundamental substances which gave origin to all forms of material.

In particular, Aristotle identified 4 elements: earth, air, fire and water, which according to his studies, if combined in the right proportions, could have originated all other substances.

At the same time Democritus from Abdera theorized the existence of tiny and indivisible particles which form all the existing material; in this way the concept of atom (from the Greek gr. ἄτομος «indivisible») was introduced for the first time.

Only in the XX century we have the scientific proof of the existence not only of the atom but of many atomic species, defined elements; their combination forms all the substances and so the material, too.

Once the most common chemical elements were characterized, it was necessary to classify them by using a criterium which could join them in a well-ordered way.

This criterium was acknowledged for the first time by the Russian chemist Dmitri Ivanovic Mendeleev who created the Periodic Table in 1865.

In time the Periodic Table has been changed due to the finding of new elements; nowadays it is possible to differentiate several element groups.

Referring to the biological organisms, we can differentiate some elements which are fundamental for life, so extremely abundant in the organisms (C, H, O, N, S...), others which are essential at low concentrations (Se, I, Co and so on...) and others totally extraneous to the living organisms, defined as xenobiotic, which are considered harmful and very toxic (i.e. lead and mercury). There is also another particular group of elements called rare earth elements (REEs), which are considered ideal candidates

for geo-referencing and traceability studies in food chemstry.

1.1.1 Toxic metals and Rare Earth Elements (REEs)

Metals are the toxic agents which have been known for a long time by human beings. Differently from other toxic substances, they are neither created nor destroyed by man.

Man's action (extraction and working for industrial purposes) has influenced the state of conservation of metals in nature, and has caused a diffusion and contamination of air, water, soil and food with harmful effects on our health as a consequence.

Since the ancient times (see book Plutarch, Hippocrates 370 B.C. and so on...), the pathogen activity of some metals was known, as for example mercury and lead. Later, this definition has been diffused including elements such as cadmium, aluminum, arsenic ….

The redistribution of metals in the environment takes place naturally through the biogeochemical cycles. The rain dissolves minerals and rocks by carrying them to waterways which extract and deposit materials from the lands where they flow. Finally, the water arrives at the sea where the metals can be precipitated as sediments or can be taken up to the atmosphere where they fall down again as rains, in order to be redistributed in other areas of the Planet (figure 1) (1).

Finally, we have, through the biological cycles which include the incorporation in the food chain, the accumulation of these substances, first in the plants and then in the animals.

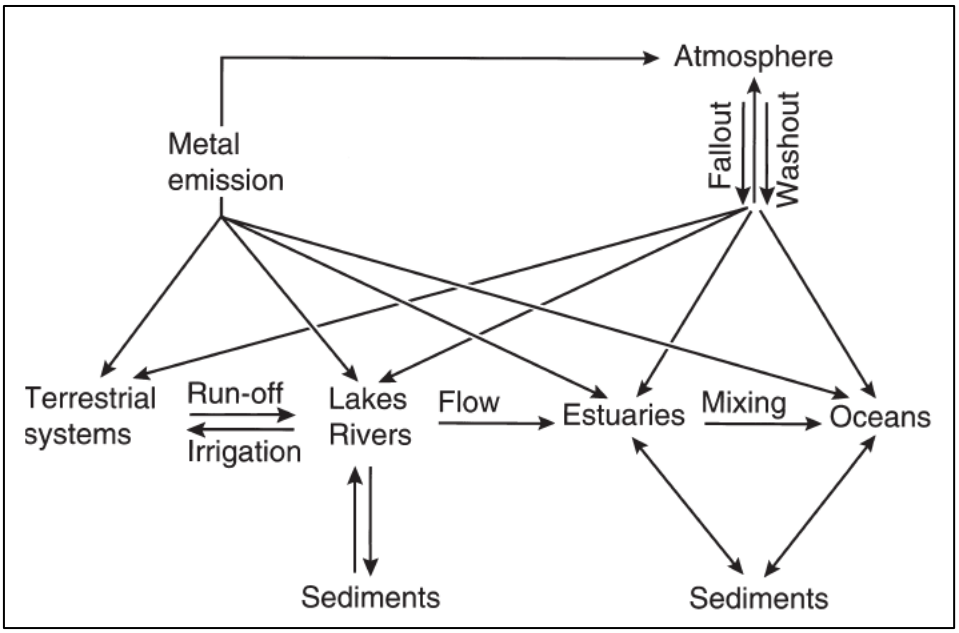

Figure 1*: transport of trace elements in the environment (1).*

Moreover, human activity has determined the formation of new compounds and a big increase in the world distribution of these elements.

The metals come in contact with man through water, air, food and drugs. Some examples of how these elements are in relation one to each other can be the case of the disaster of Minamata and the case of the Itai-Itai disease.

Minamata case in Japan

The Minamata disease takes its name from the Japanese town of Minamata and it has been documented for the first time in May 1956 (2,3).

In 1908 the Chisso Corporation (Chisso Co. Ltd) opened a chemical factory, in Minimata, for the production of fertilizers; later, it expanded and included the production of acetylene, acetaldehyde, acetic acid, vinyl chloride and octanol. The chemical plant became the most advanced center of Japan both before and after the Second World War.

The chemical reaction to produce acetaldehyde requires the use of mercury sulfate

as catalyzer; it produces, as a residual by-product of the reaction, a small quantity of methylmercury (MeHg) (National Institute Minamata Disease) (4).

This highly toxic compound was released through the wastewaters of the factory in the Minimata Bay, from the beginning of the production in 1932 until its interruption in 1968.

The methylmercury accumulated first in the ichthyofauna and then through the food chain, among the inhabitants of the area who have a diet highly rich in fish and seafood coming from the Minamata Bay.

The geographical distribution of Minamata disease[3] cases is shown in figure 2.

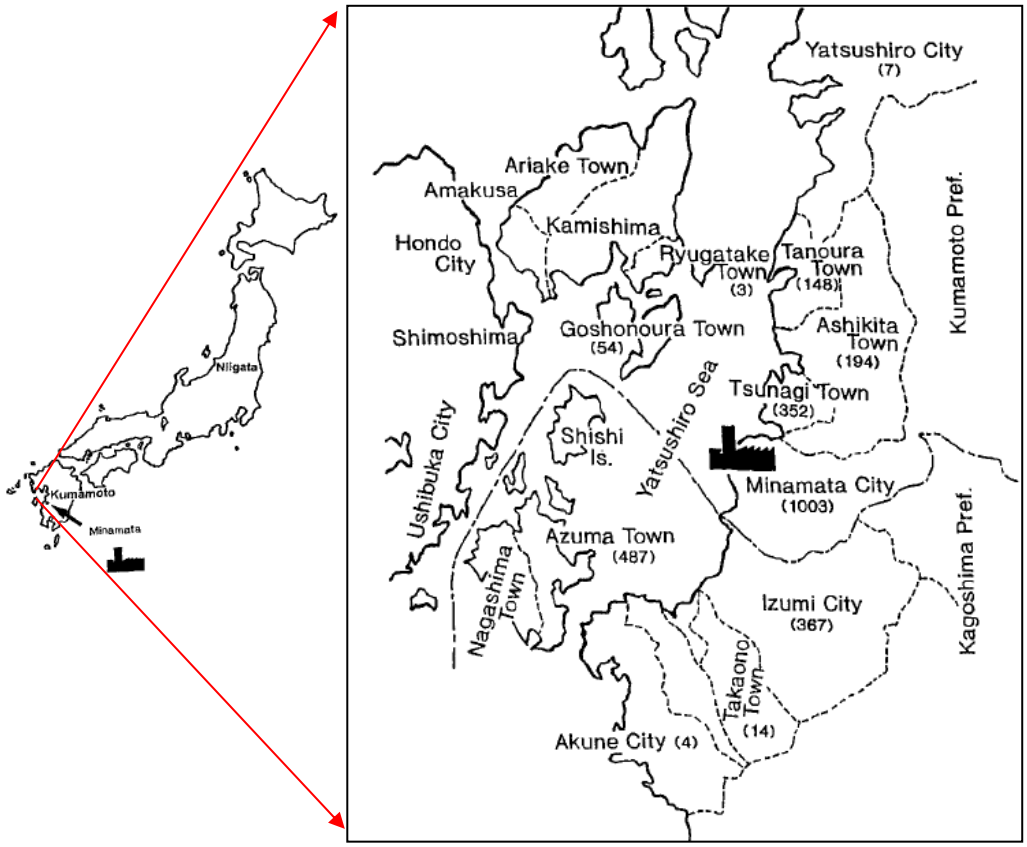

***Figure 2**: Map of Japan with Minamata Bay (3).*

Among those inhabitants, the following symptoms were observed: sensory alterations (similar to those caused by glues), ataxia, dysarthria, reduction of field of

view, hearing ailments and tremors (5).

The exposition of the fetus to methylmercury, after the mother had eaten contaminated fish, caused much more serious consequences compared to those observed in the adults, because MeHg can cross the placenta and readily pass through the blood-brain barrier in pregnant women (6).

Cases of brain paralysis, hypoplasia of neurons of the brain cortex, growth break off and destruction of neurons could be observed (7-9).

This resulted in extreme fetal abnormalities and neurotoxicity (i.e., microcephaly, blindness, severe mental and physical developmental retardation) even among infants born from mothers with minimal symptoms (6).

In this case, the syndrome took the name of “congenital Minamata disease” (10,11).

The Minamata syndrome is also known as “laughing dead”, because the patient dies with a sort of smile on his face, due to the tetanus paralysis of the face (trismus).

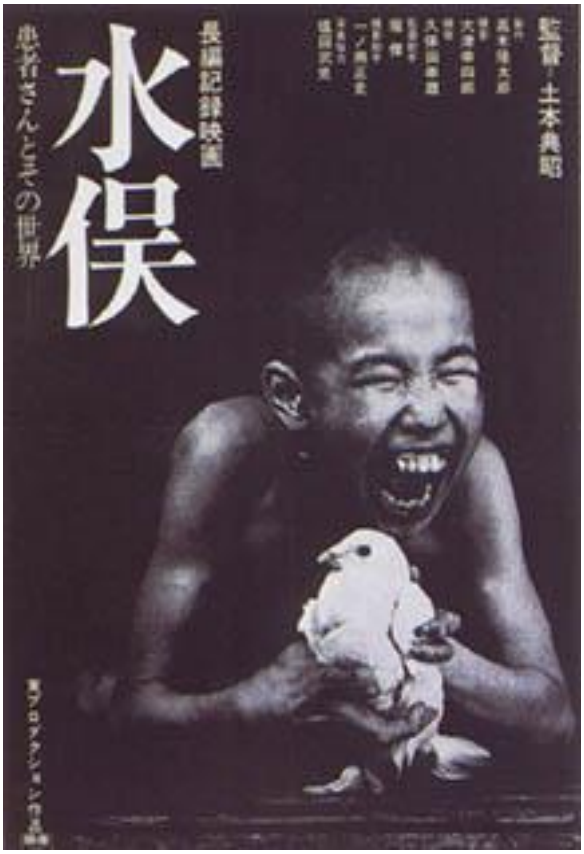

An epidemic case of Itai-Itai

Cai et al. (1995) found an epidemic form of "Itai-Itai disease" in the people of a group of villages situated on the banks of the Zhang River and the Fujang River in the Province of Jianxi in the south of China (figure 3).

They also analyzed the people who lived in the villages near the banks of the Youxian River, who did not show the same syndrome.

As the etiology of the disease was known, they evaluated the concentration of cadmium in the urine, hair and nails of ill people (villages of Zhang and Fujiang) and of healthy people (villages near Youxian); they found a high concentration of the metal in the former ones and normal concentration in the latter.

They looked for the presence of the metal in food and in the soils, eventually, they found the sources in two tungsten mines upstream of the two rivers, which

discharged pollutants in the waters destined to be used by farmers to irrigate agricultural fields including rice patties (12).

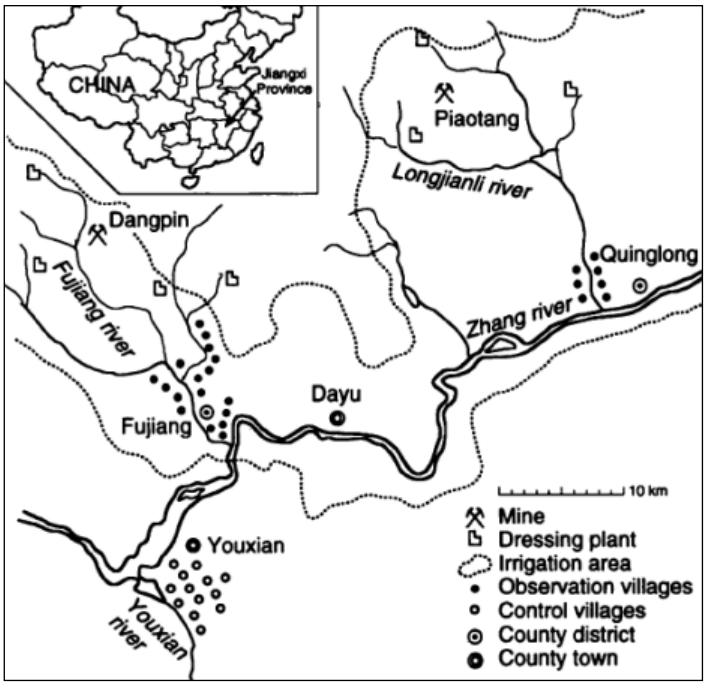

***Figure 3**: geographical map of South China (12)*

Regarding the toxic heavy metals, they are further discussed independently hereafter.

1.1.1.1 Lead

Among the most toxic elements, the most widespread is lead, in fact, its presence can be found almost in any biological system. It has no physiological function in the living organisms, neither plant nor animal, and for this reason, it is toxic if it surpasses a limited amount. However, the definition of this limit, for any organism, is a problem that has no easy solution.

Children are the most affected by this metal because lead changes many functions linked to their development and, in addition, some systems of defense in children, such as the blood-brain barrier, are not completely formed and effective (13).

The first people who extracted and used lead were the Egyptians, the Jews and the

Phoenicians (14). Thanks to its Physical-chemical characteristics, lead was widely used (i.e.to vitrify the porous surface of ceramics, to coin money etc), even though it was extremely dangerous for human health.

The ancient Romans realized about the neurotoxic effects caused by lead poisoning, in fact the saying “mad as a painter” comes from the use of “Pompeii red”, which consisted in lead oxide (15). Another example of “lead poisoning” among the ancient Romans was caused by the use of a sweetener called sapa (lead acetate) which was obtained by cooking the grape must in lead containers (16).

Lead poisoning was therefore known since the ancient times and although in the following centuries the documented cases in the literature are occasional, the pathology appears again in the documents of the XIX century, when in the period of industrialization, it reaches vast proportions. In 1920, the introduction of tetraethyl lead in fuels, caused serious damage to the public health, until it was banned in the 1980s. However, the use of tetraethyl lead was so large that it caused a big diffusion in the atmosphere, as witnessed by a 200-fold increase of lead in the ice in Greenland (17).

Lead, as an environmental pollutant, can come from several sources that can be worked or not; among those one can mention: industrial emissions (i.e. PM10), tetraethyl lead added to fuel (TEP) from 1923 to 1975, lead piping, kitchen tools, food boxes welded with lead, lead paints, mining, waste batteries, lead welding, pesticides which were used in the past in agriculture (arsenate) and contaminated food (18).

Lead is most commonly absorbed through the respiratory system, gastrointestinal tract (gastroenteric) and through transdermal means (19).

The inhaled absorption has significantly decreased since the lead compounds in fuels have been replaced by adding benzene as an antiknock, even if a new problem was created since benzene can cause leukemia. The gastroenteric absorption is not uniform in the exposed people: in particular, the affecting factors are age and diet (19).

Children, and all people who have a diet lacking in iron, calcium and zinc, absorb lead much more quickly and easily (20). Excretion takes place both by urine and by feces (21).

After absorption, about 90% of the lead is deposited and accumulated in the bone tissue and in the hemopoietic mallow. In this last case in particular, it interferes with the synthesis of the heme group and of the hemoglobin in the erythroid precursors (22). When the bone is remodeled also lead and likewise calcium, is redistributed in the organism (23).

Even from very low lead levels, we can notice some pathologic effects on different tissues, up to high levels showing acute intoxication.

At low lead levels, a reduction of the intellectual quotient IQ (24), hearing deficiency and some developmental and behavioral disorders in children can be observed.

As the concentration increases it is possible to note some alterations of the metabolism of vitamin D (22), variations in the enzymatic expression in the erythrocytes or in their precursors, anemia due to the underproduction of hemoglobin, headache, perception of metallic flavour in the mouth, lack of appetite, constipation, abdominal colic, tremors, kidney damage with excretion of uric acid, neuropathy and encephalopathy (25).

In pregnant women, lead has a very hidden action because it is able to cross the placenta and spread in the fetal tissues (26). This can cause extremely serious malformations such as anencephaly, or spina bifida (18).

In conclusion, it is better to remember that even with concentrations which are classified as nonpathological, lead can have important toxic effects if there are other toxic elements like for example cadmium and mercury.

1.1.1.2 Mercury

Among all metallic elements, mercury is the only liquid at standard temperature conditions; it appears in two oxidation states: elemental mercury (Hg^0), and mercuric

state (Hg^{2+}) (27).

In the most oxidized state mercury can bind one or two carbons originating stable organic molecules, among which methylmercury (CH_3Hg^+) is the more toxic and represented (28,29).

In the Middle Ages, the alchemical practices caused substantial poisoning from mercury, which was known, at that time, as ”quick silver”.

In the last century, other poisoning effects has been detected, for example, the neurotoxic effects deriving from fumes of mercury as a professional pathology of the leather tanners.

Due to its physical properties, mercury is used in the manufacturing of barometers, thermometers, hydrometers, pyrometers, UV lamps and many other special tools (30,31).

Other fields of use of Hg include the production of mirrors, gold and silver extraction, electrical rectification (32,33).

In addition, tattoo pigments, protective paints, pesticides and medicines (Thymesoral) may contain mercury (34-37).

Lastly, there is a source of iatrogenic exposure to mercury which is given by dental amalgams, used until a few years ago in dental practice. Scientific research demonstrate that it is possible to correlate excreted urine mercury after chelation therapy with the number of such amalgams (38).

As a result of human industrial activities, mercury is diffused into the environment as vapor, falling to the ground with rains, then accumulating in surface waters (37).

Despite the main source of mercury vapors is the earth's crust, industrial vapors are the ones most absorbed by man as the main cause of environmental pollution (39).

Indeed, it has been shown that human activities have caused a steady rise in mercury vapors over the last two centuries (40-42).

Once emitted, mercury tends to accumulate in saline and soft waters and is converted here by methanogenic bacteria into methylmercury. In this form, the metal enters the food chain bioaccumulating into larger concentrations from microorganisms to

predatory fish (42) (figure 4).

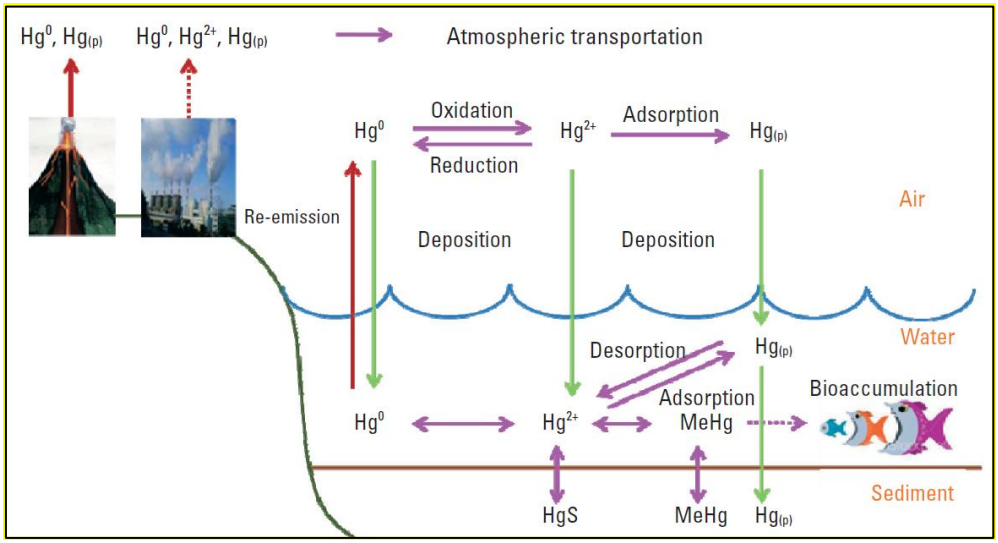

***Figure 4**: biogeochemical cycle of mercury (42)*

Mercury dust and its vapors enter the body through the respiratory system, via the gastrointestinal tract and the skin (43,44).

There are two possible types of intoxication: acute and chronic. The first case causes abdominal pain, nausea, vomiting, enteric and kidney damage and death within 10 days (43,44).

Chronic intoxication, on the other hand, appears variable in symptoms, including muscle tremor, spasms at the extremities, mouth inflammation, gums, and falling teeth (43,44).

Mercury causes a pronounced lipid peroxidation of red blood cells in the hemopoietic system, probably inhibiting the activity of glutathione peroxidase (GPX) and superoxide dismutase (SOD) (45).

Several cases of interaction between the element and the immune system are reported in the literature: Hg not only has the ability of immunosuppression, but there is evidence that it can also yield immunostimulatory signals in various species,

including humans and rodents (46).
The formation of immunocomplexes is the cause of renal impairment of glomerulonephritis reported on both guinea pigs (47) and humans (48).
At last, there is an observable alteration of the nervous system which manifests with irritable behavior, apprehensive states, mood swings, depression, memory disorders, learning problems, impairment of social behavior, and low intelligence quotient (49).
Also, the neurotoxic effect is very relevant on adults and fetuses, as described above paragraph 1.1.1 .

1.1.1.3 Cadmium

Cadmium has a rather recent story when compared to lead and mercury: it was discovered in 1817 and it has been used in the industrial field starting from the half of the XX century. It can be used to produce batteries, fertilizers, and pigments for paints and plastic materials and in the galvanization processes. Moreover, cadmium is a residual product of extraction processes of other metals (50).
The main way cadmium is absorbed by the human body isthrough the gastroenteric system. Cadmium accumulates in cultivated plants, on polluted soils or by irrigation with water; from here, it gradually biaccumulates in the food chain (51). It can also be accumulated in a very efficient way by shellfish and mollusks (52).
Also, the cigarette smoke represents an important source of exposure: according to some estimates, a cigarette contains from 1 to 2 ug of cadmium and about 10% of it is inhaled (53).
Cadmium shows strong nephrotoxicity even if the origin of this process is indirect. In fact cadmium, after its enteric absorption, goes to the liver in the bloodstream where it stimulates the synthesis of metallothionein (MT), which has the capacity to bind cadmium (figure 5). The complex Cd-MT is partly stored in the hepatocytes and partly transported to the kidneys, where it is accumulated in the lysosomes of the cells of this organ, and it causes necrosis (54). (figure 6)

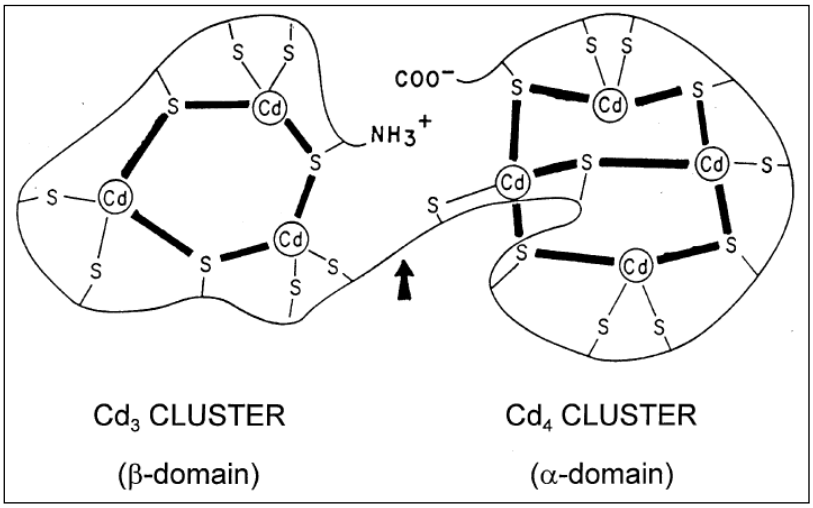

Figure 5*: Schematic structure of a metallothionein. The domain alpha coordinates four atoms of cadmium, while the domain beta joins three (54).*

Depending on the exposure, a person may manifest acute or chronic intoxication.

The acute toxicity by ingestion of contaminated food can cause sickness, vomiting and abdominal pains, while, if it is due to vapor inhaling, it can cause pneumonia with pulmonary edema (52).

The chronic intoxication can cause pathologies of the tubule and of the kidney glomerulus (55), damaging the metabolism of the vitamin D and of the PTH (56).

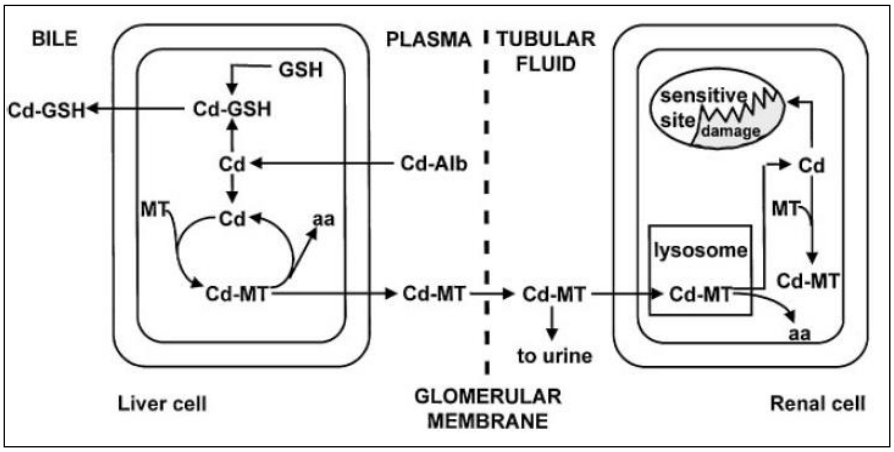

Figure 6: *A proposed model for the pathogenesis of the nephropathy caused by cadmium(54)*

It is possible to have osteomalacia and osteoporosis caused by an interference with calcium metabolism, leading to bone deformation and pain which are typical of the "Itai-Itai" disease (12) (cfr paragraph 1.1.1).
Moreover, there are hypertension, cardiovascular disorders, lymphocytosis and microcytic anemia-hypochromic, emphysema, chronic pulmonary obstruction and behavior alterations and intellectual deficit.
Cadmium is classified as a category I carcinogenic by the International Agency for Research on Cancer (IARC) which is put in relation to lung cancer caused by cigarette smoke (57).

1.1.1.4 Aluminum

Aluminum is one of the elements which is the most present on our Planet because it is the third in abundance to form the earth crust. Its reactivity lets it join with +3 valence to oxygen givers such as phosphates or citrates.
It is normally present in inert forms, but in the last few decades, aluminum has become more bioavailable by acid rain which has accentuated the toxicity.
Humans can absorb aluminum from different sources, especially at home. In particular, it can be absorbed by aluminum sheets or bowls used to pack food, dishes, cutlery, coffeepots or cans made of this metal (58).
Dishes, in particular, can yield large quantities of aluminum if they are used to cook or eat acidic foods such as tomatoes and its derivatives.
Aluminum is also present in some medicines such as antacids, based on aluminium hydroxide , vaccines, which have been added with aluminum as an adjuvant, and some herbal compounds (59).
Aluminum chloride is often used in drinking water processes to flocculate impurities (58), while aluminum chloride is used in cosmetics and deodorants as an astringent (59).
Inside the human body, aluminum shows the most toxic effects on the respiratory,

gastroenteric, skeletal systems and on the central nervous system. In fact it interferes with the absorption of calcium, iron, and fluorides (60); in healthy patients, after the consumption of high quantities of antiacids, or in patients on dialysis, it has been shown to be a cause of osteomalacia due to its capacity to join phosphorus causing a lack of phosphates in the bones (61).

It can also cause constipation due to the intestinal inhibition of peristalsis, caused by the interference with cholinergic signals (60).

The consequences of the professional exposure to aluminum dust are mainly consisting in pulmonary fibrosis (62,63).

The capacity of aluminum to join calmodulin can cause serious consequences on the nervous system, because of the alteration of the transport tubular activity.

This last toxic activity seems to be particularly insidious and marked because it is connected to various neurologic and neurodegenerative pathologies, also depending on the age (64).

Among the most emerging ones, there are the Alzheimer Disease, the Parkinson Disease (PD), the Amyotrophic Lateral Sclerosis (ALS), the Gulf War Syndrome (GWS), Autism Spectrum Disorders (ADS), the syndrome of Guam (complex ALS-PD of Guam), the Dialysis Human Dementia Syndrome and other rare and less known diseases (64). Aluminum can substitute iron in some proteins (e.g. transferrin) (65,66), and it forms complexes with glutamate and citrate that can pass the blood-brain barrier (BBB) (67,68), causing oxidative stress in the central nervous system.

Referring to what has been explained hereabove, in 1989 a mixed committee of experts FAO/OMS about food additives (JECFA) has recommended a weekly provisional and tolerable dose (PTW) of 7,0 mg/kg body weight of Al, but this limit has been modified in 2007 by reducing it to 1.0 mg/kg body weight, because they have found some potential toxic effects on the developing reproductive system and on the nervous system (69).

1.1.1.5 Arsenic

Even if it is not a real metal but a semi-metal, arsenic is such a diffused and toxic element that it is normally associated with the heavy metals class. In nature, it is diffused in both its oxidation states +3 and +5 which are normally forming inert mineral structures. The real danger consists in the environmental mobilization and dispersion of this element which, in this way becomes more reactive and absorbable. We can distinguish organic compounds from inorganic ones: the former can be further divided into trivalent (arsenic trioxide, sodium arsenite, arsenic trichloride) and pentavalent (arsenic pentoxide, ac. arsenic, lead and calcium arsenate) forms (70).

The latter ones are present in both trivalent and pentavalent states and in methylated form, following the bio-methylation made by the microorganisms of soil and of salt and fresh waters (71).

Arsenic is mainly dispersed in the environment by human activities, in particular as a byproduct of extraction and working of some metals as lead, copper, zinc, but also by the glass and chemical industry. There is also a specific arsenic compound, the copper acetoarsenite, also called "Paris green", added as preservative to chipboard and plywood (72).

We can't overlook the massive use, which was done in the past, of arsenic-based pesticides and herbicides which have dispersed huge quantities of this element in the soils and waters which were intended for agriculture. Even if today these products have been banned and replaced with other herbicides and organic pesticides, arsenic is still present and can be found in a lot of food, for example, rice (73).

As any other xenobiotic elements, arsenic is metabolized by the liver and excreted by the kidneys. The hepatic metabolization in human body consists in the methylation of both the trivalent and pentavalent forms with production mono- and di- methyl arsenic (MMA and DMA). In this way, it is possible to obtain less toxic compounds which have a simpler excretion by kidney way (74).

In fact, the As(V) is reduced to As(III) which reacts with the S-adenosylmethionine (SAM) and is methylated to MMA and DMA (75).
Arsenic changes the functionality of mitochondrial enzymes which are involved in the cellular respiration (76); in particular, it interferes with the action of the succinate dehydrogenase and it uncouples the oxidative phosphorylation.
This causes an increase in the production of hydrogen peroxide which helps the formation of the different radical species (ROS), it causes damage to DNA and therefore potentially starts the development of cancer (74).
Moreover, the chronic exposure to low amounts of arsenic can cause serious damage to human health: ailment, fatigue, dermatitis and eczema of allergic-type and, in most serious cases, hepatic injuries followed by jaundice, cirrhosis, ascites, and also neurological damages by demyelination of nerve fibers (77).
A further danger of the chronic intoxication by arsenic is found in the mimic capacity of phosphorus which enables it to replace itself in the DNA, causing alterations in the structure and mutations. That's why IARC and EPA classified it as carcinogenic (group I), respectively in 1987 and 1988 (78).

1.1.1.6 Nickel

Nickel is a ubiquitous metal which is mainly present as an oxide, sulfide, and silicate. There are several sources of exposure, for example, cigarettes, automotive exhaust gas, and certain kinds of food as chocolate, cocoa, soy, nuts, hydrogenated oils and coffee (79).
Nickel can also be found in nickel-cadmium batteries (Ni-Cd), materials and prosthesis for dental use, costume jewelry and pigments for glass and pottery.
The ordinary excretion of nickel is linked to the cysteine or other thiolic compounds (glutathione) or amino acids (histidine, aspartic acid, arginine) (80).
Most of the absorbed nickel comes from drinks and food and the concentration can change a lot, according to the geographical area, the kind of diet and the water supply

(81).

According to the chemical shape of the element and physiological factors, the absorption in the intestinal tract has a variation from 1% to 10%. The presence of nickel in the urine shows a recent exposure and changes a lot from day to day (82).

The most clinically relevant manifestations are dermatosis, contact dermatitis, and atopic dermatitis (83). Moreover nickel exposure seems to hypersensitize the immune system, so promoting the appearance of allergic responses to various antigens (84). Finally, nickel changes enzyme functions replacing the zinc in the active sites of enzymes where it is the cofactor, by modifying the function (85).

Nickel compounds are considered human carcinogens and metallic nickel is possibly a human carcinogen (86).

A last important observation concerns an evident greater sensitivity to these effects in females.

1.1.1.7 Rare Earth Elements (REE)

Rare earths are a particular group of elements considered ideal candidates for georeferencing and traceability studies on food products (87).

They are a group of 17 chemical elements, precisely scandium, yttrium and the lanthanides. Scandium and yttrium are considered rare earths because they are generally found in the same mining deposits of the lanthanides and they have similar chemical properties.

The elements belonging to the REEs are found in the earth crust in relatively high concentrations, so the name "rare earths" is not due to the abundance, but to the difficulty in extracting and separating processes.

Lanthanides have aroused particular interest, because, due to their chemical similarity, they could not be submitted to phenomena of selective fractionation in the distribution of concentration from the soil, to the plant and finally to the fruit (the REEs do not have any role in the plant physiology) (88,89).

This is particularly true regarding food products which do not undergo any

transformations before commercialization (vegetable products, saffron, raw nuts, etc).

On the contrary, those products which derive from more complex processes (for example, wine), where the base product is transformed before the commercialization, can show an alteration in the REEs profile during transformation. In fact, in this case, it is necessary to consider the contribution of each process on the final REEs profile.

1.1.2 Elemental Profiling

Elemental profiling consists in the determination of all the elements contained in a sample; in line of principle, this profile includes all the elements (alkaline and alkaline-earth metals, transition metals, non-metals, lanthanides) but it is usually focused to the determination of heavy metals, potentially toxic elements (as Al, …..) and rare earths.

To date, elemental profiling is a widely used approach in basic research; it usually exploits an inductively coupled plasma (ICP) for the atomization of the sample, coupled to mass spectrometry (ICP-MS) or to optical emission (ICP-OES or ICP-AES) for the detection. ICP-MS represents a powerful tool for the quantitative determination of about 60 elements of the periodic table at trace (ppb-ppm) and ultra-trace (ppb and sometimes ppt) concentration levels.

This technique has many advantages:

- in a single analysis it allows to determine the whole elemental profile of the analyzed sample
- it allows very rapid analysis
- it is able to detect minimum concentrations distinguishing different isotopes of the same element
- it guarantees high sensitivity and reproducibility

From the scientific literature it emerges that elemental profiling focuses mainly on two different research areas: health studies and food authentication and traceability

studies. In the first case it is used in the health field to monitor the concentrations of elements in biological samples such as urine, plasma, blood, hair, saliva, nails, tumor tissues (90-95), with the final aim of confirming suspicions of chronic intoxication. Some recent studies relate different metals with neurodegenerative diseases such as Parkinson's disease, Alzheimer's disease, Amyotrophic Lateral Sclerosis (ALS) and autoimmune diseases such as multiple sclerosis (MS) (96). Studies so far have involved in particular, lead, mercury, aluminum, cadmium but a complete elemental profiling could shed on the correlation between the elements and their possible synergistic effects in influencing the onset, development and progression of these diseases, thus representing a significant step forward in their prevention and treatment. This area of research has developed in recent decades due to a strong and continuous introduction of metals and other elements into the environment. Some emblematic examples are: lead derived from petrol (97,98), mercury accumulated in fish (99,100), arsenic accumulated in rice (101). A further field of investigation has emerged in recent years concerning the dispersion of rare earth elements (REEs) in the environment due to components of computers, mobile phones and other last generation devices not properly disposed of. The replacement of mercury thermometers with thermometers using an alloy consisting of gallium, indium and tin represents a further potential source of metal pollution that is worth monitoring due to the unclear effects of these elements on human health (102,103).

The second field of research that exploits elemental profiling is food science. In this case it can be used for the characterization of food from a nutritional point of view or for traceability and authentication studies of different food products.

The elemental characterization of food can have a preventive function, both to avoid the excessive consumption of food at risk for heavy metals accumulation (e.g. mercury in tuna), and to encourage the consumption of food rich in micro and macro nutrients.

In traceability studies, elemental profiling makes it possible to relate a product to its territory. Seeds and fruits are in facts a natural site of bio-accumulation of metals

inside the plant. Traceability studies usually involve the determination of REEs since these elements are accumulated by plants without being fractionated: the REEs profile of the soil is thus reflected in the fruit (104). This principle is at the basis of traceability studies, focused to verify if the REEs profile remains unchanged from the soil to the final product; this principle has already been demonstrated for some short supply chains, such as that of paprika (105). For the longer production chains, the maintenance of the REEs profile is not always verified and must be evaluated from time to time (106).

On the other hand, in authentication studies for frauds identification, a link between food and territory is nor searched for but elemental profiling is used to differentiate equivalent food products from different areas without univocally binding them to the territory.

The amount of data obtained from elemental profiling does not allow a classic univariate approach to the problem, considering one variable (isotope) at a time (for example, the determination of 45 elements in 100 samples would lead to 4500 data), but rather makes it essential to apply techniques that provide a chemometric multivariate statistical treatment.

Chemometrics is a branch of analytical chemistry focused to the development and application of statistical methods for problem solving and the analysis of data in the chemical field and more generally in applied sciences.

Unlike most statistical and analytical procedures that tend to transform into univariate all the problems, even those that are intrinsically multivariate, this allows a multivariate approach to the system under investigation. Multivariate methods allow to take into account all the variables involved, making it possible to evaluate the correlations between the system descriptors and identify both synergisms and antagonisms.

For the particular application to problems treated in this PhD thesis, two main tools of multivariate analysis were exploited (107): pattern recognition methods, useful for recognizing existing structures in the data, such as groupings present in samples

and / or variables with a similar behavior; classification methods, able to identify mathematical models for the differentiation of the samples in different classes. Pattern recognition tools are unsupervised methods, i.e methods where no *a priori* hypotheses are formulated on how the samples are grouped, aimed to display data in a compact and easily readable way, so that the homogeneous groups can be recognized within the sample set. Among the unsupervised techniques, Principal Components Analysis (PCA) is undoubtedly the most widespread, together to cluster analysis (CA).

Classification tools are instead supervised methods that, unlike the previous ones, are based on the assumption that the existence of groups or classes is already known and defined. This condition may derive from the fact that the samples are conceptually separated in theoretical classes or may derive from a previous identification of groups of samples by PCA or CA. Classification methods are aimed to identify the variables mostly responsible for the separation of the classes of samples, i.e. the identification of candidate markers. Each class is then described by a mathematical model that can be applied to unknown samples to evaluate their belonging to one class or another. Among the classification mostly exploited in traceability and authentication studies, we find Linear Discriminant Analysis (LDA) (108,109), Principal Component Analysis – Discriminant Analysis (PCA-DA) (108, 109), Partial Least Squares – Discriminant Analysis (PLS-DA) (108,109) and Soft Independent Model of Class Analogy (SIMCA) (108,109).

In literature, several papers are present about traceability and authentication studies exploiting multivariate statistics on elemental profiling For example, Aceto et al. (106) studied the possibility to use lanthanides (La, Ce, Pr, Nd, Sm, Eu, Gd, Tb, Dy, Ho, Er, Tm, Yb, Lu) as chemical markers in a traceability study about the Moscato d'Asti wine production chain; soils, grapes and musts were analyzed by ICP-MS. The effect played by oenological practices on the REEs distribution was evaluated. In this work, PCA and CA were applied and proved that the lanthanides fingerprint is kept unaltered in the passage from soils to grapes and musts; alterations are instead

observed on the wine after clarification treatments using bentonites.

Another paper Bontempo et al. (110) reports the possibility of tracing the geographical origin, in tomato and derivatives along the production chain (juice, passata and paste) by Isotope Ratio Mass Spectrometry, Inductively Coupled Plasma Mass Spectrometry and Ion Chromatography. The samples used in this study came from three different Italian regions (Piedmont, Emilia Romagna, and Apulia). The traceability of these products was demonstrated: excellent discrimination among products from the three regions was achieved by applying linear discriminant analysis (LDA) on 17 parameters (Gd, La, Tl, Eu, Cs, Ni, Cr, Co, d34S, d15N, Cd, K, Mg, d13C, Mo, Rb and U).

Another study is about the Red Onion of Tropea (Calabria, Italy), an Italian product of excellence, registered on the European list of "Denominations of Origin and Protected Geographical Indications" on March 28, 2008 with Reg. CE n. 284/2008 of the Commission (111); in this study, Furia et al. (112) developed a reliable classification model of onion samples in groups corresponding to “Tropea” and “non-Tropea” categories. The concentrations of 25 elements (Al, Ba, Ca, Cd, Ce, Cr, Dy, Eu, Fe, Ga, Gd, Ho, La, Mg, Mn, Na, Nd, Ni, Pr, Rb, Sm, Sr, Tl, Y, and Zn) in onion samples with PGI brand (120) and onion samples not cultivated following the production regulations (80) were analyzed by ICP-MS. Different chemometric approaches were tested: LDA SIMCA, and back-propagation artificial neural networks (BP-ANN). Satisfactory results (prediction ability >90%) were obtained.

Finally, Spiros et al. (113) discriminated ‘‘Fava Santorinis’’ from other yellow split peas, by four classification methods applied to REEs and trace elements determination by ICP-MS. In this paper, orthogonal projection analysis (OPA), Mahalanobis distance (MD), PLS-DA and k nearest neighbors (KNN) were applied. OPA provided the best results 100% accuracy).

When multivariate tools are applied to elemental profiling, particular attention must be paid to data pretreatment. Since the absolute concentrations of the elements usually decreases along the production chain, their use in traceability and

authentication studies is unfeasible. Elemental concentrations are usually normalized, that is scaled with respect to a reference analyte that has to remain unchanged in the samples under investigation.

As for the elements to be used as normalizing factors, studies are present in literature that use as normalizing factors different elements such as strontium, barium, lanthanum or rubidium. The choice is usually driven by the fact that the chosen element must remain unchanged within the samples under analysis. In other cases, the most adequate standardization factor needs to be identified in order to solve the problem.

1.1.3 Chemometrics Theory

Hereafter, the multivariate statistical methods used in this Ph.D. thesis will be briefly presented.

1.1.3.1 Data pretreatment

When multivariate techniques are applied, data pretreatment is usually necessary to provide reliable results. The most exploited scaling technique is autoscaling, consisting in a two steps procedure: data are first mean centered so that the new average value for each variable equals 0; then, the data are normalized by the standard deviation of each variable independently, so that the new variables have all unit variance. This scaling is useful to provide variables accounting for the same amount of information, thus eliminating scale effects.

Here, autoscaling was always applied when applying PCA or other multivariate statistical techniques.

When multivariate tools are applied in traceability studies based on elemental profiling, it is preferable to deal with ratios rather than with the absolute concentration of the elements since this last one naturally decreases passing from soil to the fruit and so on along the production chain.

Data were therefore scaled for each analyte independently since each analyte could

be used as a normalizing factor, by the expression:

$$x'_{i,j} = \frac{x_{i,j}}{x_{i,k}} \; i \neq k \; (1)$$

where $x'_{i,j}$ is the normalized value for the *i*-th sample and the *j*-th analyte, $x_{i,j}$ is the concentration level of the *i*-th sample and the *j*-th analyte and $x_{i,k}$ is the concentration level of the *i*-th sample and the *k*-th analyte (where $i \neq k$).

1.1.3.2 Statistical Analysis: Principal Component Analysis (PCA)

PCA (108,109) is a multivariate statistical method allowing the representation of the objects (samples), described by the original variables (metal concentrations), in a new reference system characterized by new variables called Principal Components (PCs). The PCs are calculated hierarchically: the first PC accounts for the maximum amount of the original variance, while subsequent PCs account for the maximum residual variance, so that systematic variations are explained in the first PCs, while experimental noise and random variations are contained in the last ones. Each PC is a linear combination of the original variables and they are orthogonal to each other, thus accounting for independent sources of information. PCA provides two main tools for data analysis: the *scores,* representing the co-ordinates of the samples in the space given by the PCs; the *loadings,* representing the coefficients of the linear combination describing each PC, *i.e.* the weights of the original variables on each PC. The *scores* allow the identification of groups of samples showing similar (samples close one to the other in the graph) or different (samples far from each other) behaviors. By looking at the corresponding loading plot, it is possible to identify the variables that are responsible for the similar or different behaviors detected for the samples in the score plot. PCA was applied here after varimax rotation of the most relevant PCs; this treatment allows the maximization of the variances of all the original variables on each PC (108,109).

1.1.3.3 Partial Least Squares – Discriminant Analysis (PLS-DA)

Partial Least Square (PLS) (108,109) is a multivariate regression method establishing a relationship between one or more dependent variables (Y) and a group of descriptors (X). X and Y variables are modeled simultaneously, to find the latent variables (LVs) in X that will predict the LVs in Y. When a large number of descriptors (X variables) are present, or a large experimental error is expected, it can be quite difficult to obtain a final model with a suitable predictive ability. In these cases, techniques for variable selection are usually exploited. Here, a backward elimination (BE) strategy was applied, eliminating one variable at a time, according to the minimum error in cross-validation; variables are eliminated according to the smallest importance (114). PLS was originally proposed to model continuous responses, but it can be applied also for classification purposes by establishing an appropriate Y response matrix related to the belonging of each sample to a class. The regression is then carried out between the X-block variables (here the elemental) and the Y just established. This application for classification purposes is called PLS-DA (115,116). In this case, where three classes are present, three binary variables were added to the Y matrix, coded so that +1 means that the sample belongs to a certain cultivar corresponding to the specific column, while -1 means that the sample does not belong to the class associated to the specific column.

1.1.3.4 Principal Component Analysis – Linear Discriminant Analysis (PCA-LDA)

LDA (117-119) is a Bayesian classification method providing the classification of the objects taking into consideration at the same time the multivariate structure of the data. Each object is classified in a particular class g if the so-called discriminant score D_g is minimum:

$$D_g(x_i) = \left(x_i - \bar{x}_g\right)^T S_g^{-1}\left(x_i - \bar{x}_g\right) + \ln\left|S_g\right| - 2\ln P_g \quad (5)$$

where, $\mathbf{S_g}$ is the covariance matrix of class g; $\bar{x}_g$ is the centroid of class g, x_i is the vector representing the i-th object and P_g is the prior probability of class g. In LDA,

$\mathbf{S_g}$ is approximated with the pooled (between the classes) covariance matrix; this corresponds to considering all the classes as having a common shape (i.e., the average, weighted over the degrees of freedom, of the shape of the present classes). The variables contained in the LDA model discriminating the classes can be chosen by a stepwise algorithm, selecting iteratively the most discriminating variables. Here, a forward selection (FS) procedure was applied: at each iteration, the variable guaranteeing the best Non-Error-Rate (NER%) in cross-validation was added to the final model. FS-LDA was applied to the principal components rather than to the original variables. The loadings of the PCs allow the calculation of the final weight of each original variable on the LDA model built on the PCs.

1.1.3.5 Evaluation of the classification performances

The classification performances can be evaluated both in fitting and cross-validation by the calculation of several indexes. *The confusion matrix* is a matrix reporting the true classes on the rows and the assigned classes on the columns. Given G classes, each element n_{kl} represents the number of samples belonging to class k and assigned to class l. The diagonal values $n_{gg,}$ corresponding to each g-th class, are the correct assignments (i.e. samples correctly assigned to a class), while the extra-diagonal elements correspond to the miss-classifications (i.e. samples of a class erroneously attributed to another class). The sum of each row is the number of samples belonging to the corresponding g-th class (n_g), while the sum of each column is the number of samples assigned to the corresponding g-th class (n'_g). All the indexes related to the classification performances can be calculated starting from the confusion matrix:

Precision is the capability of a classification model to not include samples of other classes in the considered class. For each class g, it is calculated as the percentage ratio of the number of samples correctly assigned to class g (n_{gg}) and the total number of samples assigned to class g (n'_g).

Sensitivity is the capability of a classification model to correctly recognize samples

belonging to the *g*-th class. It is calculated as the percentage ratio of samples correctly assigned to class *g* (n_{gg}) and the total number of samples belonging to class *g* (n_g).

Specificity is the capability of the *g*-th class to reject the samples of all the other classes. It is calculated as:

$$Sp_g = \frac{\sum_{k=1}^{G}(n'_k - n_{gk})}{n - n_g} * 100 \qquad \text{for } k \neq g \quad (3)$$

where *G* is the number of classes and n'_k is the total number of samples assigned to class *k*:

$$n'_k = \sum_{g=1}^{G} n_{gk} \quad (4)$$

Accuracy is the percentage ratio of the overall correctly assigned samples, considering all the classes contemporarily.

The ***Non Error Rate*** *(NER%)* is the average of the class sensitivities, while the *Error Rate (ER%)* is the complement to 100% of the NER%.

1.2 Bibliography

1. Beijer K., Jernelöv A. (1986) Sources, transport and transformation of metals in the environment In: Friberg L, Nordberg GF and Vouk VB (eds) Handbook on the Toxicology of Metals. Amsterdam: Elsevier, 68-84.
2. Eto K. (1997) Pathology of Minamata Disease. Toxicol. Pathol. 25, 6: 614-623.
3. Harada M. (1995) Minamata Disease: Methylmercury Poisoning in Japan Caused by Environmental Pollution. Crit Rev Toxicol. 25(1):1-24.
4. NIMD: Report of the Social Scientific Study Group on Minamata Disease, In the Hope of Avoiding Repetition of a Tragedy of Minamata Disease, National Institute for Minamata Disease, p. 13.
5. Kumamoto University Study Group (1968). Pathology of Minamata desease. In: Minamata Disease, M Kutsuna (ed). Shuhan, Kumamoto, Japan, pp. 141-

252.

6. Crammer M., Gilbert S., Crammer J. (1996) Neurotoxicity of mercury-indicators and effects of low-level exposure overview. Neurotoxicology. 17 (1): 9-14.
7. Takeuchi T., Kambra T., Morikawa N., Matsumoto H., Shiraishi Y., and Ito H. (1959) Pathologic observations of the Minamata disease. Acta Pathol. Jpn. 9(suppl.): 769-783.
8. Matsumoto H., Koya G., and Takeuchi T. (1965) Fetal Minamata disease: A neuropathological study of two cases of intrauterine intoxication by methylmercury compound. J. Neuropathol. Exp. Neurol. 24: 563-574.
9. Choi B.H., Lapham L.W., Amin-zaki L., and Saleem T. (1978) Abnormal neuronal migration, deranged cerebral cortical organization, and diffuse white matter astrocytosis of human fetal brain: A major effect of methylmercury poisoning in utero. J. Neuropathol. Exp. Neurol. 37: 719-733.
10. Takeuchi T. (1977) Pathology of fetal Minamata disease. Pediatrician 6: 69-87.
11. Takeuchi T., Matsumoto H., and Koya G. (1964) A pathological study of fetal Minamata disease diagnosed clinically as so-called infantile cerebral palsy. Adv. Neurol. 8(4): 145-161 (in Japanese).
12. Cai S., Yue L., Shang Q., Nordberg G. (1995) Cadmium exposure among residents in an area contaminated by irrigation water in China. Bull World Health Organization. 73, 359–367.
13. Needleman H.L., Schell A., Bellinger D. et al. (1990) Long-term effects of childhood exposure to lead at low doses: An eleven-year follow –up report. N Engl J Med. 322:82-88.
14. Woolley D.E. (1984) A perspective of lead poisoning in antiquity and the present. Neurotoxicology. 5(3):353-61.
15. Gilfillan S.C. (1965) Lead poisoning and the fall of Rome. J Occup Med. 7:53-60.

16. Nriagu J.O. (1983) Occupational exposure to lead in ancient times. Sci Total Environ. 31(2):105-16.
17. Ng A., Patterson C. (1981) Natural concentrations of lead in ancient Arctic and Antarctic ice. Geochimica et Cosmochimica Acta. 45,11, 2109-2121.
18. Ugazio G. Compendio di Patologia Ambientale. Edizione Minerva Medica pp 11-24 (2008).
19. https://www.atsdr.cdc.gov/csem/lead/docs/CSEM-Lead_toxicity_508.pdf
20. Bruening K., Kemp F.W., Simone N., Holding Y., Louria D.B., Bogden J.D. (1999) Dietary calcium intakes of urban children at risk of lead poisoning. Environ Health Perspect. 107:431-435.
21. Skerfving S., Gerhardsson L., Schutz A., Stromberg U. (1998) Lead—biological monitoring of exposure and effects. J Trace Elem Exp Med. 11:289–301.
22. Goyer R.A., Rhyne B.C. (1973) Pathological effects of lead. Int Rev Exp Pathol. 12:1–77.
23. Pounds J.G., Long G.J., Rosen J.F. (1991) Cellular and molecular toxicity of lead in bone. Environ Health Perspect. 91:17–32.
24. Needleman H.L., Schell A., Bellinger D. et al. (1990) Long-term effects of childhood exposure to lead at low doses: An eleven-year follow –up report. N Engl J Med. 322:82-88.
25. Goyer R.A. (1990) Lead toxicity: From overt to subclinical to subtle health effects. Environ Health Perspect. 86:177–181.
26. Gundacker C., Hengstschläger M. (2012) The role of the placenta in fetal exposure to heavy metals. Wien Med Wochenschr. 162(9-10):201-6.
27. Kim M.K., Zoh K.D. (2012) Fate and Transport of Mercury in Environmental Media and Human Exposure. J Prev Med Public Health. 45:335-343.
28. Tchounwou P.B., Yedjou C.G., Patlolla A.K., and Sutton D.J. (2012) Heavy Metals Toxicity and the Environment. EXS. 101: 133–164.
29. Bensefa-Colas L., Andujar P., Descatha A. (2011) [Mercury poisoning]. Rev

Med Interne. 32(7):416-24.
30. Clarkson T.W. et al. (2003) The toxicology of mercury – current exposures and clinical manifestations. N Engl J Med. 349: 1731.
31. http://www.who.int/ceh/capacity/Mercury.pdf
32. Bengtsson U.G.,Hylander L.D. (2017) Increased mercury emissions from modern dental amalgams. Biometals. 30:277–283.
33. Clarkson T.W., Vyas J.B., and Ballatori N. (2007) Mechanisms of Mercury Disposition in the Body. American Journal Of Industrial Medicine. 50:757–764.
34. Thum C.K., Biswas A. (2015) Inflammatory complications related to tattooing: a histopathological approach based on pattern analysis. Am J Dermatopathol. 37(1):54-66.
35. Rodrigues J., Branco V., Luc J., Holmgren A., Carvalho A. (2015) Toxicological effects of thiomersal and ethylmercury: Inhibition of the thioredoxin system and NADP+-dependent dehydrogenases of the pentose phosphate pathway. Toxicology and Applied Pharmacology. 286, 216–223.
36. Tchounwou P.B., Ayensu W.K., Ninashvilli N., Sutton D. (2003) Environmental exposures to mercury and its toxicopathologic implications for public health. Environ Toxicol. 18:149–175.
37. Maqboola F., Niaza K, Hassana F.I., Khana F., and Abdollahi M. (2017) Immunotoxicity of mercury: Pathological and toxicological effects. Journal of Environmental Science and Health, Part C. Vol. 35, No. 1, 29-46.
38. Aposhian H.V., Bruce D.C., Alter W., et al. (1992) Urinary mercury after administration of 2, 3-dimercaptopropane-1-sulfonic acid: correlation with dental amalgam score. FASEB J. 6:2472-2476.
39. Goldman L.R., Shannon M.W. and the Committee on Environmental Health. Technical Report: Mercury in the Environment: Implications for Pediatricians. Pediatrics 2001;108;197.

40. Monteiro L.R., Furness R.W. (1997) Accelerated increase in mercury contamination in north Atlantic mesopelagic food chains as indicated by time series of seabird feathers. Environmental Toxicology and Chem. 16, 2489–2493.
41. United Nations Environment Programme. The global atmospheric mercury assessment: sources, emissions and transport. Geneva: United Nations Environment Programme; 2008, p. 13-62.
42. Kim M.K., Zoh K.D. (2012) Fate and Transport of Mercury in Environmental Media and Human Exposure. J Prev Med Public Health. 45:335-343.
43. Park J.D. and Zheng W. (2012) Human Exposure and Health Effects of Inorganic and Elemental Mercury. J Prev Med Public Health. 45(6): 344–352.
44. https://www.atsdr.cdc.gov/mmg/mmg.asp?id=106&tid=24
45. Bulat P., Dujić I., Potkonjak B., Vidaković A. (1998) Activity of glutathione peroxidase and superoxide dismutase in workers occupationally exposed to mercury. Int Arch Occup Environ Health. 71 Suppl:S37-9.
46. Pollard K.M., Pearson D.L., Hultman P., Hildebrandt B., Kono D.H. (1999) Lupus-prone mice as models to study xenobiotic-induced acceleration of systemic autoimmunity. Environ Health Perspect. 107:729.
47. Henry G.A., Jarnot B.M., Steinhoff M.M. et al. (1998) Mercury-induced renal autoimmunity in the MAXX rat. Clinical Immunology and Immunopathology. Vol 49:187–203.
48. Pelletier L., Druet P. (1995) Immunotoxicology of metals. Toxicology of Metals Handbook of Experimental Pharmacology. Vol 115, pp 77-92.
49. Stein J., Schettler T., Wallinga D., Valenti M. (2002) In harm's way: toxic threats to child development. J. Dev. Behav. Pediatr. 23, pp. S13-S22.
50. ATSDR: Cadmium (Update). Washington, DC: U.S. Department of Health and Human Services, 1998.

51. Smith S.W. (2013) The Role of Chelation in the Treatment of Other Metal Poisonings J. Med. Toxicol. 9:355–369.
52. https://www.atsdr.cdc.gov/substances/toxsubstance.asp?toxid=15
53. http://www.cdc.gov/niosh/docs/1970/76-192.html.
54. Klaassen C.D., Liu J., Choudhuri S. (1999) Metallothionein: an intracellular protein to protect against cadmium toxicity. Annu Rev Pharmacol Toxicol. 39:267-94.
55. Buchet J.P., Lauwerys R., Roels H. et al. (1990) Renal effects of cadmium body burden of the general population. Lancet. 336:699-702.
56. Friberg L., Eliner C.F., Kjellstrom T., et al. Cadmium and Health: A Toxicological and Epidemiological Appraisal. Vol II. Effects and Respose. Boca Raton, FL: CRC Press, 1986, pp 1-307.
57. IARC: Monographs on the Evaluation of Carcinogenic Risks to Humans. Vol 58. Beryllium, Cadmium, Mercury, and Exposures in the Glass Manufacturing Industry. Lyons, France: IARC(1993).
58. Fekete V., Vandevijvere S., Bolle F., Van Loco J. (2013) Estimation of dietary aluminum exposure of the Belgian adult population: evaluation of contribution of food and kitchenware. Food Chem. Toxicol. 55, pp. 602-608.
59. Bondy S.C. (2015) Low levels of aluminum can lead to behavioral and morphological changes associated with Alzheimer's disease and age-related neurodegeneration. Neurotoxicology, 52, pp. 222-229.
60. Exley C., Burgess E., Day J.P., Jeffery E.H., Melethil S., Yokel R.A. (1996) Aluminum toxicokinetics. J Toxicol Environ Health. 48: 569–584.
61. P.C., Couttenye M.M., De Broe M.E. (1996) Diagnosis and treatment of aluminium bone disease. Nephrol Dial Transplant. 11(Suppl 3) 74–79.
62. Riihimaki V., Aitio A. (2012) Occupational exposure to aluminum and its biomonitoring in perspective. Crit Rev Toxicol. 42(10) 827–853.
63. Malo J.L., Vandenplas O. (2011) Definitions and classification of work-related asthma. Immunol Allergy Clin N Am. 31(4):645–662.

64. Shaw C.A., Tomljenovic L. (2013) Aluminum in the central nervous system (CNS): toxicity in humans and animals, vaccine adjuvants, and autoimmunity. Immunol Res. 56(2-3):304-16.
65. Trapp G.A. (1983) Plasma aluminium is bound to transferrin. Life Sci. 33:311-306.
66. Murko S., Scancar J., Milacic R. (2011) Rapid fractionation of Al in human serum by the use of the HiTrap desalting size exclusion column with ICP-MS detection. J Anal At Spectrom. 26:86-93.
67. Deloncle R., Guillard O., Clanet F., Courtois P., Piriou A. (1990) Aluminum transfer as glutamate complex through blood-brain barrier. Possible implication in dialysis encephalopathy. Biol Trace Elem Res. 25(1):39-45.
68. Canales J.J., Corbalán R., Montoliu C., Llansola M., Monfort P., Erceg S., Hernandez-Viadel M., Felipo V. (2001) Aluminium impairs the glutamate-nitric oxide-cGMP pathway in cultured neurons and in rat brain in vivo: molecular mechanisms and implications for neuropathology. J Inorg Biochem. 87(1-2):63-69.
69. World Health Organization, Safety Evaluation of Certain Food Additives and Contaminants. Food Additive Series: 58, 2007 http://whqlibdoc.who.int/trs/WHOTRS940eng.pdf.
70. Crisponi G., Nurchi V.M., Crespo-Alonso M., Toso L. (2012) Chelating agents for metal intoxication. Curr Med Chem. 19(17):2794-815.
71. Lomax C., Liu W.J., Wu L. , Xue K., Xiong J., Zhou J. , McGrath S.P., Meharg A.A., Miller A.J. and Zhao F.J. (2012) Methylated arsenic species in plants originate from soil microorganisms. New Phytologist. 193: 665–672.
72. Goyer R.A. and Clarkson T.W. TOXIC EFFECTS OF METALS. CHAPTER 23. Casarett & Doull's Essentials of Toxicology, 2e Klaassen CD, Watkins JB.

73. Awasthi S., Chauhan R., Srivastava S., Tripathi R.D. (2017) The journey of arsenic from soil to Grain in Rice. Frontiers in Plant Science. 8, 20, Article number 1007.
74. NRC: Arsenic in Drinking Water. Washington, DC: National Academy Press, 1999, pp1-308.
75. Bentley R., Chasteen T.G. (2002) Microbial Methylation of Metalloids: Arsenic, Antimony, and Bismuth. Microbiol Mol Biol Rev. 66(2): 250–271.
76. Brown M.M., Rhyne B.C., Goyer R.A. & Fowler B.A. (1976) Intracellular effects of chronic arsenic administration on renal proximal tubule cells. Journal of Toxicology and Environmental Health. Volume 1, Issue 3.
77. http://www.atsdr.cdc.gov/substances/toxsubstance.asp?toxid=3
78. IARC Working Group on the Evaluation of Carcinogenic Risks to Humans. Arsenic, metals, fibres, and dusts. IARC Monogr Eval Carcinog Risks Hum. 2012;100(Pt C):11-465.
79. Medical and Biological Effects of Environmental Pollutants: Nickel, Nat. Acad. Sci, Washington DC,1975.
80. Sunderman F.W. (1989) Mechanisms of nickel carcinogenesis. Scand J Work Environ Health. 15:1–12.
81. Ambient Water Quality Criteria for Nickel, US EPA NTIS, Springfield, VA. Publ No. PB81-117715,1980.
82. https://www.atsdr.cdc.gov/toxprofiles/tp.asp?id=245&tid=44
83. Bocca B., Forte G., Pino A. and Alimonti A. (2013) Heavy metals in powder-based cosmetics quantified by ICP-MS: an approach for estimating measurement uncertainty. Anal. Methods. 5, 402-408
84. Yoshioka Y., Kuroda E., Hirai T., Tsutsumi Y. and Ishii K.J. (2017) Allergic Responses Induced by the Immunomodulatory Effects of Nanomaterials upon Skin. Exposure Front. Immunol. 8, 189.
85. Foster A.W., Osman D., and Robinson N.J. (2014) Metal Preferences and Metallation. J Biol Chem. 289(41): 28095–28103.

86. IARC, International Agency for Research on Cancer, 2012. Arsenic, metals, fibres, and dusts. Vol. 100 C, IARC, Lyon, France.
87. Aceto M. (2016) The Use of ICP-MS in Food Traceability (Book Chapter) Advances in Food Traceability Techniques and Technologies: Improving Quality Throughout the Food Chain. pp. 137-164.
88. Tyler G. (2004) Rare earth elements in soil and plant systems: a review. Plant Soil 267, 191–206.
89. Liang T., Ding S., Song W., Chong Z., Zhang C., Li H. (2008) A review of fractionations of rare earth elements in plants. Journal of Rare Earths 26, 7–15.
90. Bocca B., Mattei D., Pino A., Alimonti A. (2011) Monitoring of environmental metals in human blood: The need for data validation. Current Analytical Chemistry. Volume 7, Issue 4, 269-276.
91. Goulle J-P., Mahieu L., Castermant J., Neveu N., Bonneau L., Laine G., Bouige D., Lacroix C. (2005) Metal and metalloid multi-elementary ICP-MS validation in whole blood, plasma, urine and hair reference values. Forensic Sci. Int., 153, 39–44.
92. Chirila E., Draghici C. (2011) Analytical Approaches for Sampling and Sample Preparation for Heavy Metals Analysis in Biological Materials. NATO Science for Peace and Security Series C: Environmental Security. 1, pp. 129-143.
93. Hussein W.F., Njue W., Murungi J., Wanjau R., (2008) Use of human nails as bio-indicators of heavy metals environmental exposure among school age children in Kenya, Sci. Total Environ. 393, 376–384.
94. Alimonti A., Bocca B., Mattei D., Lamazza A., Fiori E., De Ercole M., Pino A., Forte G. (2009) Composition of essential and non-essential elements in tissues and body fluids of healthy subjects and patients with colorectal polyps. International Journal of Environment and Health. 3,2, 2009, 224-237.

95. Chung H.K., Nam J.S., Ahn C.W., Lee Y.S., Kim K.R. (2016) Some Elements in Thyroid Tissue are Associated with More Advanced Stage of Thyroid Cancer in Korean Women Biological Trace Element Research. 171(1), pp. 54-62.
96. Fulgenzi A., Vietti D., Ferrero M.E. (2017) Chronic toxic-metal poisoning and neurodegenerative diseases. International Journal of Current Research. 9,09, pp.57899-57909.
97. Caplun E.B.A., Petit D., Picciotto D.E. (1984) Lead in petrol. Endeavour. 8, 3, 135-144.
98. http://www.who.int/bulletin/archives/80(10)768.pdf
99. Carneiro M.F., Grotto D., Barbosa F. (2014) Inorganic and methylmercury levels in plasma are differentially associated with age, gender, and oxidative stress markers in a population exposed to mercury through fish consumption. J Toxicol Environ Health A. 77(1-3):69-79.
100. EFSA Scientific Committee, 2015. Statement on the benefits of fish / seafood consumption compared to the risks of methylmercury in fish / seafood. EFSA Journal, 13(1), p.3982.
101. Islam S., Rahman M.M., Islam M.R., Naidu R. (2016) Arsenic accumulation in rice: Consequences of rice genotypes and management practices to reduce human health risk. Environment International 96 139–155.
102. Nabi S. (2014) Toxic Effects of Mercury | | Springer 2014 Chapter 2, 9-14.
103. Geratherm Medical AG (2011, July 20). Galinstan Safety Data Sheet [Online]. Available: http://www.rgmd.com/msds/msds.pdf
104. Liang, T., Ding, S., Song, W., Chong, Z., Zhang, C., Li, H., 2008. A review of fractionations of rare earth elements in plants. Journal of Rare Earths 26, 7–15.
105. Brunner M., Katona R., Stefanka Z., Prohaska T. (2010) Determination of the geographical origin of processed spice using multielement and isotopic pattern on the example of Szegedi paprika. European Food research and

Technology. 231(4), 623-634.

106. Aceto M, Robotti E., Oddone m., Baldizzone M., Bonifacino g., Bezzo G., Di Stefano R., Gosetti F., Mazzucco E., Manfredi M., Marengo E. (2013) A traceability study on the Moscato wine chain. Food Chemistry. 138, 1914–1922.
107. Gonzalvez A., Armenta S., de la Guardia M. (2009) Trace-element composition and stable-isotope ratio for discrimination of foods with Protected Designation of Origin. Trends in Analytical Chemistry. 28, 11, 1295-1311.
108. Massart D.L., Vandeginste B.G.M., Deming S.M., Michotte Y., Kaufman L. (1988) Chemometrics: A textbook. Amsterdam: Elsevier.
109. Vandeginste B.G.M., Massart D.L., Buydens L.M.C., Yong S. De, Lewi P.J., Smeyers-Verbeke J. Handbook of Chemometrics and Qualimetrics: Part B. Amsterdam: Elsevier, 1998.
110. Bontempo L., Camin F., Manzocco L., Nicolini G., Wehrens R., Ziller L., Larcher R. (2011) Traceability along the production chain of Italian tomato products on the basis of stable isotopes and mineral composition. Rapid Commun. Mass Spectrom. 25, 899–909.
111. Commission Regulation (EC) No 284/2008 of 27 March 2008 registering certain names in the Register of protected designations of origin and protected geographical indications Lingot du Nord (PGI), Cipolla Rossa di Tropea Calabria (PGI), Marrone di Roccadaspide (PGI).
112. Furia E., Naccarato A., Sindona G., Stabile G., Tagarelli A. (2011) Multielement Fingerprinting as a Tool in Origin Authentication of PGI Food Products: Tropea Red Onion. J. Agric. Food Chem. 59, 8450–8457.
113. Drivelos S.A., Higgins K., Kalivas J.H., Haroutounian S.A., Georgiou C.A. (2014) Data fusion for food authentication. Combining rare earth elements and trace metals to discriminate ‘‘Fava Santorinis’’ from other yellow split peas using chemometric tools.Food Chemistry. 165, 316–322.

114. Oussama A., Elabadi F., Platikanov S., Kzaiber F., Tauler R, (2012) Detection of Olive Oil Adulteration Using FT-IR Spectroscopy and PLS with Variable Importance of Projection (VIP) Scores. J Am Oil Chem Soc. 89(10): 1807-1812.
115. Robotti E., Marengo E. (2017) Chemometric multivariate tools for candidate biomarker identification: LDA, PLS-DA, SIMCA, Ranking-PCA, Methods in Molecular Biology. Vol 1384, 237-267.
116. Marengo E., Robotti E., Bobba M., Milli A., Campostrini N., Righetti S.C., Cecconi D., Righetti P.G. (2008) Application of partial least squares discriminant analysis and variable selection procedures: A 2D-PAGE proteomic study. Analytical and Bioanalytical. 390(5), 1327-1342.
117. Fearn T. (2008) The interaction between standard normal variate and derivatives. NIR News. 19 (7).
118. Negri A.S., Robotti E., Prinsi B., Espen L., Marengo E. (2011) Proteins involved in biotic and abiotic stress responses as the most significant biomarkers in the ripening of Pinot Noir skins. Funct. Integr. Genomics, 11 (2)341–355.
119. Marengo E., Robotti E., Bobba M. (2007) 2D-PAGE maps analysis, in: A. Vlahou (Ed.), Methods in Molecular Biology Vol. 428: “Clinical Proteomics: Methods and Protocols”, Humana Press Totowa, NJ, pp. 291–325.

CHAPTER 2

2.1 Outline of the thesis

The work of this Ph.D. Thesis is focused on deepening different aspect related to the exploitation of elemental profiling. The work was therefore divided into two main areas of research: the use of elemental profiling for the solution of issues related to human health and for the development of traceability and authentication studies.

For what regards the use of elemental profiling in the area of human health, the study was focused on the monitoring for one year, by ICP-MS, of the excretion of heavy metals and other elements from a patient subjected to the chelating therapy with $CaNa_2EDTA$. The main purposes of this study were the follow-up of the therapy and the evaluation of the efficacy of the employed administration protocol.

The possible heavy metal chronic poisoning was hypothesized by the physicians, based on the anomalous clinical symptoms presented by the patient, which were apparently unrelated each other. A tentative diagnosis of Chronic Fatigue Syndrome was posed. The hypothesis was supported by the patient medical history and by laboratory investigations. In particular, the plasma level of lactic acid was constantly above the normal threshold, either at rest or under muscular stress. Such an alteration could arise from mitochondria malfunctioning in the muscles, caused by heavy metals intoxication.

Paralel to this study, we have monitored for ten days the plasma proteome of this patient subjected to chelating therapy with $CaNa_2EDTA$. The plasma proteins were analyzed with a micro-LC Eksigent Technologies system (Eksigent, Dublin, USA) interfaced with a 5600+ TripleTOF system (AB Sciex, Concord, Canada) equipped with DuoSpray Ion Source and CDS (Calibrant Delivery System). The plasma proteome coverage was increased using immunodepletion method and the proteins were quantified using the label-free SWATH-MS quantification. The analysis

allowed to get insight into the expression of the plasma proteome changes after chelation therapy, providing new information in terms of the understanding of mechanisms and effects of the treatment on the human body, rather than the pathways involved. In fact, the low-abundant plasma proteins are considered an important source of biomarkers for disease diagnosis and therapeutic monitoring.

The second part of the Ph.D. project envisages applying two different analytical techniques to perform hazelnut authentication and traceability studies.

It is very important for both the consumer and the food industry, to safeguard the protected varieties and the food quality. Due to the great commercial difference between the "Tonda Gentile delle Langhe" and the other cultivars, it is particularly important for the food industry the availability of tools for tracing the variety and the geographic provenance of hazelnuts and their derivatives along the production chain of the hazelnut paste.

Here, we have applied elemental profiling through ICP-MS and ICP-OES in an authentication study involving the production chain of hazelnut paste: from raw fruits to roasted hazelnuts, down to the final paste. The study involves three different cultivars ("Tonda Gentile delle Langhe", "Romana" and "Mortarella") and the data were treated by multivariate statistical classification methods to provide a model able to discriminate the three cultivars independently from the type of technological transformation.

The same raw hazelnut samples were also analyzed using a portable FTIR spectrometer coupled to multivariate statistical classification tools.

With this method, we want to differentiate the hazelnuts from different cultivars based on the differences in the signal intensity of their IR spectra.

Due to the rapid analysis, high sensitivity, simplicity and sample preparation, the proposed analytical methodology could be successfully used to verify the cultivar of hazelnuts, and the analysis can be performed quickly and directly on site.

CHAPTER 3

"Elemental profiling and proteomic screening of urine and plasma during a chelating therapy"

3.1 Introduction

Metal ions are probably among the toxic agents known since the longest time. Differently from other toxic compounds, they cannot be created or destroyed, yet they can change their oxidation state. Their industrial extraction, transformation and wide use have favored the contamination of air, water, soil and food, and their subsequent introduction into the vegetal and animal food chain up to human organisms (1).

Metals have spread in the environment following the widespread use of materials and substances in which they are present, such as gasoline and batteries (containing Pb), varnishes (containing Pb and Hg), pesticides (containing Pb, Hg and As), thermometers and teeth amalgams (containing Hg), pots, packages and cooking tools (containing Al), cigarette smoke (containing Pb and Cd) (2-9).

Besides, Al and Hg are found also in vaccines and drugs (10-15). Other elements present in the environment due to anthropic pollution are Sn, Th, Ni, U, Ce, Ga, Sr, Co, Mo, Bi, Ti, Rb, Ag, W, Zr, Ba, Ge, V, Sb, La, Sc (16-18).

While the toxicity of some elements (e.g. lead and mercury) is well known since centuries (19-24), in the last decades several compounds have been added to the list of the dangerous ones, like cadmium, aluminum and arsenic. These metals may accumulate in the body in targeted organs and cause organ failure following acute or chronic intoxication.

Thanks to the intervention of public health care systems, the cases of severe metal poisoning by a single element are nowadays very rare. Instead, it is increasing the

attention towards the chronic effects due to the exposition to a mixture of metals (so-called “cocktail effect”), individually at a concentration *per se* not sufficient to cause clinically relevant effects.

One medical approach to contrast metal intoxication is the chelating therapy (25). The treatment consists in the infusion of chelating agents that are able to form soluble complexes with the metal ions present in the organism. Upon chelation, the metal ion loses its toxicity and is eliminated through the urinary route. However, the chelating agents present some undesirable features. For instance, they are not specific, and therefore can bind to either toxic and useful metal ions. In addition, they may cause inflammatory/allergic reactions (25). Further, the mobilization of the metal ions in form of complexes may redistribute the toxic metal ion through the circulatory system of the patient (26, 27).

The ideal chelating agent for therapeutic application should have the following features: a) be soluble in water, b) not be metabolized, c) be able to reach the organs where the metals are stored, d) form stable and nontoxic complexes, e) be excreted through the urinary route, and f) show a low affinity for essential metal ions like calcium and zinc (28,29). Among the available agents (25,30), ethylenediaminetetraacetic acid (EDTA) is the most utilized one in the chelating therapy (31-34), due to its low side effects (35-40). EDTA is normally administered as calcium salt, since the disodium salt presents a high affinity for calcium and causes tetanic crisis due to hypocalcemia (40).

The parenteral administration permits a fast distribution of the drug in the organism, while its absorption in the gastrointestinal tract is quite low.

Furthermore, chelating therapy has been used for the treatment of several pathologies like artery diseases and neurodegenerative diseases. There are currently 11 FDA-approved chelators available and EDTA is the most utilized (32).

The role of metal toxicity in the pathogenetic mechanisms of hypertension, atherosclerosis, and coronary heart disease has already been highlighted (41). Toxic

metals induce oxidative stress, which is caused by unbalanced redox states, involving either excessive generation of reactive oxygen species (ROS) or dysfunction of the antioxidant system.

The National Center for Health Statistics estimates that more than 100,000 Americans receive chelation each year, but the inappropriate use of chelation therapy can be very dangerous (42). A large-scale controlled trial of disodium EDTA demonstrated the reduction of cardiovascular events (43): the treatment reduced clinical events in post–myocardial infarction (MI) patients, particularly in patients with diabetes (44,45). Several studies showed the efficacy of the chelation therapy in removing metals intoxication but only few blood parameters related to the oxidative status have been investigated (46).

3.2 Chelating therapy for removing metal ions intoxications

Here, we have monitored for one year, by ICP-MS, the excretion of heavy metals, from a patient subjected to the chelating therapy with $CaNa_2EDTA$.

The main purposes of this study were the follow-up of the therapy and the evaluation of the efficacy of employed administration protocol.

The possible heavy metal chronic poisoning was hypothesized by the physicians, based on the anomalous clinical symptoms presented by the patient, which were apparently unrelated each other. A tentative diagnosis of Chronic Fatigue Syndrome was posed (47). The hypothesis was supported by the patient medical history and by laboratory investigations. In particular, the plasma level of lactic acid was constantly above the normal threshold, either at rest or under muscular stress. Such an alteration could arise from mitochondria malfunctioning in the muscles, caused by heavy metals intoxication (48,49).

3.2.1 Materials and methods

3.2.1.1 The case history

The patient is a 37 years old male subject, 1.80 m tall, actual weight 52 Kg, Body Mass Index (BMI) 16.04, non smoker, non alcohol or coffee drinker. He is presently under treatment with Eutirox 100 mcg/die. Following is the relevant clinical record:

- 11 years old: development of a pollen allergy treated with desensitizing vaccines for about 20 years and an immunotherapy with allergenic extracts absorbed on aluminum hydroxide employed as adjuvant;
- 11-29 years old: de-sensitizing vaccines (about 24 subcutaneous injections per year);
- 23 years old: dietary allergies with anaphylactic shock (towards fruit and vegetables);
- 24 years old: severe weight loss; frequent myalgia, arthralgia, muscle stretching;

- 31 years old: thyroid cancer *(pT3m PN1a*, total thyroidectomy + 2 cycles of ^{131}I 3.7 GBq and 5.5 GBq); osteoporosis;
- 33 years old: elimination of the dental fillings containing mercury amalgams;
- 35 years old: basal lactic acid at 15.95 mg/dL and up to 87.17mg/dL under stress, above the CUT-OFF values (normal range 5.7-22 mg/dL).

However, analysis of a muscular biopsy from femoral quadriceps (in 2011), excluded the suspect of mitochondriopathy. Lead and aluminum were then determined in the patient blood, yet the values (lead 0.001 µg/mL and aluminum 0.0002 µg/mL) ruled out the possibility of an acute intoxication, given that the normal values for persons not professionally exposed to these heavy metals are < 0.0028 µg/mL and < 0.075 µg/mL, respectively.

Contemporarily, the dietary regimen of the patient was adjusted to limit as much as possible the intake of heavy metals.

Notwithstanding the normal plasma levels, it was hypothesized an organ-specific accumulation of heavy metals. In 2012, the patient was submitted to a chelating test with EDTA, to evaluate the potential presence of heavy metals bio-accumulated in the organism. After the first chelating agent infusion, the urine samples collected within 12 h were analyzed by the Laboratory of Toxicology (Doctor's Data Inc., St. Charles, IL USA). The 20 more toxic metals were determined by elemental analysis by inductively coupled plasma – mass spectrometry (ICP-MS). The concentrations of relevant metals were: Pb 15 µg/g creatinine (R.I. < 2 µg/g creat.), Cs 46 µg/g creat. (R.I. < 9 µg/g creat.), Cd 2 µg/g creat. (R.I. < 0.8 µg/g creat.), Ni 12 µg/g creat. (R.I. < 10 µg/g creat.), Hg 3 µg/g creat. (R.I. < 3 µg/g creat.), Tl 0.5 µg/g creat. (R.I. < 0.5 µg/g creat.) (figure 1a).

Based on these results, it was advised to continue the chelating therapy, programming control analyses in the same laboratory at the 11°, 14°, 20° infusion. (Laboratory of Toxicology, Doctor's Data Inc., St. Charles, IL USA) (figure 1b-d).

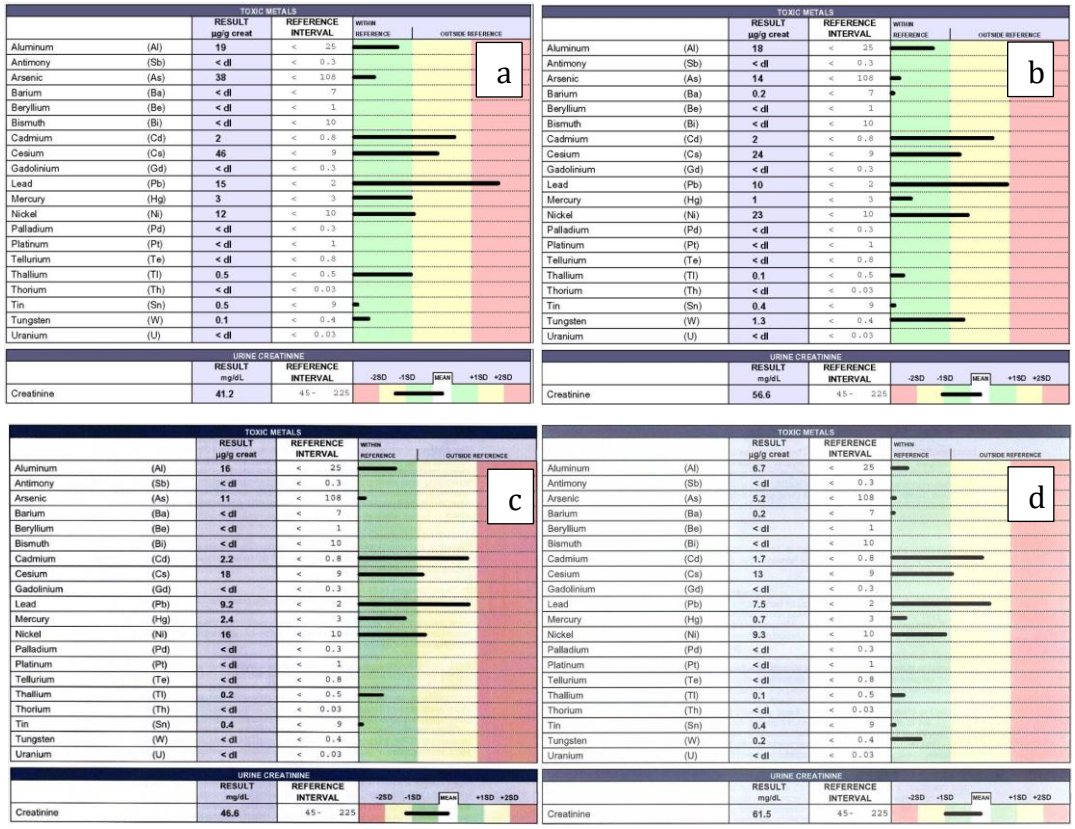

***Figure 1**: Mineralogram determined on the urine sample after the 1st (a), 11th(b), 14th (c) and 20th (d) infusion (Laboratory of Toxicology, Doctor's Data Inc., St. Charles, IL USA).*

Meanwhile, the urine samples were collected every day, for seventeen months, with the aim to monitor in our laboratory the metals excretion along time and to analyze additional metals besides those considered by the Doctor's Data lab. This systematic collection started at the 6th treatment. For the first five treatments, only the urines collected in the first twelve h post-therapy are available.

3.2.1.2 Chelating therapy protocol

The chelating therapy was administered every two weeks for a period of seventeen months. It consisted in slow intravenous infusion (3-4 hours) of 2g of EDTA as calcium-sodium salt (Salf, Brescia, Italia) diluted in 500 mL of physiological saline solution (46,50).

3.2.1.3 Sampling design

Urine samples were collected as detailed below and stored in plastic bottles at 4°C until analysis. The collection was done as follow: 3 separate samples for the urine excreted every 12 h after the infusion and 3 separate samples for the urine excreted every 24 h up to the next infusion. From the 12^{th} to the 30^{th} infusion, the three separate 12 h samples were pooled in one single sample.

The total amount of each element in the sample was normalized *versus* the duration time of the corresponding collection, so that the reference unit is μg/h.

Aliquots of each sample were preserved in Falcon tubes after supplementation of 2 mL of 69% nitric acid. The samples were labelled with a four-digit code: a letter identifying the EDTA administration (F); a number identifying the progressive EDTA administration (1-30), a letter indicating the sample (C) and a number indicating the sample progressive order after the infusion (1-44; from 1 to 3, 12 h collection samples; from 4 on, 24 h collection samples). For example, sample F6C3 refers to the sample collected after the 6^{th} infusion, from 24 h to 36 h after treatment; sample F6C4 instead refers to the sample collected after the 6^{th} infusion from 36 h to 60 h after treatment.

3.2.1.4 Reagents and instrumentation

EDTA as calcium-sodium salt (Salf, Brescia, Italia), Nitric Acid 69% Trace Select was from Fluka Analitical (Buchs, Switzerland), Multi-standard Solutions CCS1, CCS2, CCS4, CCS5, CCS6 for the calibration of the ICP-MS analysis was from Inorganic Ventures (Christiansburg, VA, USA), ultrapure water was obtained through a Millipore Milli-Q® system (Billerica, MA, USA, Microwave digester (Start D Microwave Digestion System, Milestone, Sorisole, Italy) and ICP-MS (XSeries 2 Thermo Scientific, Waltham, MA, USA) equipped with a single quadrupole mass analyzer.

The instrumental signal acquisition parameters are reported in table 1.

	CCT-KED mode	STD mode
Extraction	-161	-188
Lens 1	-1150	-1150
Lens 2	-87.1	-83.9
Lens 3	-185.5	-187.5
Pole Bias	-17.9	-2.2
Sampling Depth	130	150
Horizontal	130	120
Vertical	676	665
Cool	14.8	14.8
Auxiliary	0.82	0.82
Nebuliser	0.9	0.92
Forward power	1400	1400
D1	-53.3	-40
Focus	-10.4	12
CCT Gas 1	5	0
D2	-122	-129
DA	-32.9	-31.4
Hexapole Bias	-20	-4
	Survey Scan Setup	**Main Run Setup**
Sweeps	5	10
Dwell Time	600	10000
Channels Per Mass	10	1
Channel Spacing	-	0.02

Table 1: *ICP-MS experimental settings. Forward Power is expressed in W; Cool, Auxiliary and Nebuliser in L min^{-1}; CCT Gas1 in mL min^{-1}; Sweeps, Channel per mass, and Channel per spacing in arbitrary units; Dwell time in ms; all other parameters in V.*

Each calibration curve was calculated by means of the following seven standard solutions: 0.0001 μgL^{-1}, 0.001 μgL^{-1}, 0.01 μgL^{-1}, 0.1 μgL^{-1}, 1 μgL^{-1}, 10 μgL^{-1}, 100 μgL^{-1}, covering a concentration range of 7 orders of magnitude. A weighted least

square fitting was used, weighting the errors by the inverse of the concentration level. Table 2 reports the LOD and LOQ for each investigated isotope, determined by the calibration curve method (51,52).

Element	LOD	LOQ	Element	LOD	LOQ	Element	LOD	LOQ
7Li	0.030	0.045	**90Zr**	0.015	0.040	**159Tb**	0.00010	0.00040
27Al	0.020	0.060	**93Nb**	0.0013	0.0038	**163Dy**	0.00060	0.0020
45Sc	0.061	0.092	**95Mo**	0.13	0.19	**165Ho**	0.00060	0.0018
47Ti-CCT	0.40	1.3	**98Mo**	0.13	0.19	**166Er**	0.0013	0.0040
47-Ti	0.13	0.40	**103Rh**	0.0012	0.0033	**169Tm**	0.00050	0.0020
51V-CCT1	0.041	0.062	**88Sr**	0.048	0.072	**172Yb**	0.0015	0.0040
52Cr-CCT1	0.024	0.073	**89Y**	0.0020	0.0060	**175Lu**	0.0010	0.0030
55Mn-CCT1	0.0022	0.0066	**105Pd**	0.0070	0.020	**178Hf**	0.0020	0.0050
56Fe-CCT1	0.34	0.52	**107Ag**	0.0090	0.027	**180Hf**	0.0020	0.0060
59Co-CCT1	0.015	0.022	**111Cd**	0.0080	0.012	**181Ta**	0.0025	0.0075
60Ni-CCT1	0.16	0.24	**118Sn**	0.010	0.040	**182W**	0.0011	0.0033
62Ni-CCT1	0.14	0.20	**120Sn**	0.010	0.030	**186W**	0.0011	0.0034
63Cu-CCT1	0.20	0.30	**121Sb**	0.0010	0.0030	**187Re**	0.0020	0.0060
64Zn-CCT1	0.70	2.0	**133Cs**	0.025	0.038	**193Ir**	0.00080	0.0024
65Cu-CCT1	0.16	0.25	**138Ba**	0.0040	0.020	**195Pt**	0.0050	0.0075
66Zn-CCT1	0.70	2.0	**139La**	0.0010	0.0030	**205Tl**	0.00050	0.0014
71Ga	0.0071	0.011	**140Ce**	0.0015	0.0050	**206Pb**	0.013	0.020
72Ge	0.040	0.060	**141Pr**	0.00090	0.0030	**207Pb**	0.013	0.020
74Ge	0.010	0.015	**146Nd**	0.0012	0.0035	**208Pb**	0.013	0.020
75As-CCT1	0.14	0.21	**147Sm**	0.0010	0.0030	**209Bi**	0.0010	0.0030
78Se-CCT1	0.50	0.80	**151Eu**	0.00010	0.0010	**232Th**	0.0020	0.0060
78Se	0.30	0.40	**153Eu**	0.00040	0.0010	**238U**	0.00090	0.0030
85Rb	0.0050	0.016	**157Gd**	0.0010	0.0030			
87Rb	0.014	0.040	**158Gd**	0.0011	0.0033			

***Table 2**: LOD and LOQ values for all isotopes expressed in μgL^{-1}.*

Principal Component Analysis (PCA) and graphical representations were performed by Statistica v.10 (Statsoft Inc, Tulsa, OK, USA) and Unscrambler X (CAMO Software, Oslo, Norway).

3.2.1.5 Optimization of the mineralization procedure

The mineralization procedure underwent optimization by experimental design techniques: two levels were investigated for what regards the final concentration of HNO_3 in the sample (2%W/W and 5%W/W). The mineralization at the two different concentration levels was repeated both using or not a microwave digester, providing 4 experimental conditions. The microwave program was the following: to 180°C in 15 minutes and 15 minutes at 180°C (maximum power 1200 W).

For evaluating the best mineralization conditions three samples collected at the 23^{th} EDTA infusion were used (F23C1, F23C2 and F23C3). Each experimental condition was applied to three different aliquots of each sample to evaluate the experimental variability. Each experimental replicate was evaluated by three instrumental replications. For all the samples the elemental profile was determined by ICP-MS, consisting in 59 different isotopes. All concentration levels inferior to the LOQ were substituted by zero. The data collected were treated by Principal Component Analysis (PCA) after autoscaling.

Figure (2a) represents the score plot of the first two PCs (PC_1 = 55% and PC_2 = 23% of the overall variance): mineralization conditions with HNO_3 2% are indicated as circles, while with HNO_3 5% with triangles; the marker is white without microwaves while it is black if microwaves are used. The score plot indicates that PC_1 mainly accounts for the differences between the three types of samples, notwithstanding the amount of nitric acid used for mineralization or the use of microwaves.

Looking at the corresponding loading plot (figure 2b), it is possible to state that C3 samples show a larger concentration of almost all the analytes (positive loadings on PC_1) with the exception of Mn, Zn, Pb, Fe and Hf (negative loading on PC_1), while

C1 and C2 samples show an opposite behavior. Looking at the second PC, for all the three types pf samples the mineralization with 2% HNO_3 is always at more negative scores than the treatment at 5%. The mineralization with NHO_3 2% is particularly ineffective for Mn, Pb, Fe, Zn, Hf, Cu and Cr (positive loading on PC_2). Moreover, at 2% the use of microwaves is not to be preferred. For what regards the mineralization with HNO_3 5%, the use of the microwaves does not produce a significant effect. The mineralization of the samples with HNO_3 5% and without the use of microwaves is to be considered the best choice.

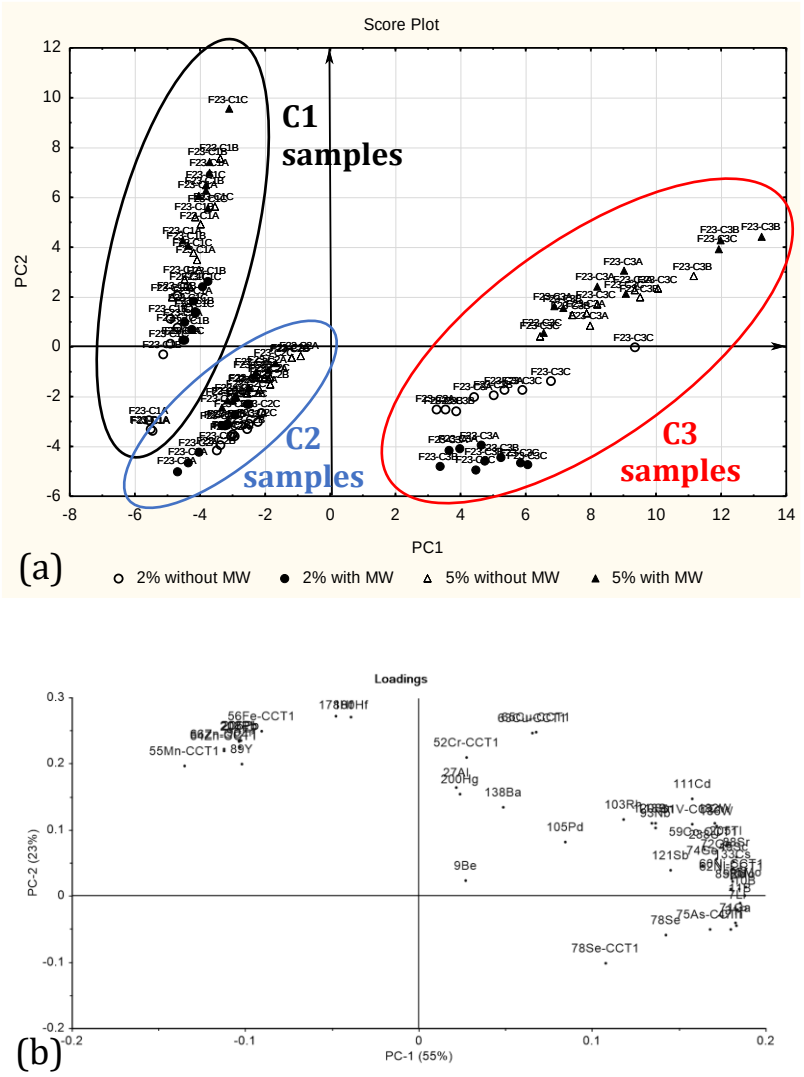

Figure 2: *score plot (a), loading plot (b)*

3.2.1.6 Determination of the elemental profile in urine samples

All urine samples were treated as follows: 25.000 mL aliquots of the samples contained in the Falcon tubes were added with 1.385 mL of HNO_3 69% (5% final concentration of nitric acid). The samples were diluted 1:5 v/v with ultrapure MilliQ water to obtain a 1% final concentration of nitric acid, and then analyzed with ICP-MS.

3.2.2 Results

The temporal charts report the sampling order on the *x* axis and the total amount excreted, normalized *vs* the sampling time, on the y axis (μg/h). Therefore, the total amount excreted is obtained by multiplying the *y* value for the collection duration time of the specific sample.

The samples in the temporal charts are labelled according to five different classes: C1, C2, C3, C4 and "basal excretion". While C1 to C4 indicate the first four samples collected after each infusion, the samples labelled as "basal excretion" correspond to all the others, collected beyond 60 h post-therapy (when its effect likely is terminated). Though in principle the latter could be affected by the chelating therapy, we can assume these as "basal excretion" since, after a rapid decrease in samples C1 to C4, the concentration of metal excreted in these samples tends to become stable.

For the sake of clarity, we shall discuss the analytes separately in the following four categories:

- Toxic elements: Pb, Cd, Al, Cr, Cs, Tl, Rb, As, Ni, Ga, Sn, W.
- Microelements: Mn, Zn, Fe, Cu, Se, Mo, Co
- Rare earths: Sc, Y, La, Ce, Pr, Nd, Sm, Eu, Gd, Tb, Dy, Ho, Er, Tm, Yb, Lu.
- Other elements: Hf, Ag Zr, Nb, Rh, Pd, Sb, Ba, Ta, Re, Ir, Bi, Li, V, Ti, Ge, Sr, Pt, Th, U.

For all graphical representations, the samples are reported on the x-axis according to the increasing collection time, while the excretion (in μg/h) is reported on the y-axis.

3.2.2.1 Toxic elements

The temporal charts for the elements belonging to this category are reported in Figures 3-6.

Pb, Cd, Al, Cr (Figure 3a-d) - For this group of elements there is a clear difference between sample C1 and the others. The chelating therapy shows very effective in the first 12 h samples (C1), where the concentrations of the four elements is very high in all the EDTA infusions. Pb concentration for the first samples slightly decreases after the 7^{th} cycle of chelating therapy, and then it remains constant, though at levels much higher than the concentrations of the other samples. Five samples collected at 36 h from the therapy show an excretion higher than the other samples of the same type (one of which shows Pb>1.2 µg/h). For Cd, the concentration of the first samples slightly increases along time, yet it is always much higher than for the other samples (0.09-0.20 µg/h). For Pb, the metal excretion within 12 h after infusion is almost constant (about 0.4 µg/h) for all the 30 treatments. From these data, we conclude that the chelating therapy sequestrates preferentially the tissue deposited Pb, rather than circulating Pb. A same consideration holds for Cd, though at a lower concentration level. Al shows an increase of the excretion in C1 samples (0.5-1.9 µg/h). For Cr, the excretion in the first samples is in the range 0.02-0.05 µg/h, while in other samples are in the range 0-0.02 µg/h.

The very few exceptions are the samples taken 36 h after the infusion, which show a high excretion (Cr >0.15 µg/h) with respect to the other samples of the same type (probably due to an accidental patient exposition). Same considerations hold for Pb. For Al, Cd and Cr, a daily excretion is also noticeable in samples collected beyond the 36h post-therapy.

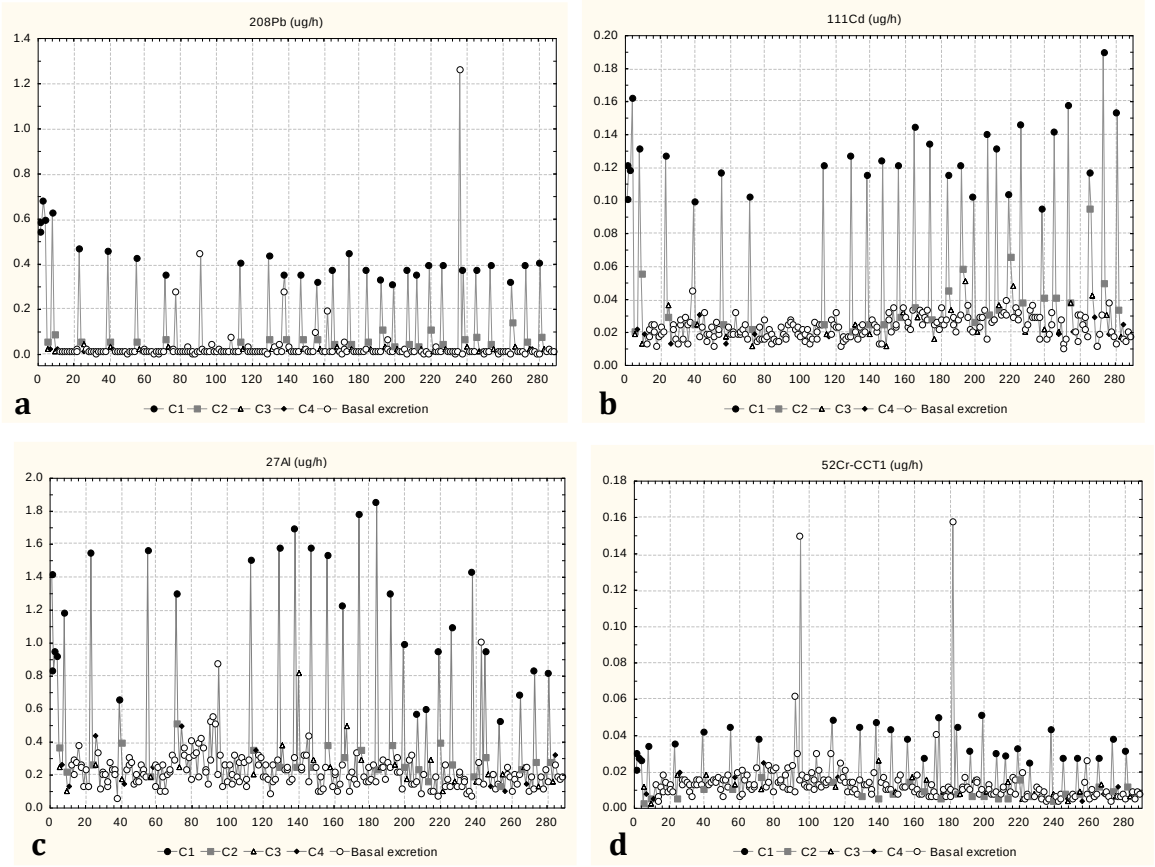

Figure 3: *Pb (a), Cd (b), Al (c), Cr (d)*

Cs, Tl, Rb (Figure 4 a-c) – These elements also show a clear difference between C1 samples and the others. Cs excretion in the first samples decreases from the first to the 18th infusion (from 2.5 µg/h to 0.5 µg/h); for Tl the decrease is from 0.02 µg/h to 0.005 µg/h, while Rb passes from 200 µg/h to 100 µg/h. All these three analytes show a relevant increase of the concentration in the first samples: after the 18th infusion for Cs and Tl, and after the 24th infusion for Rb. For the latter, the excretion corresponding to the first sample of the 30th EDTA administration is extremely high, reaching a level of 500 µg/h. The basal excretion of these elements has increased with respect to the first period of the chelating therapy, yet the samples of the first 12 h constantly show an excretion higher than the others.

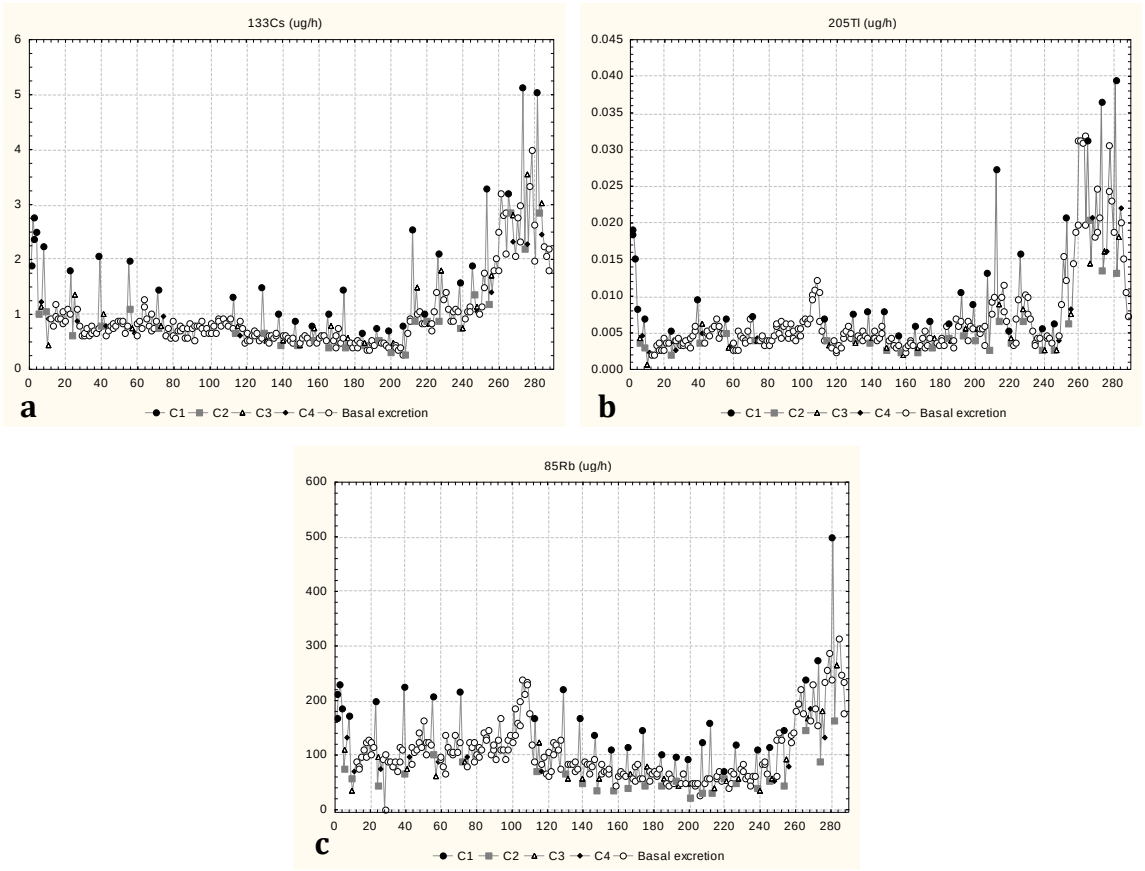

Figure 4: *Cs (a), Tl (b), Rb (c)*

As, Ni, Ga (Figure 5 a-c) - These elements show an atypical behavior, in that apparently no effect of the chelating therapy is detectable. For Ni, the excretion varies in the range 0.4-1.6 µg/h up to the 15th EDTA administration and then decreases to 0.2-0.6 µg/h; for Ga, the excretion is of the same order of magnitude as for Cd (0.04-0.12 µg/h), following a peculiar trend. The behavior of As is variable, between 0.1 and 3.2 µg/h. The patient's diet with rice could have influenced the variable excretion of As.

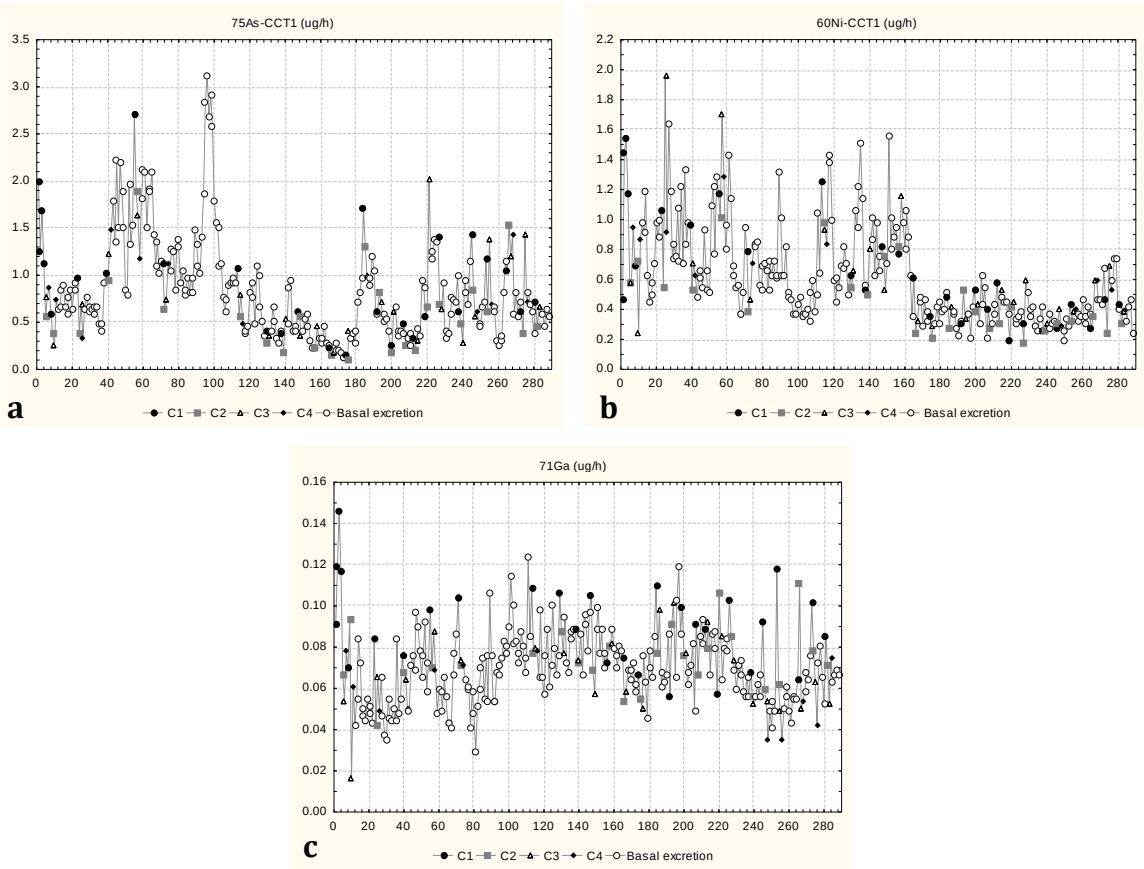

Figure 5: *<u>As (a), Ni (b), Ga (c)</u>*

<u>Sn, W</u> (Figure 6 a-b) - For Sn, in spite of the low excretion, a clear difference is evident between the first samples after the EDTA administration and the others, showing that the chelating therapy had a remarkable effect on this element. W shows an increase of its excretion in some of the first samples (e.g. for the 9th and 11th infusions).

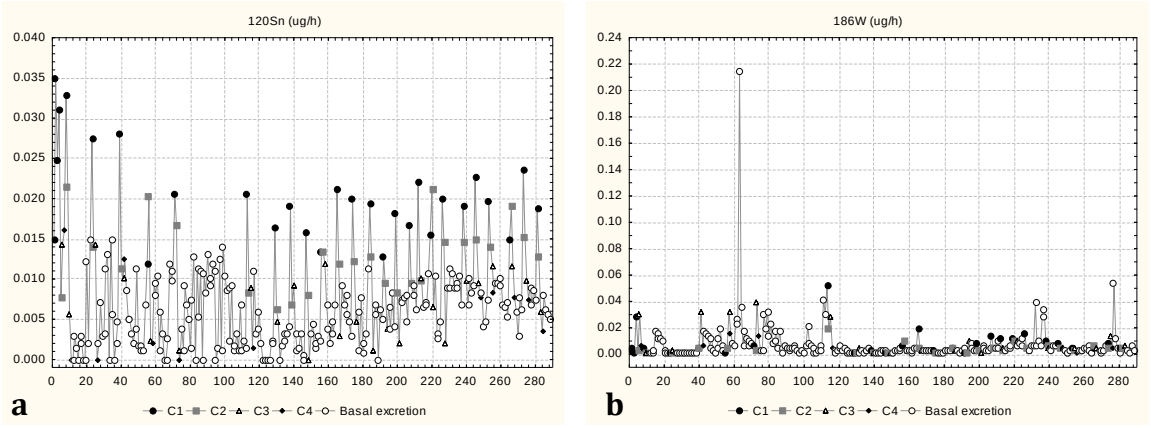

Figure 6: *Sn (a), W (b)*

3.2.2.2 Microelements

Temporal charts of these elements are reported in figures 7 and 8.

Mn, Zn, Fe, Cu (Figure 7 a-d) – The excretion of these elements is maximal in the first samples after the EDTA infusion for the whole treatment period, indicating that the chelating therapy is effective. The excreted amounts are within the range 600-1000 µg/h for Zn, 1-1.8 µg/h for Mn, 27.5-30 µg/h for Fe and 1-3.5 µg/h for Cu. In the case of Cu, the amount excreted shows an increasing trend along time. The excreted amounts of Mn and Fe are higher than the basal amount also for the second and third samples after the EDTA administration, while for Zn only for the second. These data indicate that the maximal excretion is within the first 12 h, but their elimination remains higher than normal for at least 36 h after the treatment. These amounts for the second samples are within the range 0-50 µg/h for Zn, 0.18-0.5 µg/h for Mn and 3-8 µg/h for Fe.

The amount of Zn released within the first 12 h after treatment is remarkable, between 600 and 1000 µg/h, which corresponds to an excretion of Zn of about 7.2 - 12 mg within the first 12 h after the treatment (Zn RDA 15 mg/die) (53).

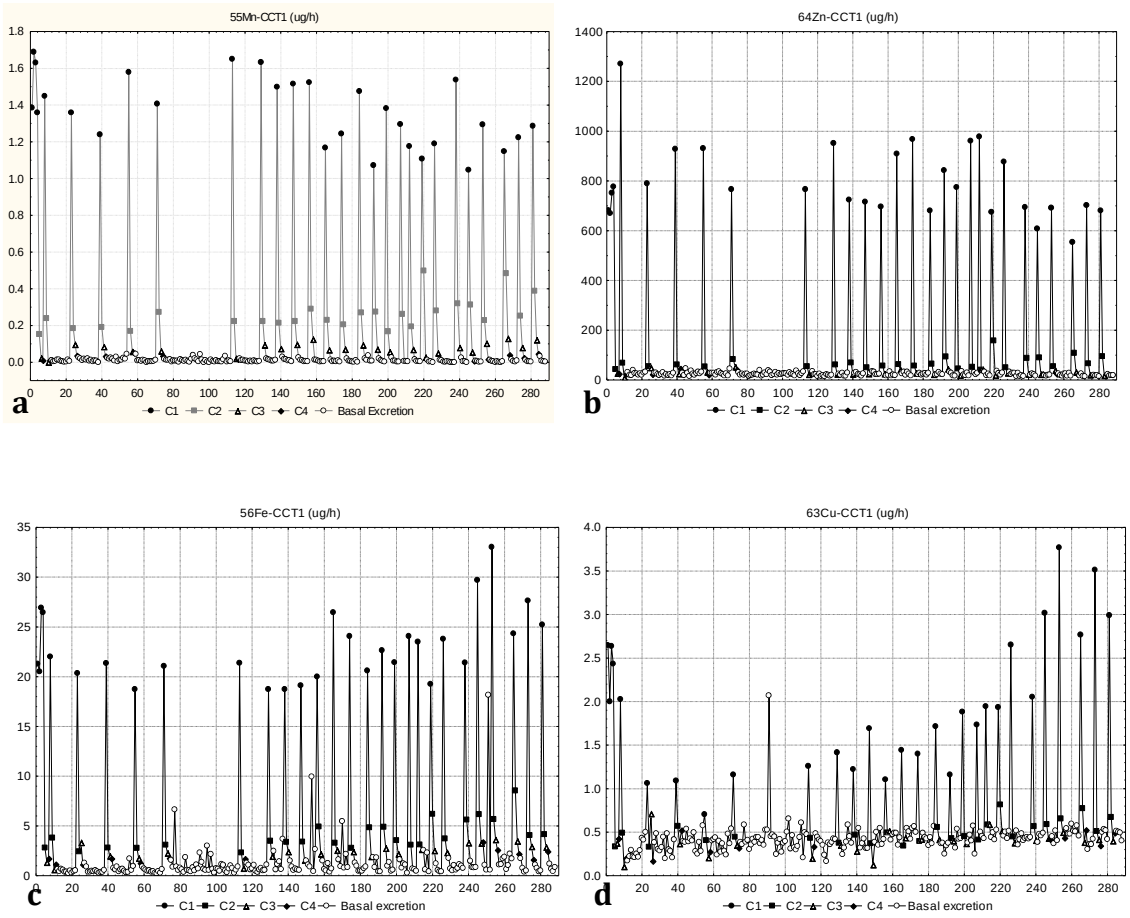

Figure 7: *Mn (a), Zn (b), Fe (c), Cu (d)*

Se, Mo and Co (Figure 8 a-c) - These elements show a variable behavior along time. As for other elements, the excreted amount is larger for the first sample after the chelating therapy administration (particularly relevant for Co) and around the second half of the monitored period for Se. The basal elimination is very variable along time, especially for Se, whose excretion likely reflects the patient's intake of supplements.

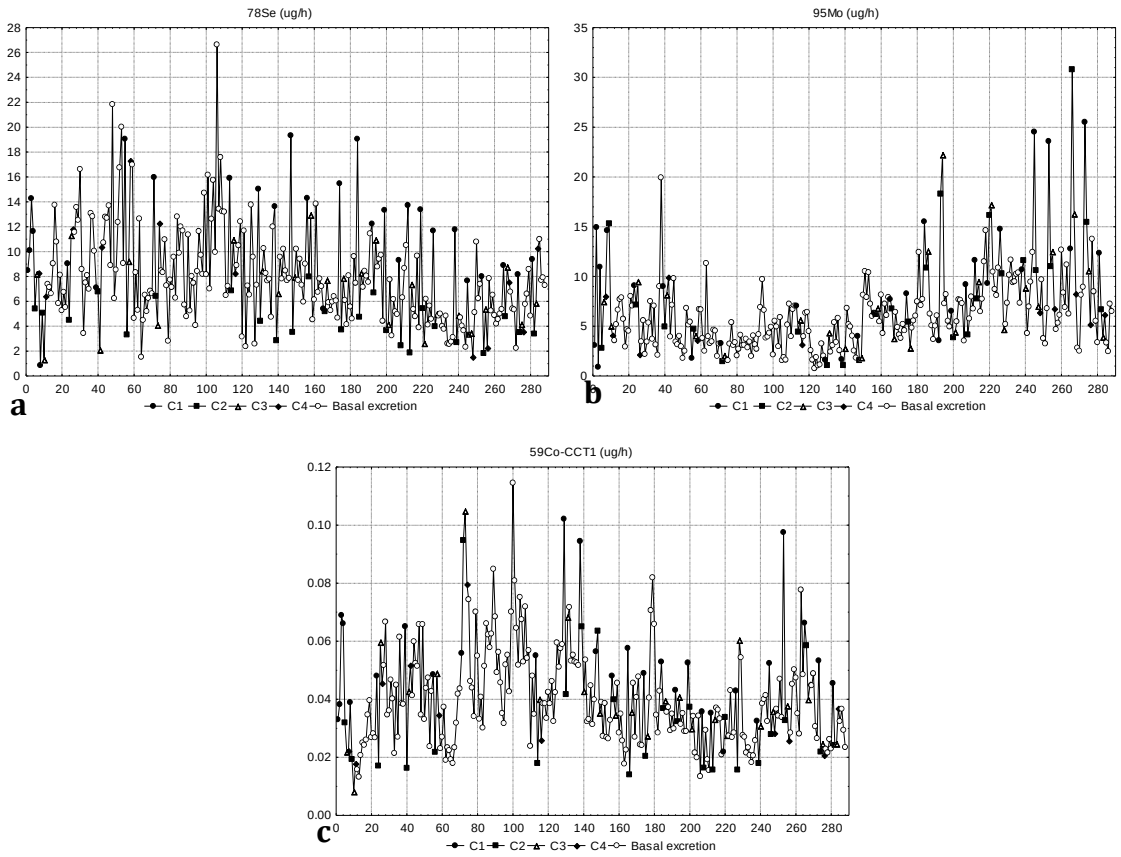

Figure 8: *Se (a), Mo (b), Co (c)*

3.2.2.3 Rare earths and other elements

Temporal charts of the excretion of the rare earths (Sc, Y, La, Ce, Pr, Nd, Pm, Sm, Eu, Gd, Tb, Dy, Ho, Er, Tm, Yb, Lu) and other elements (Sr, Ti, Hf, Ag, Zr, Rh, Sb, Ba, Li, V, Ge, U) are reported in figures 9 to 15.

Among rare earths and other elements, only the ones that present a significant behavior are reported; the other elements present significant excretion amounts only for some sporadic samples. Their presence can be related to a dietary effect, but nevertheless the chelating therapy seems to confirm its efficacy, at least for the first samples after the patient treatment.

Sc (Figure 9) – its excretion is very variable, in the range 0.4-1.8 µg/h. Above all, in the second part of the treatment it can be observed a not very sensitive effect of the chelating therapy: the first samples after the chelating agent administration are always slightly more concentrated than the other ones.

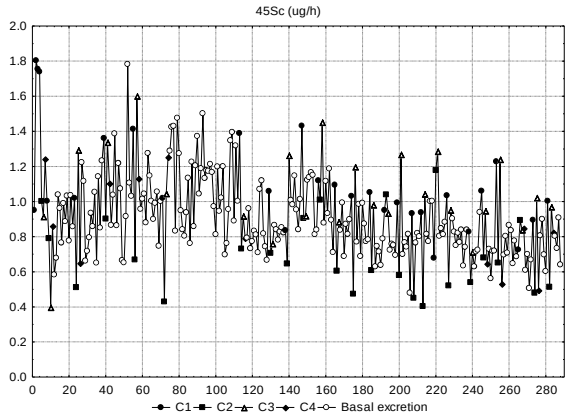

Figure 9: *Sc (a)*

La, Nd and Ce (Figure 10 a-c) - There is a noticeable excretion of these elements only for the first samples after the EDTA administration. This behavior can only be due to an accumulation of these elements in the patient's tissues and organs, since the basal excretion is almost zero.

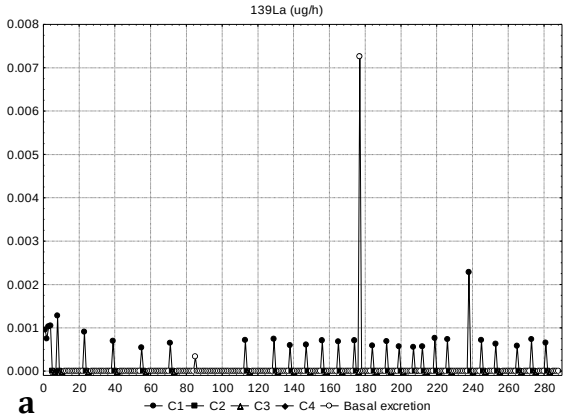

a

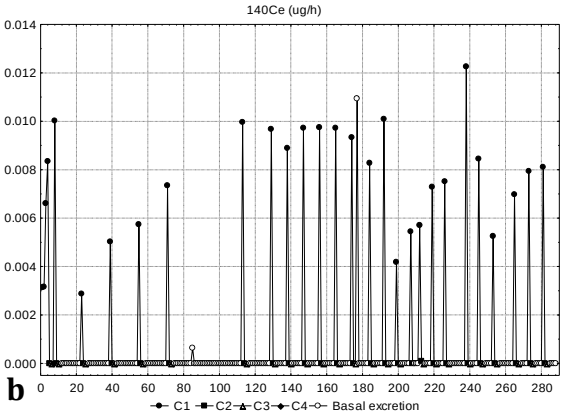

b

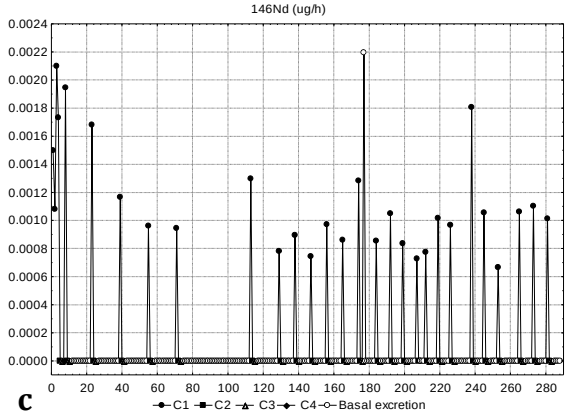

Figure 10: *La (a), Nd (b), Ce (c)*

Sr and Ti (Figure 11 a-b) show a slight effect of the chelating therapy in C1 samples. The excreted amounts pass from 2 to 15 µg/h for Sr and from 30 to 120 µg/h for Ti (with a peak of 210 µg/h). The excretion of Ti is relevant: it must be remarked that during the therapy the patient consumed dietary supplements free from TiO_2.

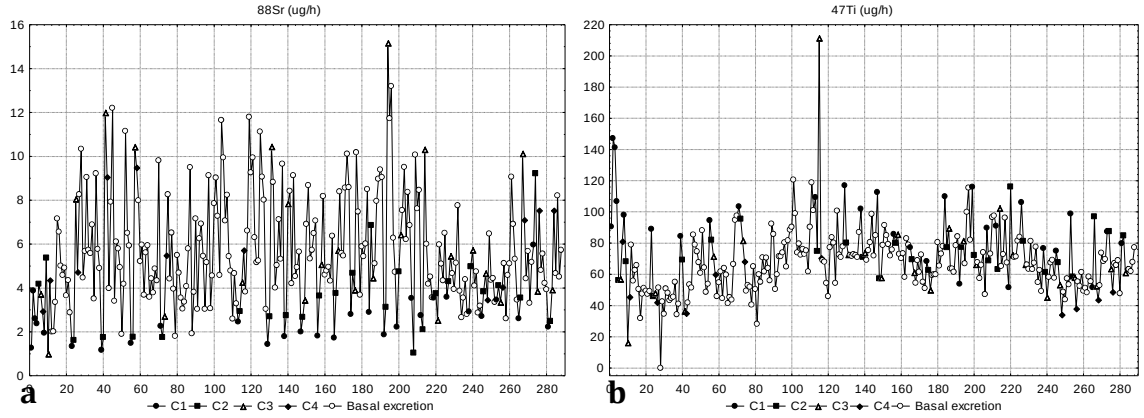

Figure 11: *Sr (a), Ti (b)*

Hf, Ag, Zr (Figure 12 a-c) – The excretion of these elements resembles that of the rare earths La, Ce and Nd. In fact, there is a clear difference between the C1 samples and all the other samples, that present negligible amounts. The chelating therapy seems to be effective for the first 12h only, for their urinary elimination. As for La,

Nd and Ce, this behavior can only be related to their accumulation in the patient's tissues and organs, since no basal excretion is recorded. The amounts excreted for Zr equal those of Pb and the concentration levels are by far greater than for rare earths (0.001 µg/h for rare earths and 0.5 µg/h for Zr).

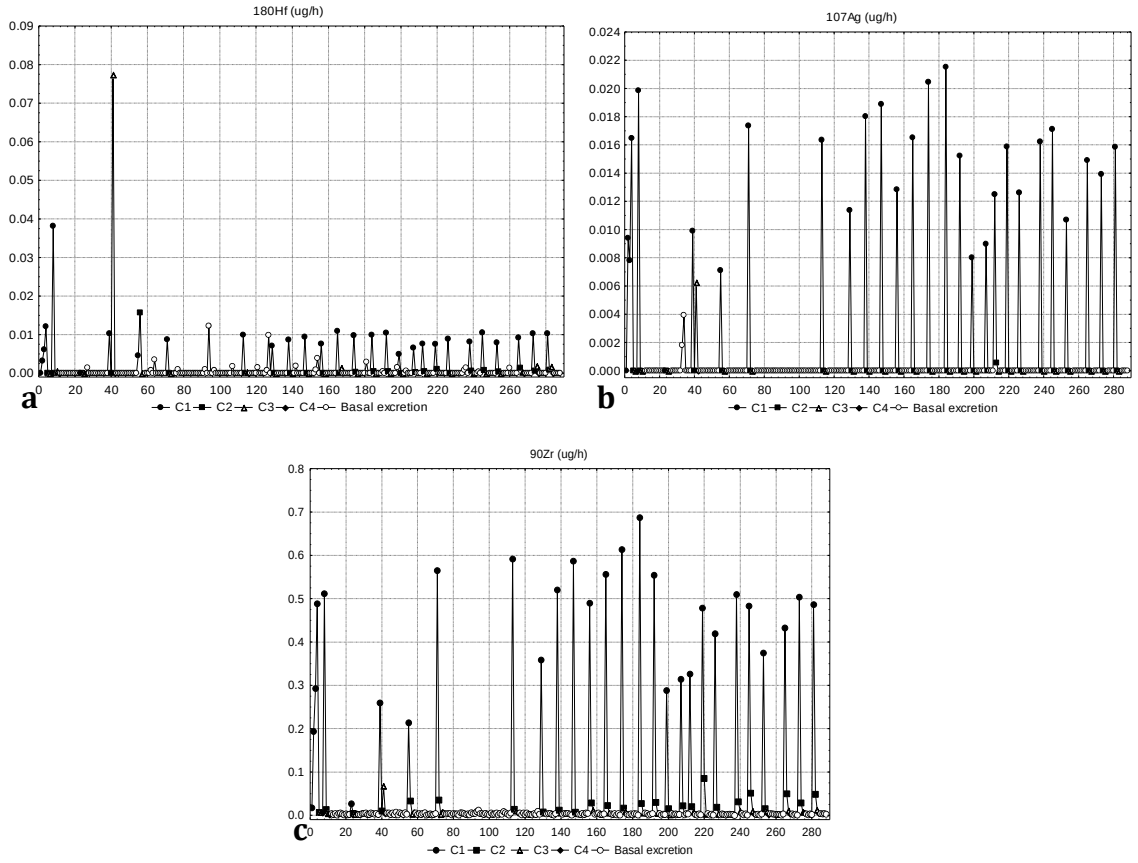

Figure 12: *Hf (a), Ag (b), Zr (c)*

Rh, Sb (Figure 13 a-b) – They show a variable behavior, but the basal elimination is very small and very variable. There is a small effect of the chelating therapy as the first samples after the EDTA administration show larger excretion than the other ones.

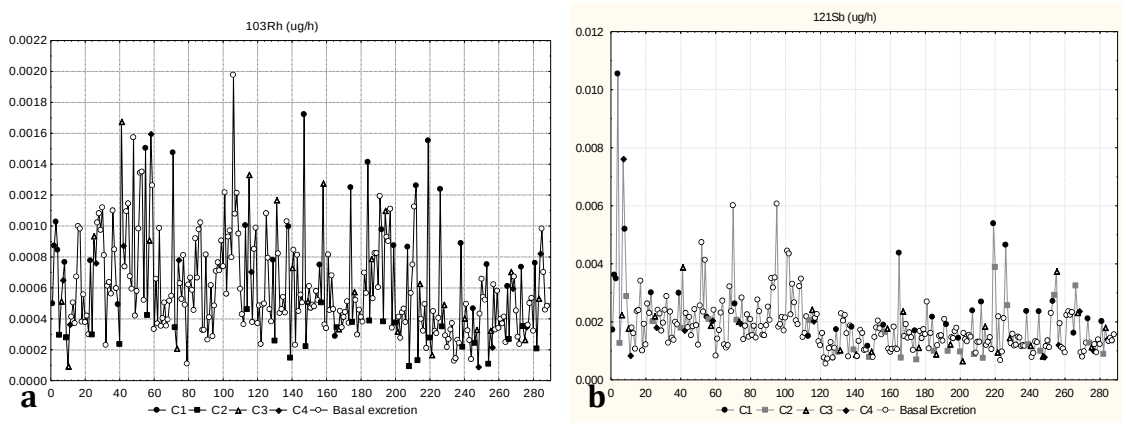

Figure 13: *Rh (a), Sb (b)*

Ba, Li, V, Ge (Figure 14 a-d) – These elements do not show the usual effect of the chelating therapy and are characterized by a variable excretion along time. There is no peculiar trend, with the exception of V that shows a decreasing excretion, with a slight effect of the chelating therapy on C1 samples in the second half of the patient's treatment. The excreted amounts pass from 0.02 to 0.10 µg/h for Ba, from 0.05 to 0.4 µg/h for V.

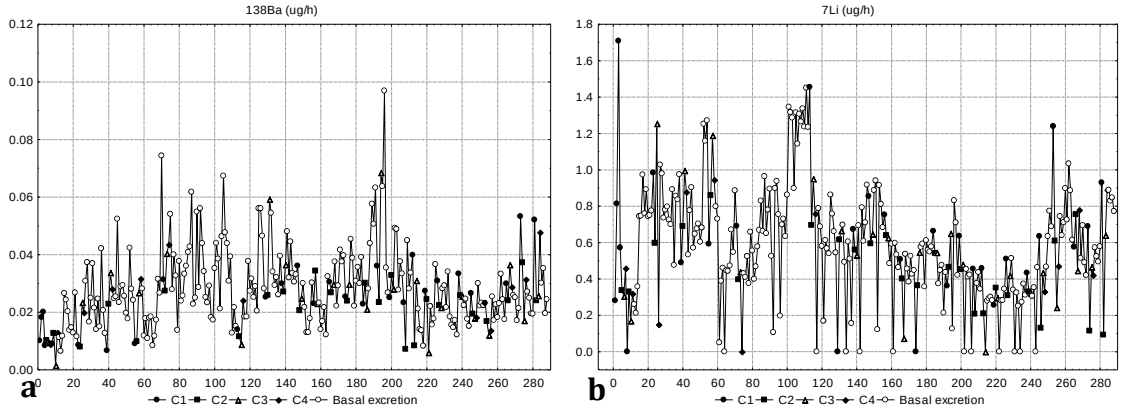

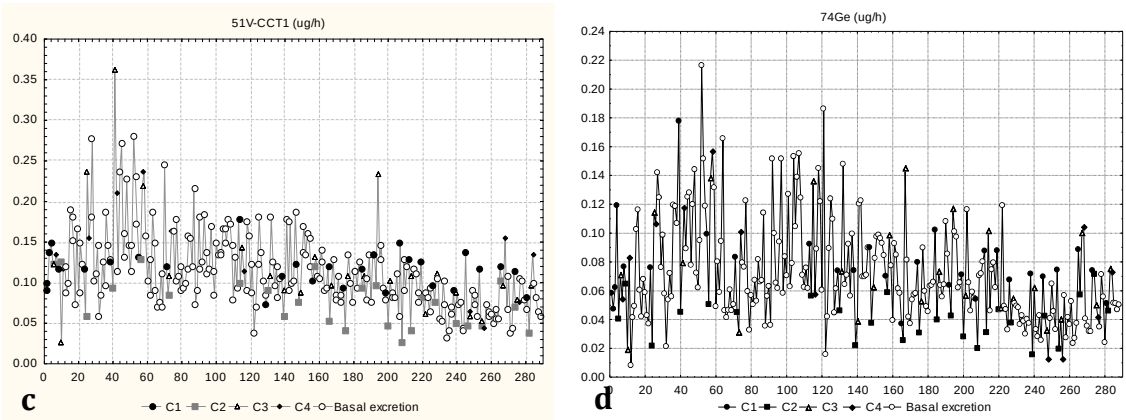

Figure 14: *Ba (a), Li (b), V (c), Ge (d)*

U (Figure 15) – This element shows a detectable basal excretion only after the 8th administration. For the last infusions a slight effect of the chelating therapy on the C1 samples can be recognized.

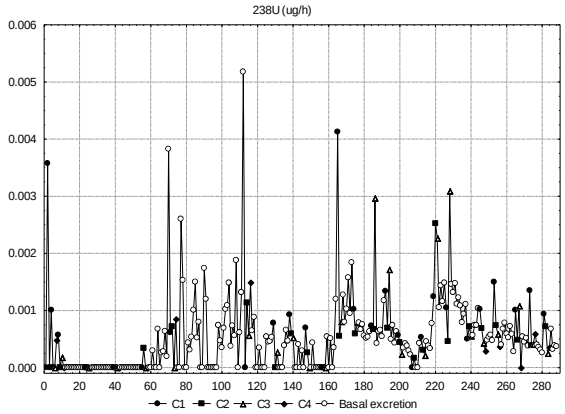

Figure 15: *U (a)*

3.2.2.4 Principal Component Analysis

The data were arranged in a matrix of dimensions 288 x 70 (288 being the collected samples and 70 the isotopes determined by ICP-MS). The data were autoscaled and PCA was carried out by applying a varimax rotation to the first 7 PCs that explain about 65% of the overall information (PC_1: 23.67%, PC_2: 10.15%, PC_3: 7.63%: PC_4:

6.62%, PC_5: 6.2%, PC_6: 5.89%, PC_7: 5.59%). The results confirm those obtained by the temporal charts already discussed, allowing the identification of groups of elements with a similar behavior:

- Al, Mn, Zn, Fe, Y, Zr, Ag, Cd, Ce, Nd and Pb: characterized by an excretion that is completed within 12 or 24 h after treatment with a not negligible basal excretion.
- V, Se, Ge, Rh, Ba, Mo, Ga, Ti, Sr, and U: characterized by an excretion that is larger 12h after treatment and a basal excretion that increases in the first half of the monitoring period and then decreases.
- Nb, Pd, Ta, Hf, Ir, Th and Bi: characterized by an excretion that is larger 12h after treatment but with some samples characterized by a particularly large excretion. Rb, Cs and Tl: characterized by an excretion larger 12h after treatment but with a not constant basal excretion up to the 10^{th} drip, then a considerable increase is recorded. This behavior could have two main causes: an increased assumption or an increased excretion induced by the chelating therapy.
- rare earths: the excretion is completed within 12h after treatment and almost no basal excretion is recorded.
- W, Ni, Sc and As: the excretion of these elements is larger in the first part of the treatment, also for what regards the basal values, then the basal excretion decreases; for the overall monitoring period, excretion after 12h is larger with respect to the other samples.

Figures 16 to 22 report the loading and score plots of the first seven PCs calculated. The loading plots are reported separately for each PC: the loadings are reported on the y-axis while the original variable on the x-axis; the variables are represented by different symbols according to their belonging to the group of toxic elements, essential elements, rare earths or others. The score plots are also reported separately for each PC: the scores are reported on the y-axis while the samples on the x-axis, according to the order of collection; the samples are represented by different symbols

according to their belonging to C1, C2, C3, C4 group or to the group of samples characterized by basal excretion. In the score plots, the samples are reported on the x-axis according to the increasing collection time, while the scores along the corresponding PC are reported on the y-axis.

Table 3 reports the % of explained variance and the % of cumulative explained variance for each PC (varimax rotated PCs were sorted and renamed according to a decreasing % of explained variance). The first 7 PCs explain about 65% of the overall information.

Looking at the first PC (Figure 16 a), Al, Mn, Zn, Fe, Y, Zr, Ag, Cd, Ce, Nd and Pb show all positive loadings, while Sr shows negative loadings. The corresponding score plot (figure 16 b) shows that C1 samples are characterized by an excretion larger than other samples for the listed elements (the behavior is opposite instead for Sr); after the 10th drip also C2 samples show an excretion slightly larger than that corresponding to basal conditions. This behavior indicates for these elements an excretion that is completed within 12 or 24 h after treatment; however, basal excretion must not be neglected.

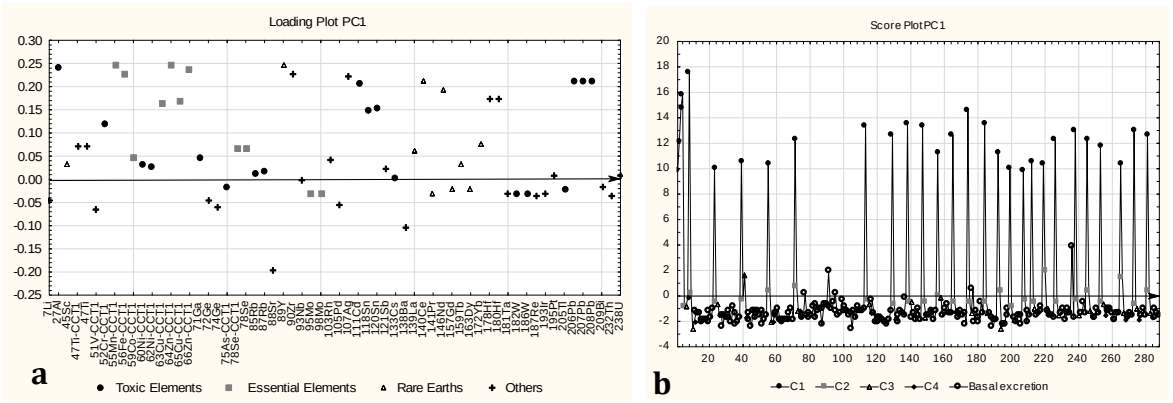

Figure 16

PC_2 (Figure 17 a) shows positive weights for V, Se, Ge, Rh, Ba (and in a minor way for Li, Co and Sr). As for the previous case, C1 samples (figure 17 b) show excretions

larger than that of other samples and in this case the basal excretion is quite variable: it increases in the first half of the monitoring period and then decreases.

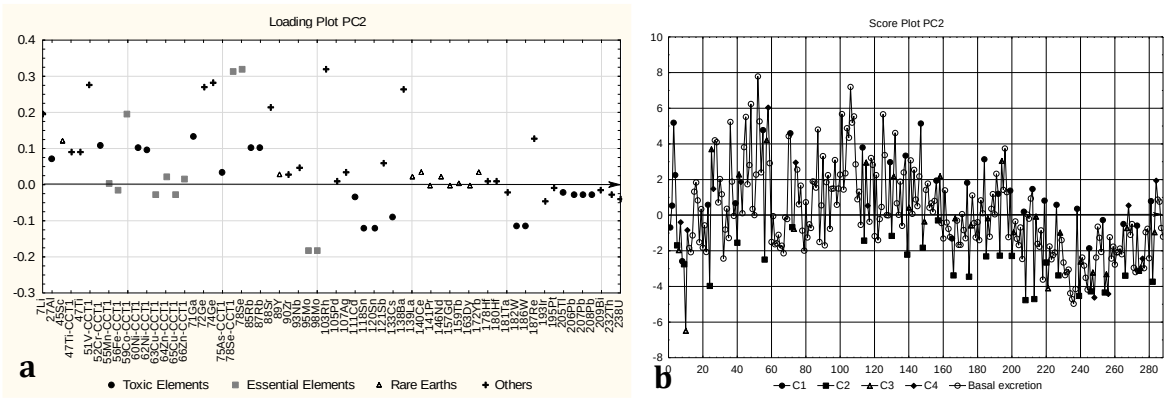

Figure 17

PC_3 (Figure 18 a) shows positive weights for Nb, Pd, Ta, Hf, Ir, Th and Bi; the score plot (figure 18 b) highlights some samples characterized by a particularly large excretion but, zooming in the plot, C1 samples show again an excretion larger than other samples.

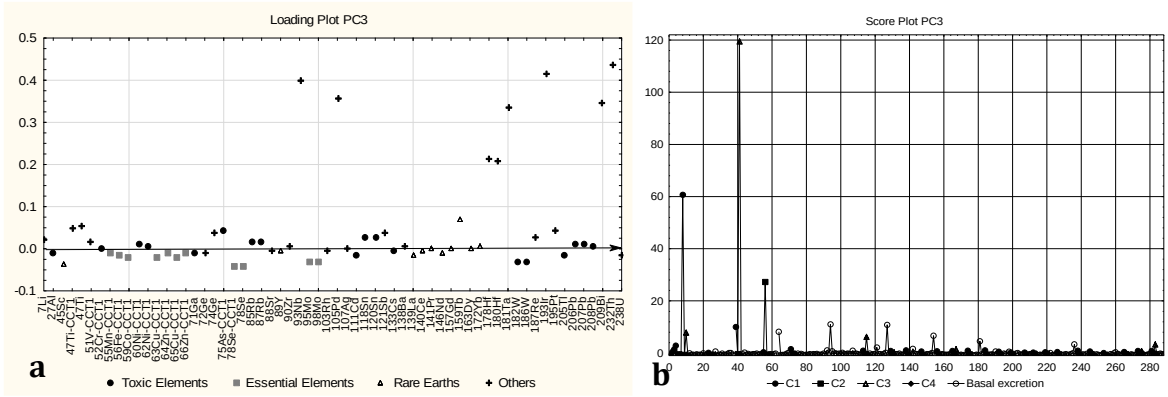

Figure 18

PC_4 (Figure 19 a) shows positive loadings for Mo, Ga, Ti, Sr, Ba and U; for these elements the basal excretion is quite variable (it increases and then decreases) but

also in this case C1 samples are characterized by an excretion larger than the other samples (figure 19 b).

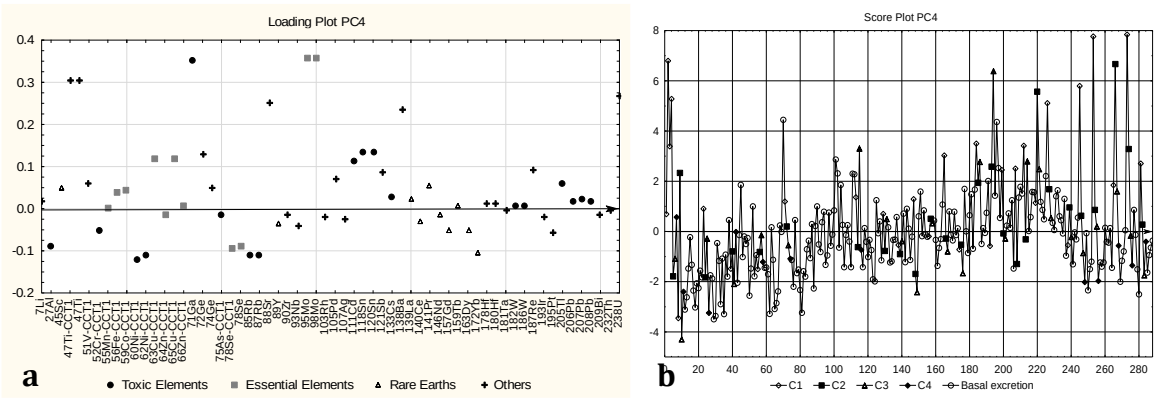

Figure 19

The fifth PC (Figure 20 a) carries information about Rb, Cs and Tl. These elements show a particular behavior (figure 20 b): in general C1 samples show a larger excretion but in addition, basal excretion seems almost constant up to the 10th drip, then a considerable increase is recorded. This behavior could have two main causes: an increased assumption or an increased excretion induced by the chelating therapy.

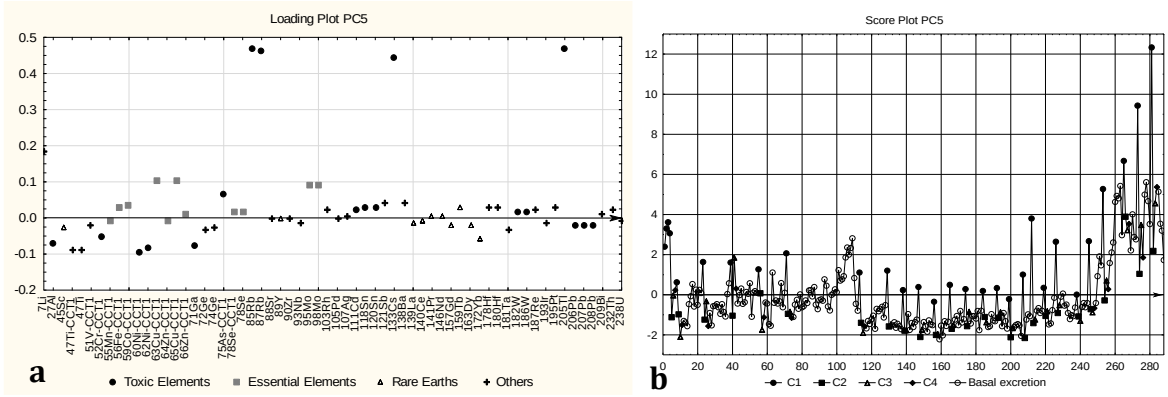

Figure 20

The sixth PC (Figure 21 a) explains the contribution of a group of rare earths (La, Yb, Pr, Dy, Gd); the corresponding score plot (figure 21 b) shows some samples characterized by an extremely large excretion if compared to the other samples, and in general the excretion of C1 samples is larger than for other samples, in particular after the 10th drip.

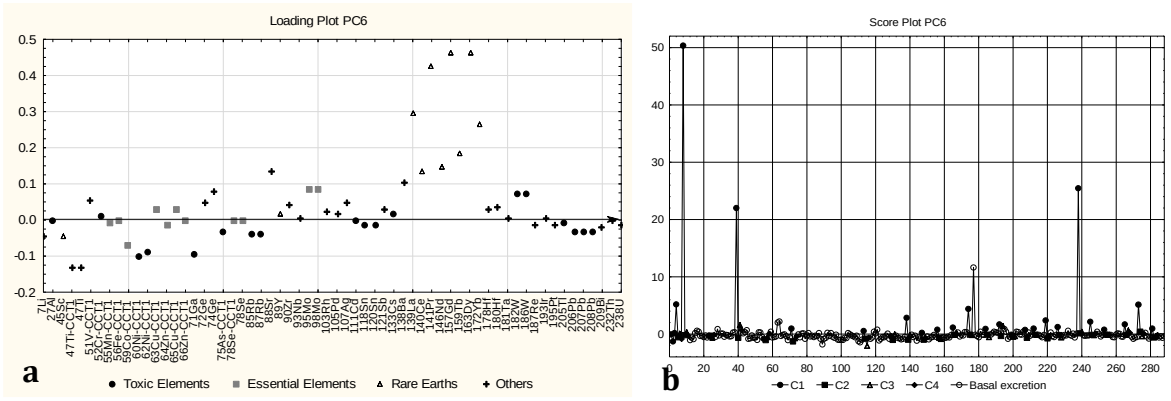

Figure 21

The 7th PC (Figure 22 a) shows the contribution of W, Ni, Sc and As (positive loadings). The excretion of these elements is larger in the first part of the treatment (figure 22 b), also for what regards the basal values, then the basal excretion decreases; however, for the overall monitoring period, C1 samples show a larger excretion with respect to the other samples.

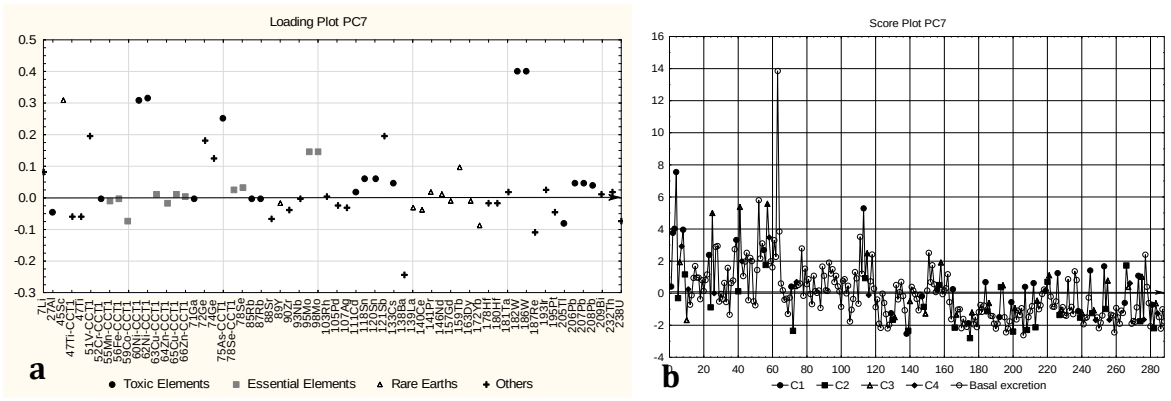

Figure 22

3.2.3 Discussion

Table 4 reports the total absolute amounts and the total amounts excreted within 12h, 24h and after more than 24 h after the treatment, weighted for the collection time, for each element belonging to the four classes examined along the monitored period.

Toxic elements				
Isotopes	**Total mg**	**Excretion < 12h (μg/h)**	**Excretion < 24h (μg/h)**	**Excretion >24h (μg/h)**
27Al	2.4	1.2	7.5E-1	2.2E-1
47Ti-CCT1	6.4E2	9.1E1	8.2E1	6.5E1
47Ti	6.5E2	9.3E1	8.4E1	6.7E1
52Cr-CCT1	1.3E-1	3.6E-2	2.3E-2	1.3E-2
60Ni-CCT1	5.4	6.6E-1	6.9E-1	5.6E-1
62Ni-CCT1	5.5	6.7E-1	5.8E-1	5.7E-1
71Ga	6.7E-1	9.2E-2	8.3E-2	6.9E-2
75As-CCT1	7.2	9.2E-1	7.6E-1	7.5E-1
85Rb	1.0E3	1.7E2	1.2E2	1.0E2
87Rb	1.0E3	1.7E2	1.2E2	1.0E2
111Cd	2.7E-1	1.3E-1	8.4E-2	2.4E-2
118Sn	6.6E-2	2.1E-2	1.7E-2	6.0E-3
120Sn	6.4E-2	2.1E-2	1.7E-2	6.0E-3
133Cs	1.0E1	1.9	1.4	1.1
182W	6.6E-2	9.0E-3	7.0E-3	7.0E-3
186W	6.7E-2	9.0E-3	7.0E-3	7.0E-3
205Tl	7.8E-2	1.3E-2	9.0E-3	8.0E-3
206Pb	4.6E-1	4.4E-1	2.6E-1	3.2E-2
207Pb	4.3E-1	4.1E-1	2.4E-1	3.0E-2
208Pb	4.4E-1	4.2E-1	2.5E-1	3.1E-2
Essential elements				
Isotopes	**Total mg**	**Excretion < 12h (μg/h)**	**Excretion < 24h (μg/h)**	**Excretion >24h (μg/h)**

55Mn-CCT1	6.6E-1	1.4	8.3E-1	1.0E-2
56Fe-CCT1	2.0E1	2.3E1	1.4E1	1.2
59Co-CCT1	3.7E-1	5.4E-2	4.3E-2	3.8E-2
63Cu-CCT1	4.7	1.9	1.2	4.3E-1
64Zn-CCT1	5.1E2	7.9E2	4.4E2	2.3E1
65Cu-CCT1	4.7	1.9	1.2	4.3E-1
66Zn-CCT1	5.2E2	8.0E2	4.5E2	2.5E1
78Se-CCT1	6.8E1	11.27	7.90	6.97
78Se	7.1E1	11.80	8.26	7.30
95Mo	6.3E1	9.8	9.1	6.3
98Mo	6.4E1	1.0E1	9.3	6.5
Rare earths				
Isotopes	**Total mg**	**Excretion < 12h (μg/h)**	**Excretion < 24h (μg/h)**	**Excretion >24h (μg/h)**
89Y	7.9E-4	2.2E-03	1.2E-03	n.d.
139La	6.3E-4	7.8E-04	4.1E-04	4.0E-05
140Ce	3.1E-3	7.5E-03	3.9E-03	6.0E-05
141Pr	7.8E-05	9.1E-05	4.7E-05	5.2E-06
146Nd	5.0E-4	1.1E-03	5.9E-04	1.2E-05
147Sm	1.3E-05	3.8E-05	2.0E-05	n.d.
151Eu	7.8E-06	2.2E-05	1.2E-05	n.d.
153Eu	8.5E-06	2.5E-05	1.3E-05	n.d.
157Gd	1.8E-05	5.3E-05	2.8E-05	n.d.
158Gd	8.8E-06	2.5E-05	1.3E-05	n.d.
159Tb	2.2E-05	4.5E-05	2.4E-05	6.6E-07
163Dy	1.5E-05	4.2E-05	2.2E-05	n.d.
165Ho	9.2E-06	2.6E-05	1.4E-05	n.d.
166Er	7.7E-06	2.2E-05	1.1E-05	n.d.
169Tm	9.5E-06	2.7E-05	1.4E-05	n.d.
172Yb	3.9E-05	1.1E-04	5.9E-05	n.d.
175Lu	7.3E-06	2.1E-05	1.1E-05	n.d.

Other elements				
Isotopes	**Total mg**	**Excretion < 12h (μg/h)**	**Excretion < 24h (μg/h)**	**Excretion >24h (μg/h)**
7Li	5.3	6.3E-1	5.4E-1	5.5E-1
45Sc	8.3	1.1	9.1E-1	8.6E-1
51V-CCT1	1.0	1.2E-1	1.0E-1	1.1E-1
72Ge	7.0E-1	8.9E-2	7.3E-2	7.2E-2
74Ge	6.4E-1	7.9E-2	6.0E-2	6.7E-2
88Sr	5.5E1	2.5	3.0	5.9
90Zr	1.8E-1	4.2E-1	2.3E-1	3.1E-3
93Nb	5.1E-3	1.6E-03	1.1E-03	4.9E-04
103Rh	5.3E-3	9.5E-04	6.3E-04	5.5E-04
105Pd	7.5E-2	5.3E-03	6.3E-03	7.9E-03
107Ag	4.8E-3	1.3E-02	6.9E-03	2.4E-05
121Sb	1.6E-2	2.9E-03	2.3E-03	1.6E-03
138Ba	2.7E-1	2.5E-02	2.3E-02	2.9E-02
178Hf	6.4E-3	9.1E-03	5.1E-03	3.3E-04
180Hf	6.1E-3	8.9E-03	5.1E-03	3.1E-04
181Ta	5.9E-4	3.9E-04	2.4E-04	4.8E-05
187Re	1.1E-3	1.0E-04	6.9E-05	1.2E-04
193Ir	2.3E-4	1.0E-04	8.1E-05	2.0E-05
195Pt	1.7E-3	2.3E-04	1.4E-04	1.8E-04
209Bi	2.3E-4	1.9E-04	1.4E-04	1.6E-05
232Th	2.5E-3	7.3E-04	6.8E-04	2.3E-04
238U	5.2E-3	8.7E-04	6.9E-04	5.3E-04

***Table 4**: Amount of analytes excreted during the overall period considered (Total mg), weighted excretion of the analytes expressed as μg/h within 12h, 24h and after 24h after treatment.*

The weighted amounts are calculated summing up the absolute amounts of the corresponding samples and dividing for the corresponding sum of collection time (expressed in h). The absolute amounts are indicated as total excreted mg, while the

weighted amounts are expressed as µg/h. Some elements show a high total excretion, e.g. Zn (>500 mg), Ti (>600 mg), Rb (>1 g), Mo (> 62 mg), Cs (>10 mg), Sr (>55 mg), Sc (>8 mg).

Figures 23, 24, 25 and 26 represent the weighted amounts excreted within 12 h, 24 h and after more than 24 h after treatment of toxic (figure 23), essential (figure 24), rare earths (figure 25) and other elements (figure 26).

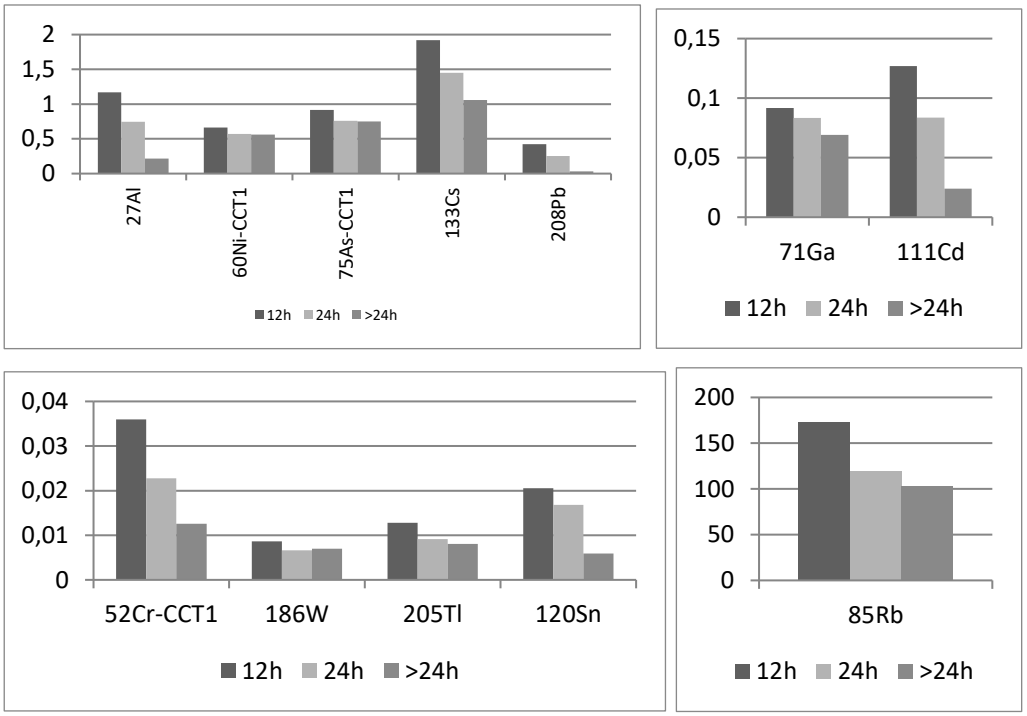

Figure 23: *Bar diagrams of the weighted excretion (in ug/h) within 12h, 24h and after more than 24h after treatment of each toxic element.*

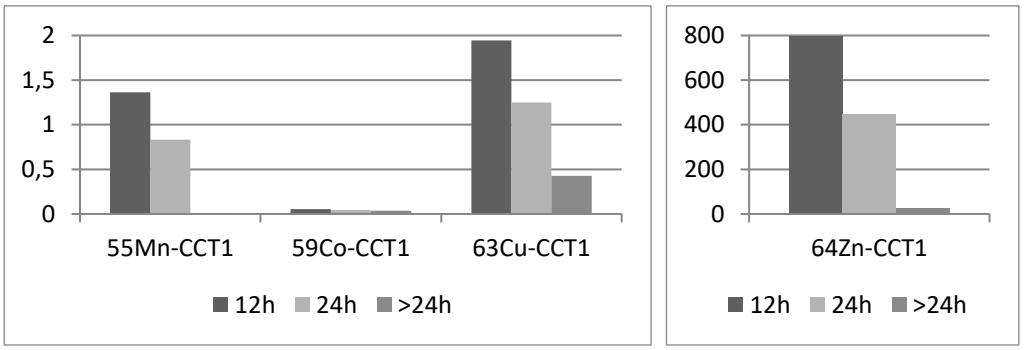

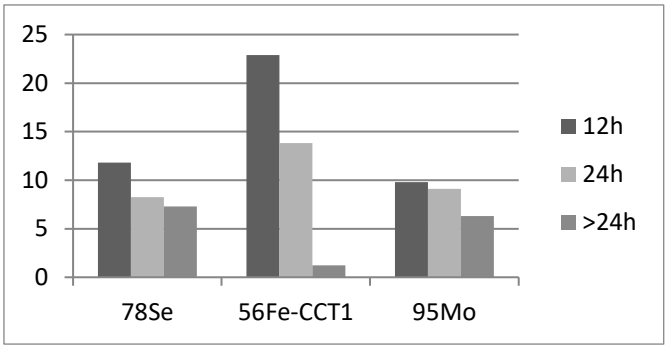

***Figure 24**: Bar diagrams of the weighted excretion (in ug/h) within 12h, 24h and after more than 24h after treatment of each essential element.*

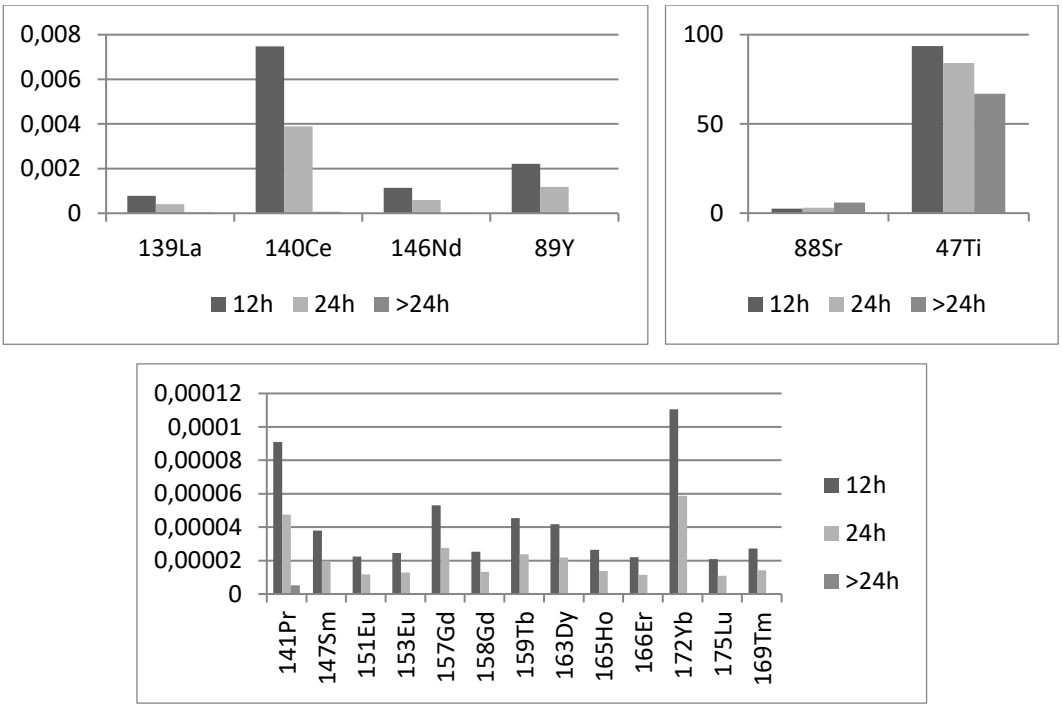

***Figure 25:** Bar diagrams of the weighted excretion (in ug/h) within 12h, 24h and after more than 24h after treatment of each rare earth.*

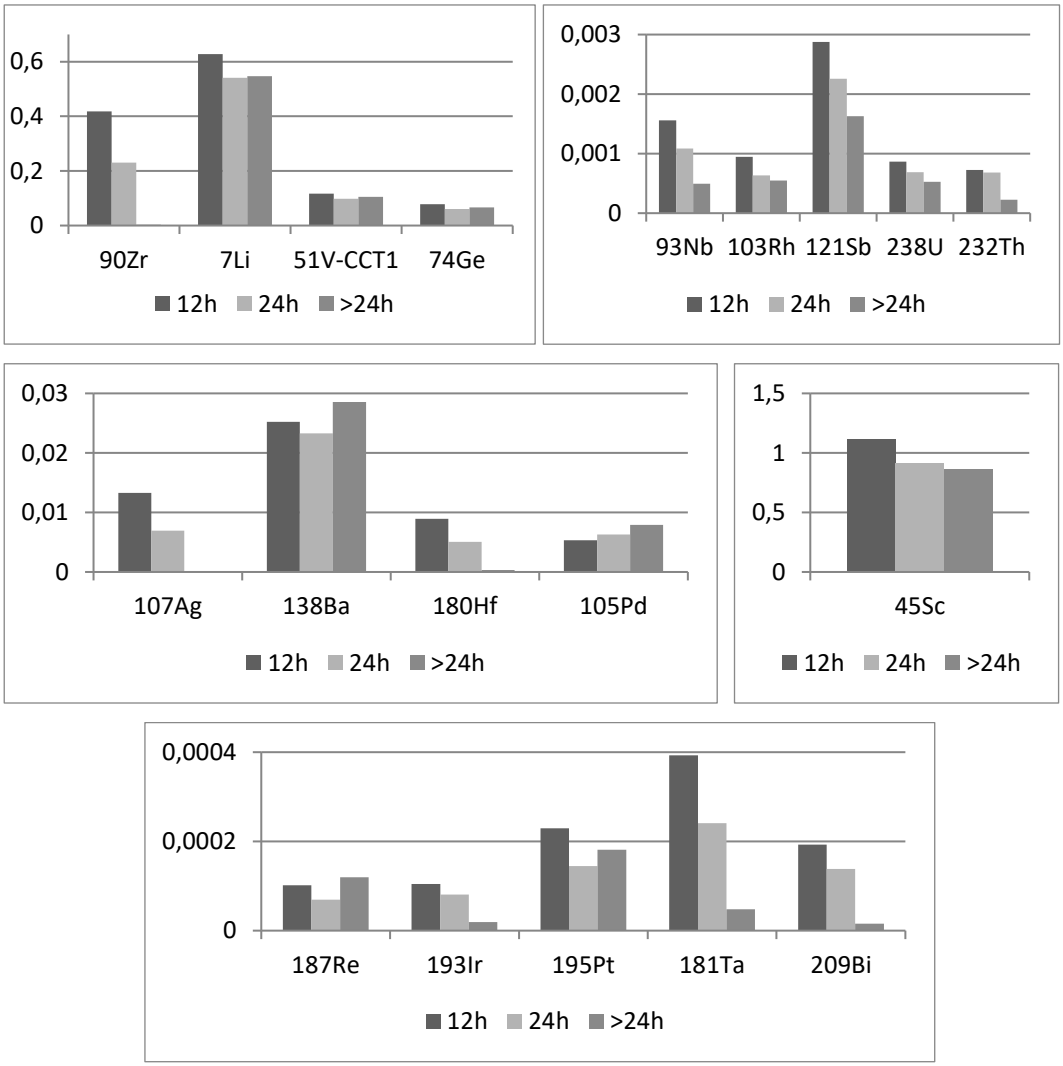

Figure 26: *Bar diagrams of the weighted excretion (in ug/h) within 12h, 24h and after more than 24h after treatment of each other element.*

The majority of the investigated elements shows the effectiveness of the chelating therapy, with a larger excretion within 12 h after the treatment, decreased values within 24 h and nearly zero after 24 h. This same pattern is shared by Pb (toxic elements), Mn, Zn, Fe (essential elements), all the rare earths, and Zr, Ag, Hf, Ir, Ta, Bi (other elements). A positive effect of the chelating therapy is also recorded for elements showing a larger excretion within 12 h, reduced values within 24 h and

constant or even very low values after 24 h of treatment. For these elements, however, the basal excretion is not negligible. This pattern is characteristic of a wide range of elements: Al, Ni, As, Cs, Ga, Cd, Cr, W, Tl, Sn, Rb (toxic elements); Co, Cu, Se, Mo (essential elements); Ti, Nb, Rh, Sb, U, Th, Sc (other elements). Peculiar patterns are observed for elements belonging to the fourth class:

- V, Ge, Li, Ba, Pt, Re show a larger excretion within 12 h, a decrease within 24 h and then an increase after 24 h. We conclude that these elements show an effect of the chelating therapy comparable with the basal excretion.
- Pd and Sr show excretions after 24 h higher than in the first 24 h post-therapy. For these elements, the chelating therapy shows no significant effect.

3.2.4 Conclusions

The systematic collection of the urine samples for 17 months permitted to monitor the excretion of metals from the organism contemporarily identifying the anomalous excretions following the pharmacological treatment. The results confirm the efficacy of the chelating therapy in the elimination of the heavy metals accumulated in the organism, as indicated by the fact that the majority of the elements shows an excretion peak in the 12 h after the EDTA administration.

For metals as Cd, As, Al, Cr, Rb, Ti, and others, the excretion continues also 36 h after the treatment, showing a pattern defined as “basal excretion”. The ICP-MS analyses confirm, on the other hand, the results of the mineralograms, and further provide a clearer view of the situation, with the evidence of an increased number of bioaccumulated elements, e.g. Rb (1.0 g in 17 months), Ti (0.65g in 17 months), Sr (0.055 g). The large excretion of Rb, whose toxic effect has been scarcely investigated, is worth of further investigation in order to clarify the origin of its presence in the patient’s body and its potential patho-physiological effects.

It is worth of note that microelements such as Zn, Mn, Fe and Cu (and in a minor way for Co), which act as co-enzymes and co-factors, were eliminated in the C1

samples. Thus, it is advisable to introduce adequate dietary supplements in the time interval between two EDTA administrations, in order to restore the reservoir of these elements and so avoiding side-effects from their depletion. In fact, the protocol used in the present treatment excludes the intake of vitamins and minerals, since they might reduce the EDTA effect.

From a mere clinical point of view, the utility of the chelating therapy was further confirmed by the improvement of the general conditions of the patient that after the 8^{th} treatment reported 3 main effects: 1) improvement of his memory, concentration capability and muscular strength, with a decrease of the joints instability; 2) restoration of physiologic libido; 3) decrease of the dietary intolerances, with reintroduction in his diet of foods that were previously causing allergic reactions. The positive effects reported by the patient became stable after the 20^{th} chelation. Since then, he has continued the treatment with EDTA for 10 further administrations. After 15 months from the last chelation therapy, the positive effects are only slightly reduced.

Two general conclusions arise from the present study:

1. The unhealthy condition of the patient was not attributable to a chronic intoxication from a single element. Instead, the tissue accumulation of a mixture of elements possibly contributed to the Fatigue syndrome-like symptoms.
2. The chelating protocol could be implemented to optimize EDTA chelating efficacy and to minimize the collateral effects. In fact, the effect of EDTA almost ends within 24 h after the treatment (25).

Further to be considered is the unbalance between administered EDTA and elemental excretion: the overall amount of EDTA administered equals 0.146 mol, while the overall elements excreted are about 0.0072 mol (calculated within 24 h after EDTA administration). It follows that EDTA is administered (at least in this case) at a very high dose with respect to the amount effectively exploited for metals chelation. Thus,

a more frequent and low-dose administrations of EDTA could be more effective and less harmful.

Another strategy (54) consists in exploiting a combination of two chelating agents with different mechanisms of action. This approach, known as “Combination Therapy”, improves the mobilization of the metals from the body, reducing the dose of the chelating agent potentially toxic and avoiding the re-distribution of the toxic metals between different body organs (55). An example (56) is given by the combined administration of monoisoamyl DMSA (MiADMSA) and EDTA in mice: this strategy is effective to limit lead chronic toxicity, reducing the amount of lead in the body and avoiding the death of neural cells.

To our knowledge, the data here reported represent the most complete dataset regarding the long-term monitoring of a chelating therapy. The present results provide insights on the therapy effects and suggest some adjustments to improve its strength and efficacy.

3.3 Plasma proteome profile during a chelating therapy

The analysis of blood proteins is very important in order to understand a disease pathway and to identify biomarkers, but also to evaluate the effect of a therapy. Low-abundant plasma proteins are considered the most promising biomarkers for disease diagnosis and for therapeutic monitoring. To this aim, several immunodepletion methods for the reduction of high abundant proteins were developed during the last decade and, today, they are widely employed in discovery studies (57).

None of the previous studies were however performed to investigate the expression of the plasma proteome changes after chelation therapy. Such feature may indeed to a large extent provide new general information in terms of the understanding of mechanisms and effects of the therapy on the plasma proteome rather than on the pathways involved.

In the present study, we have monitored for ten days the plasma proteome of a patient with heavy metal chronic poisoning subjected to the chelating therapy with Ca-Na-EDTA. The plasma proteins were quantified using shotgun proteomics: the concentration of the most abundant proteins was reduced by immunodepletion method in order to increase the proteome coverage and to quantify the low-abundant one. The samples were analyzed using the label-free SWATH-MS quantification method (58,59) and the results were processed using statistical and bioinformatic tools.

3.3.1 Materials and Methods

3.3.1.1 Chelating therapy protocol, subject and plasma collection

The chelating therapy protocol and the subject were already described in paragraphs 3.2.1.1 and 3.2.1.2.

Blood samples were collected during the three days before the chelation treatment and one, two and six days after the therapy. Plasma samples were obtained from 3 ml of fresh blood, obtained by venipuncture and centrifugation at 400×g. Each

plasma sample was harvested and separated into aliquots and frozen at −80°C until the analysis.

3.3.1.2 Plasma sample preparation

Twelve µL of plasma were depleted of high abundant proteins using the Seppro IgY14 spin column kit (Sigma-Aldrich Inc., St. Louis, MO, USA) following the manufacturer protocol. The method is used to bind human serum HSA, IgG, fibrinogen, transferrin, IgA, IgM, haptoglobin, alpha2-macroglobulin, alpha1-acid glycoprotein, alpha1-antitrypsin, Apo A-I HDL, Apo A-II HDL, complement C3 and LDL (ApoB) and thus to increase the identification of low-abundant proteins. The sample was transferred into an Amicon Ultra-0.5 mL 3 kDa centrifugal filter (Millipore, Billerica, MA, USA) following the manufacturer protocol, to collect the high molecular weight proteins. The sample was then subjected to denaturation with TFE (trifluoroethanol), to reduction with DTT (dithiothreitol) 200 mM, alkylation with IAM (Iodoacetamide) 200 mM and the complete protein trypsin digestion with 2 µg of Trypsin/Lys-C (Promega, Madison, WI, USA). The peptide digests were desalted on the Discovery® DSC-18 solid phase extraction (SPE) 96-well Plate (25 mg/well) (Sigma-Aldrich Inc., St. Louis, MO, USA). The SPE plate was preconditioned with 1 mL of acetonitrile and 2 mL of water. After the sample loading, the SPE was washed with 1 mL of water. The adsorbed proteins were eluted with 800 µL of acetonitrile:water (80:20 v/v) (60). After desalting, the sample was vacuum evaporated and reconstituted with 20 µL of 0.05% formic acid in water. 2 µL of stable-isotope-labeled peptide standard (DPEVRPTSAVAA, Val- 13C515N1 at V10, Cellmano Biotech Limited, Anhui, China) was spiked into the samples before the LC-MS/MS analysis, and used for the instrument quality control (61).

3.3.1.3 LC-MS/MS analyses

The plasma proteins were analyzed with a micro-LC Eksigent Technologies system (Eksigent, Dublin, USA) that included a micro LC200 Eksigent pump with flow module 5-50 µL, interfaced with a 5600+ TripleTOF system (AB Sciex, Concord, Canada) equipped with DuoSpray Ion Source and CDS (Calibrant Delivery System). The stationary phase was a Halo C18 column (0.5 x 100 mm, 2.7 µm; Eksigent Technologies Dublin, USA). The mobile phase was a mixture of 0.1% (v/v) formic acid in water (A) and 0.1% (v/v) formic acid in acetonitrile (B), eluting at a flow-rate of 15.0 µL min^{-1} at an increasing concentration of solvent B from 2% to 40% in 30 min. The injection volume was 4.0 µL and the oven temperature was set at 40 °C. For identification purposes the samples were subjected to a data dependent acquisition (DDA): the mass spectrometer analysis was performed using a mass range of 100–1500 Da (TOF scan with an accumulation time of 0.25 s), followed by an MS/MS product ion scan from 200 to 1250 Da (accumulation time of 5.0 ms) with the abundance threshold set at 30 cps (35 candidate ions can be monitored during every cycle). The ion source parameters in electrospray positive mode were set as follows: curtain gas (N_2) at 25 psig, nebulizer gas GAS1 at 25 psig, and GAS2 at 20 psig, ionspray floating voltage (ISFV) at 5000 V, source temperature at 450 °C and declustering potential at 25 V.

For the label-free quantification the samples were subjected to cyclic data independent analysis (DIA) of the mass spectra, using a 25-Da window: the mass spectrometer was operated such that a 50-ms survey scan (TOF-MS) was performed and subsequent MS/MS experiments were performed on all precursors. These MS/MS experiments were performed in a cyclic manner using an accumulation time of 40 ms per 25-Da swath (36 swaths in total) for a total cycle time of 1.5408 s. The ions were fragmented for each MS/MS experiment in the collision cell using the rolling collision energy. The MS data were acquired with Analyst TF 1.7 software

(AB SCIEX, Concord, Canada). Two DDA and three DIA acquisitions were performed (61-63).

3.3.1.4 Protein database search

The DDA files were searched using Protein Pilot software v. 4.2 (SCIEX, Concord, Canada) and Mascot v. 2.4 (Matrix Science Inc., Boston, USA). Trypsin as the digestion enzyme was specified for both the software. For Mascot we used 1 missed cleavages, the instrument was set to ESI-QUAD-TOF and the following modifications were specified for the search: carbamidomethyl cysteines as fixed modification and oxidized methionine as variable modification. A search tolerance of 50 ppm was specified for the peptide mass tolerance, and 0.1 Da for the MS/MS tolerance. The charges of the peptides to search for were set to 2+, 3+ and 4+, and the search was set on monoisotopic mass (64). The UniProt Swiss-Prot reviewed database containing human proteins (version 2015.07.07, containing 42131 sequence entries) was used and a target-decoy database search was performed. False Discovery Rate was fixed at 1% (61).

3.3.1.5 Protein quantification

The quantification was performed by integrating the extracted ion chromatogram of all the unique ions for a given peptide. SwathXtend was employed to build an integrated assay library, built with the DDA acquisitions, using a protein FDR threshold of 1% (65). The quantification was carried out with PeakView 2.0 and MarkerView 1.2. (ABSCIEX, Concord, Canada). Six peptides per protein and six transitions per peptide were extracted from the SWATH files. Shared peptides were excluded as well as peptides with modifications. Peptides with FDR lower than 1.0% were exported in MarkerView for the *t*-test (61).

3.3.1.6 Bioinformatics and Statistics Software

The identified proteins were classified with PANTHER Classification System (66). The regulated proteins were analyzed by using STRING software (67), which is a database of known and predicted protein-protein interactions. For functional annotation clustering and network analysis of proteins, the Cytoscape 3.1.0 plug-ins ClueGO v2.0.8 was also used (68). Statistical analysis was carried out with PeakView 2.0 and MarkerView 1.2. (ABSCIEX, Concord, Canada) (61).

3.3.2 Results

In this research the plasma proteomic profile of a patient with heavy metal chronic poisoning was monitored for ten days before and after the chelating therapy with $CaNa_2EDTA$, as reported in figure 27. The blood samples from the analysis of the three days before the therapy allowed to obtain a very robust control baseline of the patient plasma proteome, that was then compared with the proteome after the therapy with the aim of understanding the mechanisms of action, the effects and the pathways involved during the chelating therapy. The plasma samples were depleted of the high abundant proteins and subjected to proteolytic digestion. A peptide liquid chromatography separation followed by mass spectrometry analysis and database search with Protein Pilot and Mascot was then performed. SWATH-MS analyses were performed in triplicates for each analyzed sample and were imported in the PeakView software to perform the label-free quantification and the identification of regulated proteins. The data were also analyzed using multivariate analysis, for instance, principal component analysis – discriminant analysis (PCA-DA).

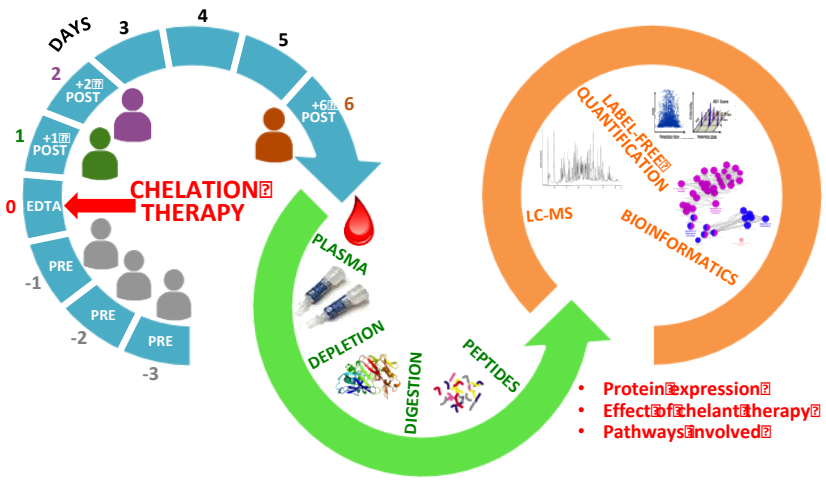

Figure 27. *Workflow of the research: the plasma proteome was monitored during three days before the therapy and until 6 days after the treatment. The highly-abundant proteins were reduced with the immunodepletion method, the proteins were then digested, analyzed with LC-MS and identified and quantified across the 10 days. Bioinformatic software were employed to extract the more important information related to the regulated proteins and the pathways involved.*

The LC-MS analysis allowed the identification of 265 proteins. The gene ontology classification of the identified proteins was carried out to characterize the plasma proteome profile of the dataset. Figure 28 shows the distribution of the proteins based on cellular components, molecular functions and biological processes. The two most abundant functions represented are catalytic activity (42%) and binding function (36%). Some few proteins associated to the antioxidant activity are also present (1%). Proteins related to cellular (19%) and metabolic processes (14%), together with the response to stimulus (11%) are also well described in the samples.

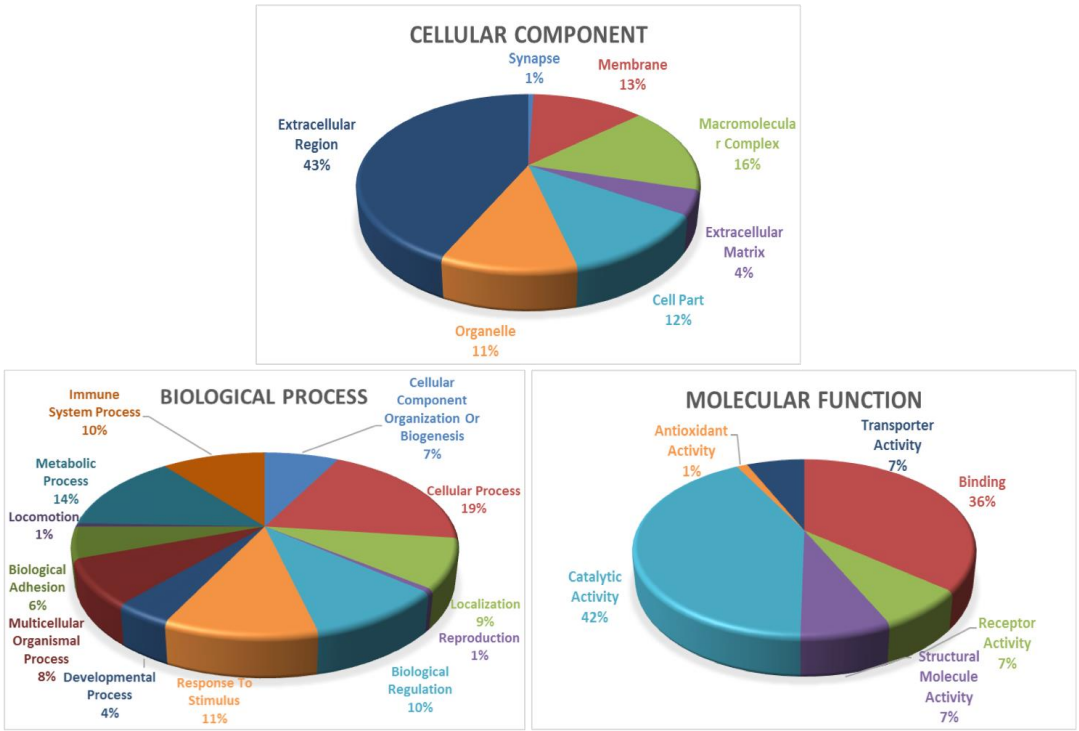

Figure 28. *Gene Ontology classification of the identified proteins based cellular component, biological process and molecular function.*

The proteins fold change of the samples collected after one, two and six days from the therapy were calculated against the average values of the three days before the treatment: a total of 58 proteins were differentially expressed in the three days after the treatment.

The heat map represented in figure 29a shows the trend of the fold change for the 58 regulated proteins: in the first day 19 proteins resulted up-regulated, while 22 were down-regulated, 17 proteins on the 58 are not regulated in the first day; in the second day 13 proteins were down expressed and 7 up regulated; after 6 days 16 proteins were down and 6 up regulated. 17 proteins were commonly regulated over the days as shown in the histogram of figure 29c that represents the log10 fold change of these proteins for each day.

Protein accession	Protein names	Gene	FC 1 DAY vs PRE	FC 2 DAYS vs PRE	FC 6 DAYS vs PRE
A1BG_HUMAN	Alpha-1B-glycoprotein	A1BG	0.63	-	-
AFAM_HUMAN	Afamin	AFM	-	-	1.43
APOC2_HUMAN	Apolipoprotein C-II	APOC2	0.61	0.70	0.68
APOC3_HUMAN	Apolipoprotein C-III	APOC3	0.46	0.62	0.56
APOE_HUMAN	Apolipoprotein E	APOE	-	0.73	-
C1RL_HUMAN	Complement C1r subcomponent-like protein	C1RL	-	-	0.69
C4BPA_HUMAN	C4b-binding protein alpha chain	C4BPA	1.94	-	-
CAH1_HUMAN	Carbonic anhydrase 1	CA1	0.49	0.60	0.51
CAH2_HUMAN	Carbonic anhydrase 2	CA2	0.19	-	-
CBPN_HUMAN	Carboxypeptidase N catalytic chain	CPN1	0.77	-	-
CFAI_HUMAN	Complement factor I	CFI	-	0.74	-
CO2_HUMAN	Complement C2	C2	0.23	-	-
CO8B_HUMAN	Complement component C8 beta chain	C8B	0.68	0.73	-
CO9_HUMAN	Complement component C9	C9	0.53	-	-
FA12_HUMAN	Coagulation factor XII	F12	0.54	0.76	0.72
FCGBP_HUMAN	IgGFc-binding protein	FCGBP	-	1.43	-
FETUB_HUMAN	Fetuin-B	FETUB	0.63	-	-
FHR2_HUMAN	Complement factor H-related protein 2	CFHR2	1.32	-	-
GELS_HUMAN	Gelsolin	GSN	0.66	-	0.76
GPX3_HUMAN	Glutathione peroxidase 3	GPX3	0.53	0.68	0.70
HEMO_HUMAN	Hemopexin	HPX	1.62	0.73	1.41
HGFA_HUMAN	Hepatocyte growth factor activator	HGFAC	0.58	-	-
HV201_HUMAN	Immunoglobulin heavy variable 2-70	IGHV2-70	-	-	0.76
HV206_HUMAN	Immunoglobulin heavy variable 4-39	IGHV4-39	2.62	-	-
IGJ_HUMAN	Immunoglobulin J chain	JCHAIN	1.33	-	-
IGLL5_HUMAN	Immunoglobulin lambda-like polypeptide 5	IGLL5	1.49	-	-
ITIH1_HUMAN	Inter-alpha-trypsin inhibitor heavy chain H1	ITIH1	-	-	1.42
ITIH4_HUMAN	Inter-alpha-trypsin inhibitor heavy chain H4	ITIH4	-	-	1.45
K1C10_HUMAN	Keratin, type I cytoskeletal 10	KRT10	-	-	0.36
K22E_HUMAN	Keratin, type II cytoskeletal 2 epidermal	KRT2	-	-	0.41
K2C1_HUMAN	Keratin, type II cytoskeletal 1	KRT1	-	-	0.35
KAIN_HUMAN	Kallistatin	SERPINA4	0.63	-	-
KLKB1_HUMAN	Plasma kallikrein	KLKB1	1.45	1.36	1.37
KNG1_HUMAN	Kininogen-1	KNG1	0.74	-	-
KV118_HUMAN	Immunoglobulin kappa variable 1-17	IGKV1-17	-	2.58	-
KV121_HUMAN	Immunoglobulin kappa variable 1D-33	IGKV1D-33	1.63	-	-

KV122_HUMAN	Immunoglobulin kappa variable 1-16	IGKV1-16	1.74	-	-
KV206_HUMAN	Immunoglobulin kappa variable 2-30	IGKV2-30	1.36	-	-
KV311_HUMAN	Immunoglobulin kappa variable 3-11	IGKV3-11	2.47	-	-
KV402_HUMAN	Immunoglobulin kappa variable 4-1	IGKV4-1	1.39	-	-
LAC2_HUMAN	Immunoglobulin lambda constant 2	IGLC2	1.35	-	-
LUM_HUMAN	Lumican	LUM	0.62	-	0.73
LV104_HUMAN	Immunoglobulin lambda variable 1-51	IGLV1-51	1.43	-	-
LV301_HUMAN	Immunoglobulin lambda variable 3-1	IGLV3-1	-	2.03	-
LV401_HUMAN	Ig lambda chain V-IV region Bau		2.10	2.29	-
LYAM1_HUMAN	L-selectin	SELL	0.72	0.75	-
N4BP2_HUMAN	NEDD4-binding protein 2	N4BP2	-	-	0.51
PEDF_HUMAN	Pigment epithelium-derived factor	SERPINF1	0.51	0.75	-
PGRP2_HUMAN	N-acetylmuramoyl-L-alanine amidase	PGLYRP2	0.63	-	-
PLSL_HUMAN	Plastin-2	LCP1	0.25	0.64	-
RET4_HUMAN	Retinol-binding protein 4	RBP4	0.58	0.73	0.61
SAMP_HUMAN	Serum amyloid P-component	APCS	2.50	1.60	-
STEA3_HUMAN	Metalloreductase STEAP3	STEAP3	-	-	0.19
TM156_HUMAN	Transmembrane protein 156	TMEM156	1.65	-	-
TRI33_HUMAN	E3 ubiquitin-protein ligase TRIM33	TRIM33	-	1.79	-
TTHY_HUMAN	Transthyretin	TTR	1.81	-	-
VTDB_HUMAN	Vitamin D-binding protein	GC	2.36	-	2.36
ZA2G_HUMAN	Zinc-alpha-2-glycoprotein	AZGP1	-	-	0.23

Table 5: *protein accessions, protein names, genes and fold changes of the modulated proteins 1, 2 and 6 days after the chelating therapy.*

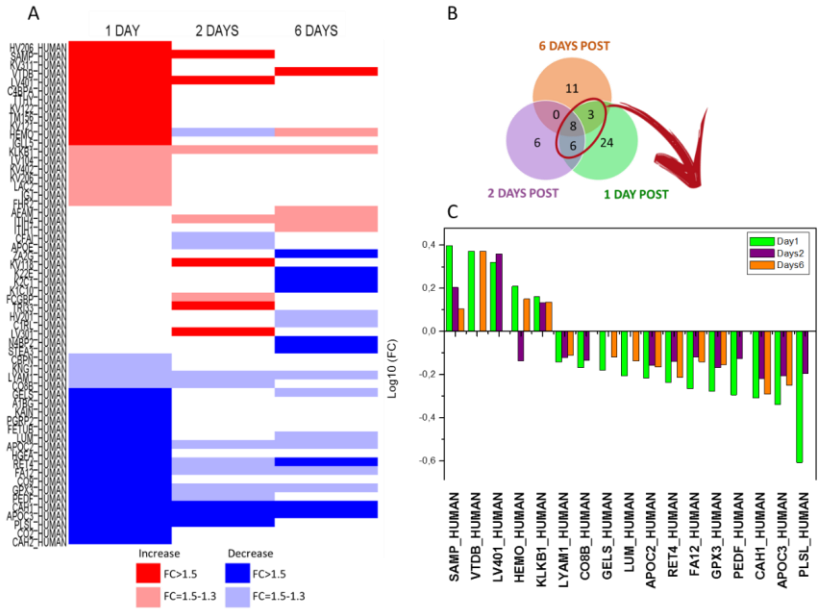

Figure 29. *Heat map of the fold changes of the regulated proteins after one, two and six days after the therapy (a); Venn diagram (b) and histogram (c) of the common regulated proteins.*

The 58 regulated proteins were submitted to the web-based tool Cytoscape to visualize the non-redundant GO terms and pathways in functionally organized networks: the resulting image, as shown in figure 30, reflects the relations between the biological terms based on the similarity of their linked gene/proteins. The analysis revealed the presence of four functional clusters linked to the complement activation, lipoprotein metabolic protein, coagulation and cellular response to metal ion. Among these four groups, the complement activation cluster is the most prominent and the proteins included in it are up and down regulated; the proteins related to coagulation, lipoprotein and cellular response to metal ion are all down regulated.

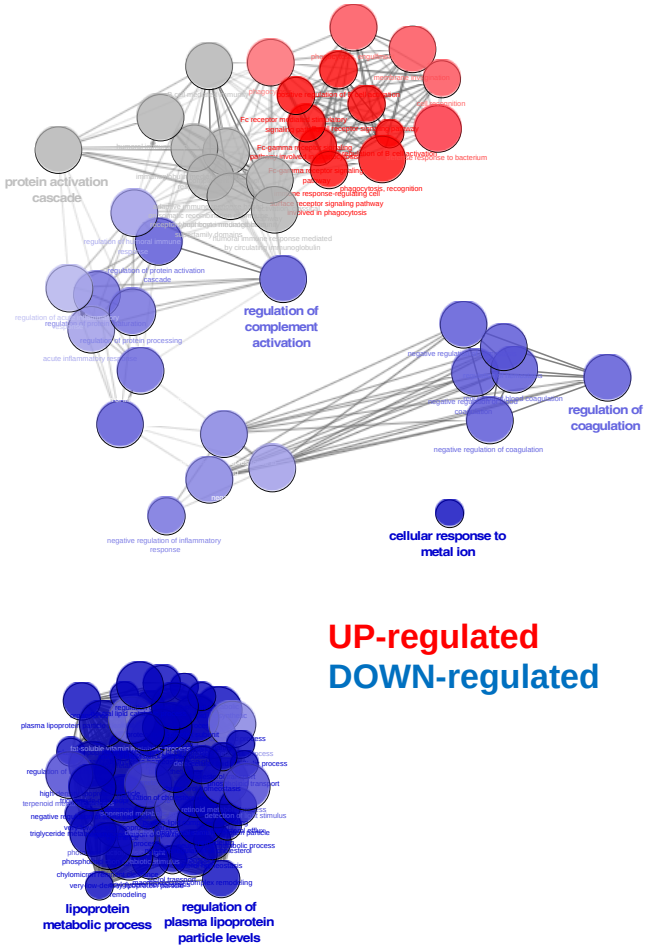

***Figure 30**: Cytoscape representation of functional clusters of regulated proteins*.

The interactions and network analysis of regulated proteins was performed using the STRING software: the analysis showed four different groups reflecting the results obtained from Cytoscape, as reported in figure 31.

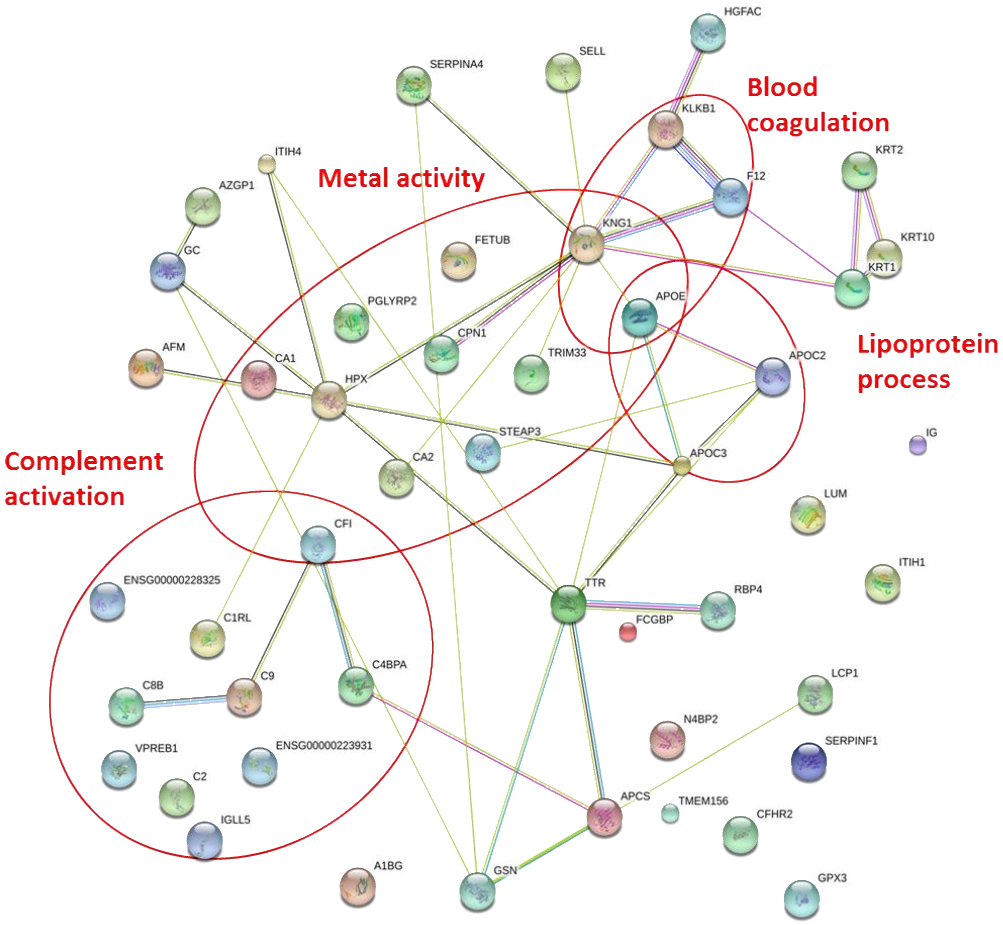

***Figure 31**: STRING network analysis of regulated proteins.*

The multivariate analysis performed using the PCA-DA method showed that the blood samples obtained before the therapy are quite similar among them and that their variability is very small. Figure 32a shows the score plot of the first two latent variables describing the dataset: the samples are correctly separated into the four classes, and in particular the first dimension is able to discriminate the “pre” and “post” state. The samples obtained before the therapy (grey) are grouped together and are well separated from the samples after the treatments. The sample obtained

one day after the therapy (green) is the farther from the controls, followed by the second day sample and the six days one, which is the closest to the pre-treatment state.

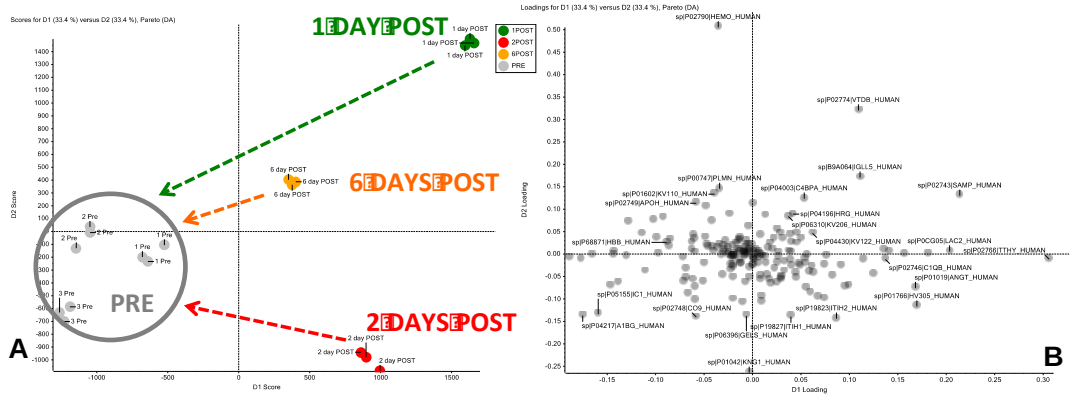

Figure 32. *Score plot (a) of the plasma samples before (grey) and one (green), two (red) and six (orange) days after the therapy. Loading plot (b) of the plasma samples.*

3.3.3 Discussion

During the chelation therapy the metal ions in the human body are chelated and eliminated through the urinary route. But this is not the only effect of EDTA on human body and plasma. The therapy is also widely used to treat heart diseases because the chelating agent can binds the calcium ions present in the fatty deposits in the arteries, which may be then swept away through the bloodstream.

As reported in the STRING and Cytoscape analysis, the main pathways related to modulated proteins are the complement activation, the blood coagulation, the lipoprotein process and the proteins linked to the metal activity. The proteins related to this two last classes are the most important for cardiovascular and metal intoxication pathologies.

For what concerns the effect of the chelating therapy on proteins related to metal ions and metal intoxication, elements like Pb and Cd have a high affinity for –SH groups in enzymes and anti-oxidative defense system and thus inhibit their activity. Moreover, the levels of glutathione (GSH), which is one of the most important components of antioxidant protection, are affected by metal intoxication.

Glutathione peroxidase 3 (GPX3) is a selenocysteine-containing antioxidant enzyme that uses excess H2O2, helping to maintain the redox balance in cells (69). During the reaction, GSH is oxidized to glutathione disulfide (GSSG). Fulgenzi et al. showed that the chelation treatment improved the oxidative and metabolic parameters in patients affected by neurodegenerative diseases, demonstrating an increase of GSH levels after the therapy (70). Our data suggests that the increasing of GSH levels may be caused by a decrease of the glutathione peroxidize, in particular the GPX3, which catalyzes the GSH oxidation. GPX3 is down-regulated because metals are chelated by EDTA and eliminated through the urinary route: thus, their concentration decreased together with the synthesis of GPX3, which is one of the major scavenger of ROS in plasma.

Plasma glutathione peroxidase concentration has also been found elevated in rheumatoid arthritis (71) and a recent paper demonstrated the efficacy of chelating therapy on this pathology (41): our findings suggests that there may be a link between the down-regulation of GPX3 caused by the treatment and the successful management of rheumatoid arthritis by chelation therapy.

We also observed the down-regulation of lumican (LUM), a proteoglycan component which binds to collagens and that was identified as overexpressed in rheumatoid arthritis with respect to spondyloarthropathy (72). It has been also implicated as an atherosclerotic marker that induces collagen fibrillogenesis in coronary atherosclerosis (73) and it has also key roles in tumor development and progression (74).

Metallothionein (MT) is a ubiquitous family of metal-binding proteins that are critical to the homeostatic control of metal levels. Since MT was discovered it has been implicated in toxic metal detoxification, oxidative stress response, and essential metal homeostasis (75). Fully saturated Zn-MT is capable of donating zinc to the apoenzymes such as Carbonic anhydrase protein (CAH1), which is a zinc-containing enzyme that catalyzes the reversible hydration of carbon dioxide, the first discovered metalloenzyme. The zinc ion can be removed from these isozymes by dialysis

against certain chelating agents (76). In our research, the concentration of CAH1 decreased after the chelation treatment, suggesting an inactivation of the enzyme after the zinc chelation.

Another important aspect of the effect of chelation therapy on human health is the one related to the reduction of cardiovascular risk. Our analysis demonstrated for the first time that the biochemical network linked to lipoprotein processes is down-regulated, in particular the Apolipoprotein Apo C-III (APOC3), Apolipoprotein Apo C-II (APOC2) and retinol-binding protein 4 (RET4) are down-expressed after the treatment. An excess of APOC2 has already been associated to increased Triglyceride-rich particles and alterations in the High Density Lipoprotein (HDL) particle distribution, factors that may increase the risk of cardiovascular diseases (77). Moreover, several studies showed the associations of circulating RET4 with obesity, insulin resistance, type 2 diabetes and cardiovascular risk factors (78). As shown in figure 7, after 6 six days the levels of APOC3, APOC2 and RET4 were still down-regulated. The role of EDTA on the removal of xenobiotic metals and its association with the cardiovascular risk factor has already been highlighted (79): our results unveiled the mechanism of how chelation can reduce major cardiovascular events.

One more protein of interest is the Pigment epithelium-derived factor (PEDF), which is a member of the serpin family secreted by adipocytes, found overexpressed in obese children and adults. Recently, elevated PEDF in children with type 2 diabetes mellitus was attributed to obesity (80). After the chelation treatment, PEDF protein is down-regulated.

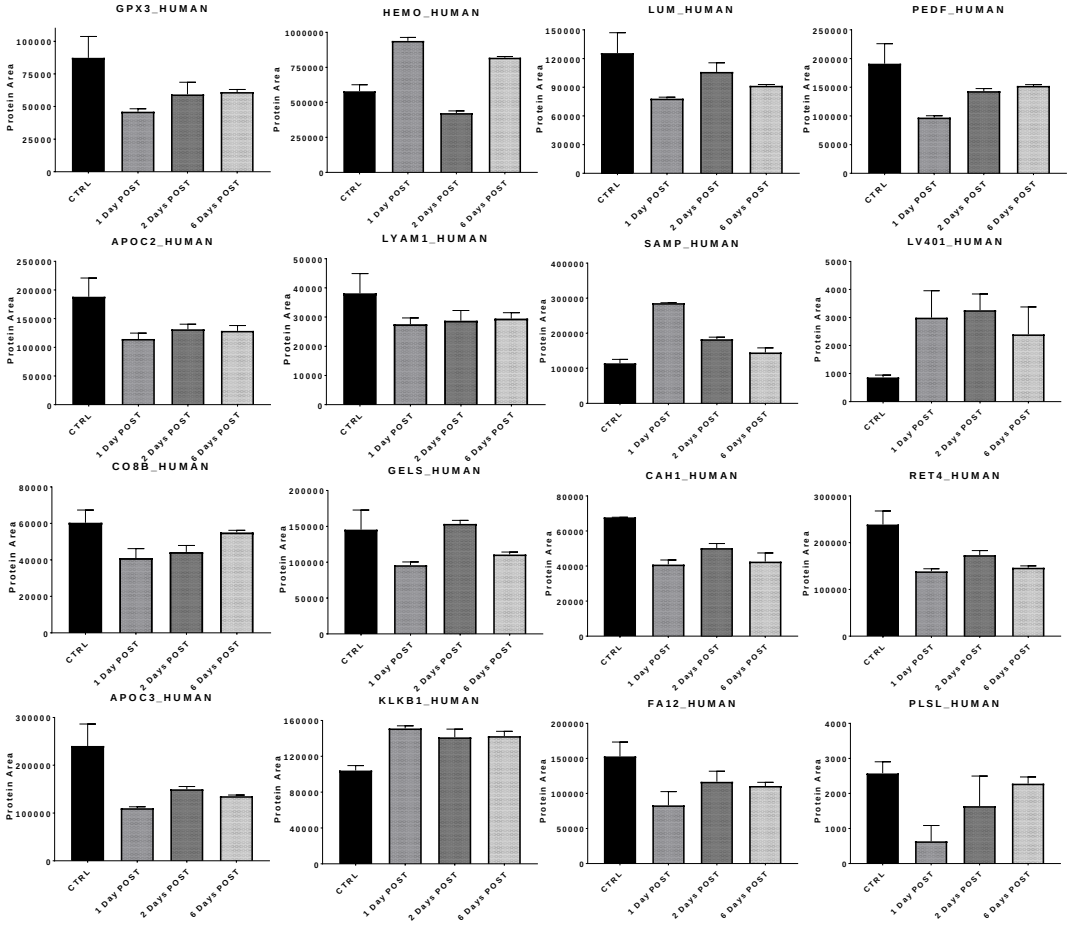

Figure 33. *Box-plot of common regulated proteins after six days of treatment: while some proteins are still modulated after six days the concentration of few of them reached the basal level*.

3.3.4 Conclusions

The aim of the present study was to understand the mechanisms of action, the effects and the pathways involved during the chelating therapy on a patient with heavy metal chronic poisoning. The plasma proteome of the patient was monitored through shotgun proteomics for ten days. Although this research is limited to only one chronic patient, this is the first study where the effect of EDTA on plasma proteome has been considered.

Our results showed a significant modulation of proteins related to redox balance in cells and elimination of ROS in plasma. Moreover, for the first time, we shed light on the mechanism of how chelation can reduce major cardiovascular events. In fact, although the effect of EDTA on cardiovascular diseases has been already studied by several projects and consortium, its effect on the broad plasma proteome was never considered. The results obtained with the shotgun proteomic approach allowed us to identify with high confidence the down regulation of proteins related to lipoprotein processes (APOC3, APOC2 and RET4), which are associated to high cardiovascular risk.

The mass spectrometry proteomics data have been deposited to the ProteomeXchange Consortium via the PRIDE (81) partner repository with the dataset identifier PXD006284.

3.4 Bibliography

1. Beijer K., Jernelöv A. (1986) Sources, transport and transformation of metals in the environment. In: Friberg L, Nordberg GF, Vouk VB (Eds.), Handbook on the Toxicology of Metals. Elsevier, Amsterdam, pp. 68-84.
2. Liu J., Goyer R., Waalkes M.P. (2007) Toxic effects of metals. In: C.D. Klaassen (Ed.) Casarett and Doull's Toxicology - The Basic Science of Poisons. 7. McGraw Hill, pp. 931-979.
3. Aposhian H.V., Bruce D.C., Alter W., Dart R.C., Hurlbut K.M., Aposhian M.M. (1992) Urinary mercury after administration of 2,3-dimercaptopropane-1-sulfonic acid: correlation with the dental amalgam score. FASEB J. 6:2472-2476.
4. Tomljenovic L., Shaw C.A. (2011) Do aluminum vaccine adjuvants contribute to the rising prevalence of autism? J Inorg Biochem. 105(11):1489-1499.

5. Tomljenovic L., Shaw C.A. (2012) Mechanisms of aluminum adjuvant toxicity and autoimmunity in pediatric populations. Lupus. 21(2):223-230.
6. Exley C. (2014) Aluminium adjuvants and adverse events in sub-cutaneous allergy immunotherapy. Allergy Asthma Clin Immunol. 10(1):4.
7. Iarc Monographs on the Evaluation of Carcinogenic Risks to Humans, A Review of Human Carcinogens: Arsenic, Metals, Fibres, and Dusts, vol. 100 C, 2012.
8. Klaassen C.D., Liu J., Choudhuri S. (1999) Metallothionein: an intracellular protein to protect against cadmium toxicity. Annu Rev Pharmacol Toxicol. 39:267-294.
9. Jarup L., Berglund M., Elinder C.G., Nordberg G., Vahter M. (1998) Health effects of cadmium exposure--a review of the literature and a risk estimate. Scand J Work Environ Health. 24(1):1-51.
10. Crépeaux G., Eidi H., David M.O., Baba-Amer Y., Tzavara E., Giros B., Authier F.J., Exley C., Shaw C.A., Cadusseau J., Gherardi R.K. (2017) Non-linear dose-response of aluminium hydroxide adjuvant particles: Selective low dose neurotoxicity. Toxicology. 375:48-57.
11. Weisser K, Stübler S, Matheis W, Huisinga W (2017) Commentary Towards toxicokinetic modelling of aluminium exposure from adjuvants in medicinal products. Regulatory Toxicology and Pharmacology. Published online, http://doi.org/10.1016/j.yrtph.2017.02.018.
12. Mold M., Shardlow E., Exley C. (2016) Insight into the cellular fate and toxicity of aluminium adjuvants used in clinically approved human vaccinations. Scientific Reports. 6:31578 DOI: 10.1038/srep31578.
13. Dórea J.G. (2017) Low-dose Thimerosal in pediatric vaccines: Adverse effects in perspective. Environmental Research. 152:280-293.
14. Geier D.A., King P.G., Hooker B.S., Dórea J.G., Kern J.K., Sykes L.K., Geier M.R. (2015) Thimerosal: Clinical, epidemiologic and biochemical studies. Clinica Chimica Acta. 444:212-220.

15. Geier D.A., Kern J.K., Geier M.R. (2017) Analytical methodology Increased risk for an atypical autism diagnosis following Thimerosal-containing vaccine exposure in the United States: A prospective longitudinal case-control study in the Vaccine Safety Datalink. Journal of Trace Elements in Medicine and Biology. 42:18-24.
16. Wilson B., Pyatt F.B. (2006) Bio-availability of tungsten in the vicinity of an abandoned mine in the English Lake District and some potential health implications. Science of the Total Environment. 370:401-408.
17. Scansetti G., Botta G.C., Spinelli P., Reviglione L., Ponzetti C. (1994) Absorption and excretion of cobalt in the hard metal industry. Science of The Total Environment. 150(1-3):141-144.
18. Frančišković-Bilinski S. (2006), Barium anomaly in Kupa River drainage basin. J Geochemical Exploration. 88(1-3):106-109.
19. Gilfillan S.C. (1965) Lead poisoning and the fall of Rome. J Occup Med. 7:53-60.
20. Nriagu J.O. (1983) Occupational exposure to lead in ancient times. Sci Total Environ. 31(2):105-116.
21. Nriagu J.O. (1983) Saturnine gout among Roman aristocrats, Did lead poisoning contribute to the fall of the Empire? N Engl J Med. 308(11):660-663.
22. Woolley D.E. (1994) A perspective of lead poisoning in antiquity and the present. Neurotoxicology. 5(3):353-361.
23. Gao Z., Ying X., Yan J., Wang J., Cai S., Yan C. (2017) Acute mercury vapor poisoning in a 3-monthold infant: A case report", Clinica Chimica Acta, vol. 465, pp. 119–122.
24. Mărginean C.O., Meliţ L.E., Moldovan H., Lupu V.V., Mărginean M.O. (2016) Lead poisoning in a 16-year-old girl: a case report and a review of the literature (CARE compliant). Medicine (Baltimore). 95(38):e4916.

25. Flora S.J.S., Pachauri V. (2010) Chelation in metal intoxication. Int J Environ Res Public Health. 7:2745-2788.
26. Flora G.J., Seth P.K., Prakash A.O., Mathur R. (1995) Therapeutic efficacy of combined meso2,3-dimercaptosuccinic acid and calcium disodium edetate treatment during acute lead intoxication in rats. Human Exp Toxicol. 14(5):410-3.
27. Crinnion W.J. (2011) EDTA redistribution of lead and cadmium into the soft tissues in a human with a high lead burden - should DMSA always be used to follow EDTA in such cases?. Altern Med Rev: J Clin Ther. 16(2):109-12.
28. Klaassen C.D. (1990) Heavy metals and heavy-metal antagonists, in Gilman AG, Rall TW, Nies AS, Taylor P (Eds), Goodman and Gilman's The Pharmacological Basis of Therapeutics. New York, Pergamon Press, pp. 1592-1614.
29. Jones M.M. (1990) Newer chelating agents for in vivo toxic metal mobilization. Comments Inorg Chem. 13:91-110.
30. Blanusa M., Varnai V.M., Piasek M., Kostial K. (2005) Chelators as antidotes of metal toxicity: therapeutic and experimental aspects. Curr Med Chem. 12:2771-2794.
31. Corsello S., Fulgenzi A., Vietti D., Ferrero M.E. (2009) The usefulness of chelation therapy for the remission of symptoms caused by previous treatment with mercury-containing pharmaceuticals: a case report. Cases Journal. 2:199-203.
32. Bamonti F., Fulgenzi A., Novembrino C., Ferrero M.E. (2011) Metal chelation therapy in rheumathoid arthritis: a case report Successful management of rheumathoid arthritis by metal chelation therapy. Biometals. 24:1093-1098.
33. Fulgenzi A., Zanella S.G., Mariani M.M., Vietti D., Ferrero M.E. (2012) A case of multiple sclerosis improvement following removal of heavy metal intoxication. Lessons learnt from Matteo's case. Biometals. 25:569-576.

34. Ferrero M.E. (2016) Rationale for the Successful Management of EDTA Chelation Therapy in Human Burden by Toxic Metals. BioMed Research International. Volume 2016, Article ID 8274504, 13 pages.
35. Crisponi G., Nurchi V.M., Crespo-Alonso M., Toso L. (2012) Chelating Agents for Metal Intoxication. Curr Med Chem. 19:2794-2815.
36. Tantanasrikul S., Chaivisuth B., Siriratanapreuk S., Padungtod C., Pleubreukan R., Boonnark T., Worahan S., Bhumiratanarak P., Chomchai C. (2002) The management of environmental lead exposure in the pediatric population: lessons from Clitty Creek, Thailand. J Med Assoc Thai. 85(Suppl 2):S762-768.
37. Mycyk M.B., Leikin J.B. (2004) Combined exchange transfusion and chelation therapy for neonatal lead poisoning. Ann Pharmacother. 38:821-824.
38. Lin-Tan D.T., Lin J.L., Yen T.H., Chen K.H., Huang Y.L. (2007) Long-term outcome of repeated lead chelation therapy in progressive nondiabetic chronic kidney diseases. Nephrol Dial Transplant. 22:2924-2931.
39. Lin J.L., Lin-Tan D.T., Hsu K.H., Yu C.C. (2003) Environmental lead exposure and progression of chronic renal diseases in patients without diabetes. N Engl J Med. 348:277-286.
40. Klaassen C.D. (2001) Casarett and Doull's Toxicology: the basic science of poisons. 6th Edn. McGraw-Hill, New York.
41. Houston M.C. (2011) Role of mercury toxicity in hypertension, cardiovascular disease, and stroke. Journal of Clinical Hypertension. 13 (8), 621–627.
42. Wax P.M. (2013) Current Use of Chelation in American Health Care, J. Med. Toxicol. 9 (4), 303–307.
43. Lamas G.A., Boineau R., Goertz C., Mark D.B., Rosenberg Y., Styliano M., Rozema T., Nahin R.L., Chappell T.L., Lindblad L., Lewis E.F., Drisko J., Lee K.L. (2014) EDTA chelation therapy alone and in combination with oral

high-dose multivitamins and minerals for coronary disease: The factorial group results of the Trial to Assess Chelation Therapy. Am. Heart J. 168, 37-44.

44. Lamas G.A., Goertz C., Boineau R., Mark D.B., Rozema T., Nahin R.L., Lindblad L., Lewis E.F., Drisko J., Lee K.L. (2013) Effect of disodium EDTA chelation regimen on cardiovascular events in patients with previous myocardial infarction: the TACT randomized trial. JAMA. 309 (12), 1241-50.
45. Escolar E., Lamas G.A., Mark D.B., Boineau R., Goertz C., Rosenberg Y., Nahin R.L., Ouyang P., Rozema T., Magaziner A., Nahas R., Lewis E.F., Lindblad L., Lee K.L. (2014) The effect of an EDTA-based chelation regimen on patients with diabetes mellitus and prior myocardial infarction in the Trial to Assess Chelation Therapy (TACT), Circ. Cardiovasc. Qual. Outcomes. 7, 15-24.
46. Fulgenzi A., De Giuseppe R., Bamonti F., Vietti D., Ferrero M.E. (2015) Efficacy of chelation therapy to remove aluminium intoxication. J Inorg Biochem. 152:214-8.
47. Myhill S., Booth N.E., McLaren-Howard J. (2009) Chronic fatigue syndrome and mitochondrial dysfunction. Int J Clin Exp Med. 2:1-16.
48. Cannino G., Ferruggia E., Luparello C., Rinaldi A.M. (2009) "Cadmium and mitochondria". Mitochondrion. 9:377-384.
49. Pacini S., Fiore M.G., Magherini S., Morucci G., Branca J.V., Gulisano M., Ruggiero M. (2012) Could cadmium be responsible for some of the neurological signs and symptoms of Myalgic Encephalomyelitis/Chronic Fatigue Syndrome. Medical Hypotheses. 79:403-407.
50. Fulgenzi A., Vietti D., Ferrero M.E. (2014) Aluminium involvement in neurotoxicity. Biomed Res. Int. (2014)1-5.

51. Vanatta L.E., Coleman D.E. (1997) Calculation of detection limits for a single-laboratory ion chromatographic method to determine parts-per-trillion ions in ultrapure water. J Chromatogr A. 770 (1-2):105-114.
52. Coleman D., Auses J., Grams N. (1997) Regulation - From an industry perspective or relationships between detection limits, quantitation limits, and significant digits. Chemometr Intell Lab. 37(1):71-80.
53. Waters R.S., Bryden N.A., Patterson K.Y., Veillon C., Anderson R.A. (2001) EDTA chelation effects on urinary losses of cadmium, calcium, chromium, cobalt, copper, lead, magnesium, and zinc. Biol Trace Elem Res. 83(3):207-21.
54. Flora S.J.S., Bhattacharya R., Vijayaraghavan R. (1995) Combined therapeutic potential of meso 2,3-dimercaptosuccinic acid and calcium disodium edetate in the mobilization and distribution of lead in experimental lead intoxication in rats. Fund Appl Toxicol. 25:233-240.
55. Flora S.J.S., Saxena G. (2004) Lead induced oxidative stress and hematological alterations and their response to combined administration of calcium disodium EDTA with a thiol chelator in rats. J Biochem Mol Toxicol 18:221-233.
56. Flora S.J.S., Saxena G., Mehta A. (2007) Reversal of lead-induced neuronal apoptosis by chelation treatment in rats: role of ROS and intracellular Ca2+. J Pharmacol Exp Ther. 332:108-116.
57. Geyer P.E., Kulak N.A., Pichler G., Holdt L.M., Teupser D., Mann M. (2016) Plasma Proteome Profiling to Assess Human Health and Disease. Cell Systems. 2(3), 185–195.
58. Gillet L.C., Navarro P., Tate S., Röst H., Selevsek N., Reiter L., Bonner R., Aebersold R. (2012) Targeted data extraction of the MS/MS spectra generated by data-independent acquisition: a new concept for consistent and accurate proteome analysis. Mol Cell Proteomics. 11, O111 016717.

59. Tate S., Larsen B., Bonner R., Gingras A.C. (2013) Label-free quantitative proteomics trends for protein-protein interactions. Journal of proteomics. 81, 91–101.
60. Guo X., Kristal B.S. (2012) The use of under-loaded C18 solid-phase extraction plates increases reproducibility of analysis of tryptic peptides from unfractionated human plasma. Anal. Biochem. 426 (1), 86–90.
61. Dalle Carbonare L., Manfredi M., Caviglia G., Conte E., Robotti E., Marengo E., Cheri S., Zamboni F., Gabbiani D., Deiana M., Cecconi D., Schena F., Mottes M., Valenti M.T. (2018) Can half-marathon affect overall health? The yin-yang of sport. Journal of Proteomics. 170, 80-87.
62. Martinotti S., Patrone M., Manfredi M., Gosetti F., Pedrazzi M., Marengo E., Ranzato E. (2015) HMGB1 Osteo-Modulatory Action on Osteosarcoma SaOS-2 Cell Line: An Integrated Study From Biochemical and -Omics Approaches. Journal of cellular Biochemistry. 117, 2559–2569.
63. Manfredi M., Martinotti S., Gosetti F., Ranzato E., Marengo E. (2016) The secretome signature of malignant mesothelioma cell lines. Journal of Proteomics. 145, 3–10.
64. Krisp C., Yang H., van Soest R., Molloy M.P. (2015) Online Peptide Fractionation Using a Multiphasic Microfluidic Liquid Chromatography Chip Improves Reproducibility and Detection Limits for Quantitation in Discovery and Targeted Proteomics. Mol Cell Proteomics. 14 (6), 1708-19.
65. Wu J.X., Song X., Pascovici D., Zaw T., Care N., Krisp C. and Molloy M.P. (2016) SWATH mass spectrometry performance using extended peptide MS/MS assay libraries. Molecular and Cellular Proteomics. 15(7), 2501-14.
66. Mi H., Huang X., Muruganujan A., Tang H., Mills C., Kang D., and Thomas P.D. (2016) PANTHER version 11: expanded annotation data from Gene Ontology and Reactome pathways, and data analysis tool enhancements. Nucl. Acids Res. 45, D183–D189.

67. Szklarczyk D., Franceschini A., Wyder S., Forslund K., Heller D., Huerta-Cepas J., Simonovic M., Roth A., Santos A., Tsafou K.P., Kuhn M., Bork P., Jensen L.J., von Mering C. (2015) STRING v10: protein-protein interaction networks, integrated over the tree of life. Nucleic Acids Res. 43, D447-52.
68. Bindea G., Mlecnik B., Hackl H., Charoentong P., Tosolini M., Kirilovsky A., Fridman W.H., Pagès F., Trajanoski Z., Galon J. (2009) ClueGO: a Cytoscape plug-in to decipher functionally grouped gene ontology and pathway annotation networks. Bioinformatics. 25 (8), 1091-1093.
69. Schmutzler C., Mentrup B., Schomburg L., Hoang-Vu C., Herzog V., Köhrle J. (2007) Selenoproteins of the thyroid gland: expression, localization and possible function of glutathione peroxidase 3. Biol. Chem. 388 (10), 1053−1059.
70. Fulgenzi A., De Giuseppe R., Bamonti F., Ferrero M.E. (2014) Improvement of Oxidative and Metabolic Parameters by Cellfood Administration in Patients Affected by Neurodegenerative Diseases on Chelation Treatment. BioMed Research International. ID 281510, 9 pages.
71. Jacobson G.A., Ives S.J., Narkowicz C., Jones G. (2012) Plasma glutathione peroxidase (GSH-Px) concentration is elevated in rheumatoid arthritis: a case-control study. Clinical Rheumatology. 31, 1543–1547.
72. Bhattacharjee M., Sharma R., Goel R., Balakrishnan L., Renuse S., Advani J., Gupta S.T., Verma R., Pinto S.M., Sekhar N.R., Nair B., Prasad T.S.K., Harsha H.C., Jois R., Shankar S., Pandey A. (2013) A multilectin affinity approach for comparative glycoprotein profiling of rheumatoid arthritis and spondyloarthropathy. Clinical Proteomics. 10(1), 11.
73. Onda M., Ishiwata T., Kawahara K., Wang R., Naito Z., Sugisaki Y. (2002) Expression of lumican in thickened intima and smooth muscle cells in human coronary atherosclerosis. Exp. Mol. Pathol. 72, 142–149.

74. Nikitovic D., Papoutsidakis A., Karamanos N.K., Tzanakakis G.N. (2014) Lumican affects tumor cell functions, tumor–ECM interactions, angiogenesis and inflammatory response. Matrix Biology. 35, 206–214.
75. Pinter T.B.J., Stillman M.J. (2014) The Zinc Balance: Competitive Zinc Metalation of Carbonic Anhydrase and Metallothionein 1. Biochemistry. 53, 6276−6285.
76. Lindskog S. (1997) Structure and Mechanism of Carbonic Anhydrase, Pharmacol. Thu. 74 (1), l-20.
77. Robert W.M. (2016) Apolipoprotein E: from cardiovascular disease to neurodegenerative disorders. J. Mol. Med. 94, 739–746.
78. Ingelsson E., Sundström J., Melhus H., Michaëlsson K., Berne C., Vasan R.S., Risérus U., Blomhoff R., Lind L., Arnlöv J. (2009) Circulating retinol-binding protein 4, cardiovascular risk factors and prevalent cardiovascular disease in elderly. Atherosclerosis. 206, 239-44.
79. Peguero J.G., Arenas I., Lamas G.A. (2014) Chelation Therapy and Cardiovascular Disease: Connecting Scientific Silos to Benefit Cardiac Patients. Trends Cardiovasc Med. 24 (6), 232–240.
80. Tryggestad J.B., Wang J.J., Zhang S.X., Thompson D.M., Short K.R. (2015) Elevated plasma pigment epithelium-derived factor in children with type 2 diabetes mellitus is attributable to obesity. Pediatric Diabetes. 16, 600–605.
81. Vizcaíno J.A., Csordas A., del-Toro N., Dianes J.A., Griss J., Lavidas I., Mayer G., Perez-Riverol Y., Reisinger F., Ternent T., Xu Q.W., Wang R. (2016) Hermjakob H. Uupdate of the PRIDE database and related tools. Nucleic Acids Res. 44 (D1), D447-D456.

CHAPTER 4

Traceability and authentication of hazelnuts and their products

4.1 Introduction

Hazelnuts are dried fruits particularly rich of group B vitamins, phosphorous, copper, calcium, proteins and essential fatty acids (1-4). For their high content of proteins (about 20%) and lipids (about 60%), hazelnuts are a valid substitute for dressings and plastic ingredients of animal origin and are therefore exploited for preparing oils and different specialties in the food industry: confectionery, nougat, candies, creams etc. In these applications hazelnuts are usually exploited as whole fruits, small grains, flour or oil, that are in turn used to produce paste, cream and other finished products. However, hazelnuts are also becoming widespread as nutraceutical ingredients, due to their content of phytosterols, recently related to the prevention of cardiovascular diseases (1,3,5-8). Recent studies confirmed, for example, that a regular consumption of hazelnuts can decrease the level of LDL cholesterol and triglycerides (1-3, 9-11).

Turkey, Spain, Italy and France are among the most important producers of hazelnuts (1,2,12,13); in 2014, FAO reports that the most important producers were Turkey, followed by Italy, Georgia and USA, other emerging producers being Azerbaijan, China, Iran, followed by Spain and France (12,14). The finest Italian varieties are:

- "Tonda Gentile Trilobata" (or "Tonda Gentile delle Langhe"). This is a Protected Geographic Indication (PGI) variety, cultivated in several districts of the provinces of southern Piedmont (Alessandria, Asti and Cuneo - Italy). The fruit is characterized by: a round shape that improves the efficiency of the mechanical shelling; delicate and characteristic aroma and flavor; a reduced content of fats that limits its rapid rancidity; a thin film surrounding the fruit,

easily removable after roasting. It is worldwide considered as the best variety and presents by far the largest prices on the market. Among all the varieties cultivated in the world, this variety is characterized by a very high commercial value since it is particularly suitable for confectionery (15,16) (European commission regulation (EC) No 1107/96 on the registration of geographical indications and designations of origin): its round shape makes its peeling very easy after roasting, so that tannins-reach peels do not affect taste (they are particularly bitter) when hazelnuts are transformed into paste; moreover, the high content of oleic acid and monounsaturated rather than polyunsaturated fatty acids, in particular with respect to cultivars from other countries, makes it more easily storable (17); finally, its quite thin shell guarantees a high yield (15,16) (European commission regulation (EC) No 1107/96 on the registration of geographical indications and designations of origin). In 1996 the TGL obtained the Protected Geographical Indication (PGI) from the European Union (EU) under the name "Nocciola Piemonte" (European commission regulation (EC) No 1107/96 on the registration of geographical indications and designations of origin) (18).

- "Tonda Gentile Romana". The shape of this variety is slightly elongated and sub-spheroidal. The fruit is medium-small, while the shell is quite thick. It is cultivated in some districts of the provinces of Rome and Viterbo (Latium, Italy).
- "Mortarella". This variety produces sub-cylindrical medium-small fruits. The shell is quite thin. The fruit is very aromatic, with a white-ivory pulp. This variety is cultivated in almost all areas of Campania region (Italy), above all for the transformation industry. It represents almost 30% of the overall Italian national production.
- "Tonda di Giffoni". Also this variety has the PGI certification and it is cultivated in several districts of the province of Salerno (Campania, Italy). Its fruits are

perfectly round, the pulp is white and the flavor is aromatic. It is particularly suitable for roasting and peeling. For these characteristics, this variety is particularly suitable for industrial transformations into grain and paste.

From an international point of view, these Italian varieties must deal with other ones characterized by a great commercial diffusion, as those cultivated in Turkey (Tombul, Cakildak, Mincane, Karafindik, Palaz and others) or Spain (Negret, Gironell, Pautet, Culplà, Tonda di Giffoni, Morell).

Hazelnuts are widespread in the food industry either as whole fruits, small grains, flour or oil, to produce paste, cream and other finished products, above all in confectionery. Different hazelnut cultivars show a different commercial value, the cultivar "Tonda Gentile delle Langhe" produced in Italy being by far the most valuable. Along the industrial production chain, hazelnuts first undergo a process of roasting to exalt their aroma, and then hazelnut paste is produced by a fine grinding of the peeled fruits.

Due to the great commercial difference between the "Tonda Gentile delle Langhe" and the other cultivars, it is particularly important for the food industry the availability of tools for tracing the variety and the geographic provenance of hazelnuts and their derivatives along the production chain of the hazelnut paste.

4.1.1 The production chain of hazelnut paste

Along the industrial production chain, hazelnuts must first undergo a process of roasting to exalt their aroma. Roasting has the purpose of dehydrating and oxidizing the fruits to increase storage time and prepare them to the different uses. It is necessary not only to improve the organoleptic properties of hazelnuts, but also for inactivating the action of microorganisms, delaying in this way their degradation. The heat treatment itself, besides the alteration of the aroma profile (19, 20) can cause modifications of vitamins (21,22), carotenoids (21), phytosterols (22), tocopherol (21), lipids (22) and fatty acids (22,23), altering both the organoleptic and

the nutritional properties of hazelnuts. For these reasons, temperature and time of roasting must be accurately controlled. Two industrial approaches are available to accomplish this step:

- static roasting (24) performed on tin pans in conventional ovens for 20-25 minutes at around 180 °C;
- dynamic roasting (25), performed in rotary or hot air flux ovens for 25-35 minutes at around 140°C. With this method heat is transferred in a more homogeneous way, favoring peeling.

Roasted hazelnuts are often further transformed into hazelnut paste both for direct human consumption and for confectionery; this process involves a fine grinding of the peeled fruits to provide a very fluid product.

While it is possible for the experts to distinguish between different hazelnuts varieties from a visual inspection of the entire fruit, unfortunately this is no more possible when the fruits are reduced to grain or paste.

4.1.2 Tools for the traceability and authentication of hazelnuts

From a commercial point of view, it is particularly important for the food industry to achieve tools for tracing the variety and the geographic provenance of hazelnuts and their derivatives, also along the transformation chain. Due to the quite different commercial value of the different varieties, studies on hazelnuts traceability and authentication are of great importance to promptly identify commercial frauds. Besides the commercial reasons, food safety hints are also gaining the attention of the consumers who are increasingly interested in traceable food for reducing the risk of food-borne diseases (26).

Traceability and authentication of typical foodstuffs has recently gained increasing attention and many papers have appeared focusing on the possibility to use different chemical characterization tools in traceability and authentication studies of different

foods (27-40). Elemental and stable isotopes profiling are certainly the most widespread techniques in this field and have been successfully applied to characterize favas (28), paprika (29), tomatoes (30), onions (31), clementines (32), cereals (33), oranges (35), honey (34, 36), saffron (38), olive oil (39, 40) and melons (41).

Different analytical methods have been applied for the classification of hazelnuts according to the different cultivar (14,42-47).

Many papers are present reporting the use of genomic approaches, as real-time polymerase chain reaction (PCR) (42-45).

However, other analytical approaches have recently been proposed, as near infrared (NIR) spectroscopy (46) or ^{1}H Nuclear Magnetic Resonance (NMR) (14, 18).

Cordero et al. (47) focused on the profiling of volatiles by comprehensive two-dimensional gas chromatography coupled to mass spectrometry, while Ciarmiello et al. (48) applied High Performance Liquid Chromatography (HPLC) to determine the phenolic profile. In the field of omics techniques, Locatelli et al. (49) used a genomic approach combined to a physical-chemical characterization and a protein fingerprinting by SDS-PAGE; Klockmann et al. (50) exploited metabolomics through Ultra Performance Liquid Chromatography Quadrupole Time-Of-Flight Mass Spectrometry (UPLC-QTOF-MS).

For what regards elemental techniques, Oddone et al. (51) applied elemental and rare earths profiling. A couple of studies are present in literature reporting applications of elemental profiling in authentication and traceability studies to the production chain of tomato products (30) and wine (52), but no studies are present referred to hazelnut products.

Spectroscopic techniques are also widely employed for food quality and safety inspections: the analysis is non-destructive and can exploit the physical-chemical information on the analyzed products (53,54). Visible and near infrared (NIR) and attenuated total reflectance (ATR) spectroscopies have already been used for

assessing the cultivar of a specific food and for authenticating the geographical origin of many products (55-58). Among the spectroscopic techniques, FTIR spectroscopy allows the detection of small differences and changes in structure and properties of biomolecules like proteins, carbohydrates and lipids altogether, when present in biological tissues and cells (59). While a recent study showed that NIR spectroscopy coupled to chemometrics was able to classify hazelnuts according to their geographic origin (60), FTIR spectroscopy has already been used to characterize the radiation-induced changes in the macro-molecular composition, concentration and structure of hazelnuts (61). The major components of lipids from hazelnuts are triacylglycerols and phospholipids, that can be detected by IR analysis. The chemical lipid profile (particularly triacylglycerols) has already been used to identify hazelnut oils on the basis of their country of origin (62). For example, French cultivars were found to be richer in triacylglycerols containing linoleic acid, while the American ones resulted richer in saturated fatty acids, since the triacylglycerol composition can be influenced by environmental factors (18).

4.1.3 Multivariate tools for the traceability and authentication of hazelnuts

In food science, multivariate screening methods and classification techniques have been successfully employed in the identification of food adulterations (63-65) and in food authentication (66-68). Principal Component Analysis (PCA), a multivariate pattern recognition method, has already been applied to describe the geographic provenance in a compact and efficient way (52). Lerma-García and coauthors (69) classified oil samples from five different botanical origins (EVOO, sunflower, corn, soybean and hazelnut) by linear discriminant analysis (LDA). Moscetti and coauthors (70) used k-nearest neighbours (KNN), soft independent modelling of class analogy (SIMCA), Partial Least Squares – Discriminant Analysis (PLS-DA) and support vector machine discriminant analysis (SVMDA) to discriminate

hazelnuts on the basis of the PDO ‘Nocciola Romana’ regulation. The best results were obtained with SVMDA and PLSDA, that showed very good recognition performances (with a classification accuracy > 95%) (18).

4.1.4 Challenges in the traceability and authentication of hazelnuts

Currently, the identification of the origin of raw hazelnuts remains a great problem for the food industry. Here, we faced this problem from two different points of view: on one hand, the use of elemental profiling for the authentication and the traceabilty of hazelnut cultivar along the production chain of hazelnut paste; on the other hand, the use of a simple, fast and accurate analytical method for their classification and authentication, based on IR spectroscopy, able to perform non-destructive analyses on the samples, with an environmentally friendly sample preparation (71). In both cases, multivariate classification tools were applied to build authentication models.

4.2 Traceability and authentication study along the production chain of hazelnut paste by elemental profiling

We applied elemental and REEs profiling through Inductively Coupled Plasma – Mass Spectrometry (ICP-MS) and ICP – Optical Emission Spectroscopy (OES) in an authentication study involving the production chain of hazelnut paste: from raw fruits, to roasted hazelnuts, down to the final paste. The study involves three different cultivars ("Tonda Gentile delle Langhe", "Romana" and "Mortarella") and the data were treated by multivariate statistical classification methods to provide a model able to discriminate the three cultivars independently from the type of technological transformation.

4.2.1 Materials and methods

4.2.1.1 Reagents

Nitric Acid 69% Trace Select and hydrogen peroxide H_2O_2 30% Trace Select were purchased from Fluka Analytical (Buchs, Switzerland); multielemental standard Solutions CCS1, CCS2, CCS4, CCS5, CCS6, for the calibration of the ICP-MS and ICP-OES, were purchased from Inorganic Ventures (Christiansburg, VA, USA). Ultrapure water was obtained through a Millipore Milli-Q system (Milford, USA).

4.2.1.2 Samples

Hazelnut samples were bought directly from local producers. Samples belong to three different cultivars: "Tonda Gentile delle Langhe", "Romana" and "Mortarella". For each cultivar, three to four different batches were available, each corresponding to a different production lot either from the same producer or from a different one, located in the same geographical area. For each cultivar, the production chain involved: raw hazelnuts, roasted hazelnuts and paste. The same production lots were available both as raw and roasted, while not all the production lots were available as

a paste. For each final sample (cultivar/type of product/lot), at least three analytical replications (from the mineralization step to the final instrumental determinations) were performed. Each cultivar was therefore characterized by 3-4 lots, each replicated 3-4 times and present as raw, roasted or paste samples. The samples available were therefore 119: 31 samples from "Romana" cultivar (12 raw, 12 roasted, 7 paste), 47 samples from "Mortarella" cultivar (16 raw, 15 roasted, 16 paste) and 41 samples from "Tonda Gentile delle Langhe" cultivar (14 raw, 14 roasted, 13 paste).

Each sample was characterized by a four-digit label: a letter indicating the cultivar (M for "Mortarella", P for "Tonda Gentile delle Langhe", R for "Romana") followed by a number indicating the lot (1 to 4), a letter indicating the type of samples (C for raw hazelnuts, T for roasted hazelnuts and P for paste) and a final progressive number indicating the analytical replication.

4.2.1.3 Sample digestion

Samples were first grinded in a mortar and put in a stove for at least 12h at 105°C until constant weight was achieved. Elemental analysis was carried out after microwave-assisted digestion using a microwave oven MDS 2000 (CEM Corporation, Matthews, NC, USA). 0.5000 g of sample (raw or roasted hazelnuts or hazelnut paste) were put in a Teflon vessel (CEM Corporation, Matthews, NC, USA) and added with 5 mL of nitric acid 69%. A first mineralization step in the microwave oven was accomplished at 630 W, with the following pressure gradient: 20 psi in 15 min with 5 min of rest time, 40 psi in 15 min with 5 min of rest time, 85 psi in 15 min with 5 min of rest time, 150 psi in 15 min with 5 min of rest time, 200 psi in 15 min with 5 min of rest time. Then 1 mL of H_2O_2 30% was added and a second mineralization step took place in the microwave oven, at 630W with a pressure gradient achieving a final pressure of 100 psi in 15 min with 5 min of rest time.

After mineralization, the solution was diluted to 50 mL with ultrapure water and further diluted 1:10 v/v with nitric acid 1% for ICP-MS analysis and 1:5 v/v with nitric acid 1% for ICP-OES analysis.

4.2.1.4 ICP-MS analysis

For the determination of metals and rare earths (45Sc, 51V, 52Cr, 55Mn, 56Fe, 59Co, 60Ni, 63Cu, 65Cu, 66Zn, 71Ga, 75As, 78Se, 88Sr, 89Y, 107Ag, 111Cd, 120Sn, 138Ba, 139La, 140Ce, 141Pr, 146Nd, 147Sm, 153Eu, 158Gd, 159Tb, 163Dy, 165Ho, 166Er, 169Tm, 172Yb, 175Lu, 187Re, 193Ir, 206Pb, 207Pb, 208Pb, 232Th, 238U) an inductively coupled plasma with mass spectrometry (ICP-MS 7700X Agilent) was used. The instrumental signal acquisition parameters are: reported in table 1.

Parameter	**Value**
Number of Points per Mass:	3
Number of repetitions	3
Total Acquisition Time	653 sec
Set Peristaltic Pump Program:	
Before Acquisition:	
Uptake speed:	0.40 rps
Uptake time:	45 sec
Stabilization time:	35 sec
After acquisition (Probe Rinse):	
Rinse speed:	10^{-2} rps
Rinse on rinse port (sample)	5 sec
Rinse on rinse port (STD)	5 sec
After Acquisition (Rinse)	
Rinse vial1	2
Rinse speed	0.30 rps
Rinse on rinse vial (step 1):	30 sec
Rinse on rinse port (Step 1):	0 sec

***Table 1**: ICP-MS experimental settings.*

Each calibration curve was calculated by means of the following 7 standard solutions: 0.000100 μgL^{-1}, 0.00100 μgL^{-1}, 0.0100 μgL^{-1}, 0.100 μgL^{-1}, 1.00 μgL^{-1}, 10.0 μgL^{-1}, 100 μgL^{-1}, covering a concentration range of 7 orders of magnitude. A weighted least square fitting was used, weighting the errors by the inverse of the concentration level. Table 2 reports the LOD and LOQ for each investigated isotope, determined by the calibration curve method (72,73).

	LOD	**LOQ**			**LOD**	**LOQ**
45Sc	0.011	0.030		**140Ce**	0.00024	0.00082
51V	0.0039	0.0053		**141Pr**	0.00038	0.00020
52Cr	0.011	0.031		**146Nd**	0.0011	0.00097
55Mn	0.0040	0.065		**147Sm**	0.0010	0.00069
56Fe	0.085	0.15		**153Eu**	0.00034	0.00010
59Co	0,00081	0.0042		**158Gd**	0.00033	0.00052
60Ni	0.016	0.094		**159Tb**	0.0011	0.0064
63Cu	0.38	0.67		**163Dy**	0.00067	0.00013
65Cu	0.56	0.68		**165Ho**	0.0010	0.0066
66Zn	0.77	2.76		**166Er**	0.00020	0.00014
71Ga	0.0037	0.0057		**169Tm**	0.00023	0.000076
75As	0.014	0.010		**172Yb**	0.00083	0.00042
78Se	0,35	0.80		**175Lu**	0.00020	0.00015
88Sr	0.0078	0.049		**187Re**	0.0014	0.0063
89Y	0.0037	0.0095		**193Ir**	0.00013	0.00043
107Ag	0.019	0.038		**206Pb**	0.011	0.14
111Cd	0.0039	0.0078		**207Pb**	0.028	0.14
120Sn	0.0044	0.041		**208Pb**	0.0044	0.13
138Ba	0.0080	0.092		**232Th**	0.00024	0.00022
139La	0.00096	0.00071		**238U**	0.00034	0.00026

***Table 2**: LOD and LOQ values for all isotopes expressed in μgL^{-1}*

4.2.1.5 ICP-OES analysis

Majority elements (Ca, Fe, Mg, Na, P, S, Si, Al) were determined by a Spectro Genesis inductively coupled plasma with optical emission (ICP-OES) (Spectro Genesisi *Ametek* – Berwyn, PA, USA) equipped with a cross-flow nebulizer, a double-pass Scott spray chamber and an ASX-260 autosampler (*CETAC Technologies* – Omaha, NE, USA). Signals were elaborated by Spectro Smart Analyzer Vision software (ver. 5.06). Plasma worked at the power of 1400 W; coolant, auxiliary and nebulizer flow rates were set at 12.00, 1.00 and 1.00 L/min respectively. Peristaltic pump run at 2 (on a scale from 1 to 5), except for preflush which was set at 4. Results were given as average value of three instrumental replications. For each analyte, the following wavelengths were used for quantification: 317.933 nm (Ca), 259.941 nm (Fe), 279.553 nm (Mg), 588.995 nm (Na), 214.914 nm (P), 182.034 nm (S), 251.612 nm (Si), 396.152 nm (Al). Each calibration curve was calculated by means of the following 5 standard solutions: 0.0100 mgL^{-1}; 0.0500 mgL^{-1}; 0.100 mgL^{-1}; 0.500 mgL^{-1}; 1.00 mgL^{-1}; 5.00 mgL^{-1}. As for ICP-MS analysis, a weighted least square fitting was used. LOD and LOQ for each investigated analyte (72,73) are reported in Table 3.

Element	**LOD**	**LOQ**
Ca	0.016	0.024
Fe	0.0048	0.0072
Mg	0.011	0.017
Na	0.045	0.067
P	0.012	0.018
S	0.027	0.040
Si	0.0088	0.013
Al	0.0057	0.0086

***Table 3**: LOD and LOQ values for all isotopes expressed in mgL^{-1}*

4.2.1.6 Software

Data analysis and all graphical representations were performed by The Unscrambler X 10.3 (Camo, Norway), Statistica v.7.1 (StatSoft Inc, Tulsa, OK, USA), Matlab R2014b (The Mathworks, Natick, MA, USA), the Classification Toolbox for Matlab (Milano Chemometrics group, University of Milano Bicocca, Italy) (53), Parvus (Prof Michele Forina, University of Genova, Italy) and Excel 2013 (Microsoft Corporation, Redmond, WA, USA).

4.2.2 Results and Discussion

Table 4 reports the concentration levels, expressed as μg/kg of product, of each analyte within each cultivar and each type of product separately, together to the corresponding standard deviation.

	Mortarella		
	Raw	**Roasted**	**Paste**
45Sc	$(6.6 \pm 2.1)10^{0}$	$(7.4 \pm 2.0)10^{0}$	$(8.0 \pm 2.5)10^{0}$
51V	$(1.28 \pm 0.28)10^{1}$	$(9.5 \pm 3.2)10^{0}$	$(1.9 \pm 1.2)10^{1}$
52Cr	$(3.5 \pm 1.9)10^{2}$	$(3.2 \pm 2.4)10^{2}$	$(5.5 \pm 4.7)10^{2}$
55Mn	$(6.9 \pm 3.3)10^{4}$	$(1.09 \pm 0.81)10^{5}$	$(7.9 \pm 2.2)10^{4}$
56Fe	$(9.3 \pm 1.6)10^{4}$	$(9.3 \pm 1.1)10^{4}$	$(9.2 \pm 1.7)10^{4}$
59Co	$(1.7 \pm 1.2)10^{2}$	$(1.29 \pm 0.60)10^{2}$	$(2.09 \pm 0.89)10^{2}$
60Ni	$(1.03 \pm 0.24)10^{3}$	$(9.9 \pm 4.9)10^{2}$	$(1.67 \pm 0.86)10^{3}$
63Cu	$(3.4 \pm 0.80)10^{4}$	$(3.48 \pm 0.58)10^{4}$	$(3.63 \pm 0.48)10^{4}$
65Cu	$(3.36 \pm 0.94)10^{4}$	$(3.49 \pm 0.59)10^{4}$	$(3.63 \pm 0.51)10^{4}$
66Zn	$(3.6 \pm 0.57)10^{4}$	$(3.69 \pm 0.48)10^{4}$	$(3.54 \pm 0.42)10^{4}$
71Ga	$(3.5 \pm 1.1)10^{0}$	$(3.4 \pm 1.4)10^{0}$	$(4.9 \pm 2.2)10^{0}$
75As	$(4.75 \pm 0.88)10^{1}$	$(4.41 \pm 0.91)10^{1}$	$(5.8 \pm 1.4)10^{1}$
78Se	$(2.7 \pm 1.5)10^{2}$	$(2.6 \pm 1.7)10^{2}$	$(2.6 \pm 1.6)10^{2}$
88Sr	$(4.1 \pm 1.6)10^{4}$	$(5.5 \pm 3.4)10^{4}$	$(4.0 \pm 1.3)10^{4}$
89Y	$(4.7 \pm 1.7)10^{0}$	$(5.9 \pm 4.0)10^{0}$	$(7.2 \pm 3.0)10^{0}$
107Ag	$(5.3 \pm 4.2)10^{1}$	$(4.9 \pm 5.1)10^{1}$	$(6.5 \pm 6.9)10^{1}$
111Cd	$(1.83 \pm 0.53)10^{1}$	$(2.6 \pm 1.4)10^{1}$	$(1.81 \pm 0.41)10^{1}$

120Sn	$(3.9 \pm 1.8)10^{1}$	$(3.5 \pm 2.0)10^{1}$	$(1.14 \pm 0.91)10^{2}$
138Ba	$(1.70 \pm 0.78)10^{4}$	$(2.1 \pm 1.2)10^{4}$	$(1.74 \pm 0.63)10^{4}$
139La	$(7.6 \pm 2.3)10^{0}$	$(7.2 \pm 5.5)10^{0}$	$(9.9 \pm 8.2)10^{0}$
140Ce	$(9.6 \pm 2.8)10^{0}$	$(6.6 \pm 3.4)10^{0}$	$(1.6 \pm 1.3)10^{1}$
141Pr	$(1.07 \pm 0.30)10^{0}$	$(7.9 \pm 3.7)10^{-1}$	$(1.8 \pm 1.6)10^{0}$
146Nd	$(4.9 \pm 1.4)10^{0}$	$(3.7 \pm 1.8)10^{0}$	$(7.6 \pm 6.4)10^{0}$
147Sm	$(9.8 \pm 2.6)10^{-1}$	$(8.6 \pm 3.6)10^{-1}$	$(1.5 \pm 1.1)10^{0}$
153Eu	$(5.8 \pm 2.5)10^{0}$	$(7.5 \pm 4.1)10^{0}$	$(6.1 \pm 2.0)10^{0}$
158Gd	$(9.5 \pm 2.5)10^{-1}$	$(7.6 \pm 3.7)10^{-1}$	$(1.4 \pm 1.1)10^{0}$
159Tb	$(5.6 \pm 3.2)10^{-1}$	$(7.7 \pm 3.6)10^{-1}$	$(1.12 \pm 0.61)10^{0}$
163Dy	$(6.1 \pm 1.4)10^{-1}$	$(5.9 \pm 2.9)10^{-1}$	$(8.1 \pm 5.0)10^{-1}$
165Ho	$(4.8 \pm 2.8)10^{-1}$	$(7.1 \pm 3.7)10^{-1}$	$(9.7 \pm 5.9)10^{-1}$
166Er	$(2.68 \pm 0.70)10^{-1}$	$(2.7 \pm 1.5)10^{-1}$	$(3.6 \pm 2.1)10^{-1}$
169Tm	$(4.7 \pm 2.4)10^{-2}$	$(3.7 \pm 2.2)10^{-2}$	$(5.6 \pm 3.3)10^{-2}$
172Yb	$(2.97 \pm 0.85)10^{-1}$	$(2.4 \pm 1.2)10^{-1}$	$(3.8 \pm 2.3)10^{-1}$
175Lu	$(4.8 \pm 2.4)10^{-2}$	$(5.3 \pm 2.7)10^{-2}$	$(7.0 \pm 3.8)10^{-2}$
187Re	$(4.6 \pm 2.9)10^{-1}$	$(7.3 \pm 4.8)10^{-1}$	$(1.04 \pm 0.61)10^{0}$
193Ir	$(1.14 \pm 0.99)10^{-1}$	$(10.0 \pm 6.0)10^{-2}$	$(8.2 \pm 3.4)10^{-2}$
206Pb	$(1.4 \pm 2.8)10^{2}$	$(7.0 \pm 5.3)10^{1}$	$(1.49 \pm 0.70)10^{2}$
207Pb	$(1.3 \pm 2.7)10^{2}$	$(6.5 \pm 4.9)10^{1}$	$(1.38 \pm 0.65)10^{2}$
208Pb	$(1.2 \pm 2.4)10^{2}$	$(5.9 \pm 4.4)10^{1}$	$(1.25 \pm 0.59)10^{2}$
232Th	$(1.66 \pm 0.55)10^{0}$	$(1.16 \pm 0.79)10^{0}$	$(3.3 \pm 3.5)10^{0}$
238U	$(1.32 \pm 0.93)10^{0}$	$(1.18 \pm 0.95)10^{0}$	$(2.3 \pm 1.2)10^{0}$
Ca	$(1.49 \pm 0.29)10^{6}$	$(1.47 \pm 0.29)10^{6}$	$(1.32 \pm 0.19)10^{6}$
Fe	$(4.49 \pm 0.63)10^{4}$	$(4.41 \pm 0.31)10^{4}$	$(4.16 \pm 0.80)10^{4}$
Mg	$(1.670 \pm 0.094)10^{6}$	$(1.65 \pm 0.12)10^{6}$	$(1.48 \pm 0.13)10^{6}$
Na	$(1.75 \pm 0.72)10^{4}$	$(1.67 \pm 0.95)10^{4}$	$(2.19 \pm 0.50)10^{4}$
P	$(2.15 \pm 0.24)10^{6}$	$(2.01 \pm 0.12)10^{6}$	$(1.97 \pm 0.20)10^{6}$
S	$(1.66 \pm 0.11)10^{6}$	$(1.66 \pm 0.16)10^{6}$	$(1.45 \pm 0.14)10^{6}$
Si	$(1.20 \pm 0.55)10^{4}$	$(1.23 \pm 0.84)10^{4}$	$(1.08 \pm 0.51)10^{4}$
Al	$(5.2 \pm 2.2)10^{3}$	$(3.6 \pm 1.5)10^{3}$	$(6.7 \pm 3.6)10^{3}$

	Piemonte IGP		
	Raw	**Roasted**	**Paste**
45Sc	$(6.3 \pm 1.4)10^{0}$	$(5.7 \pm 3.9)10^{0}$	$(6.5 \pm 1.5)10^{0}$

51V	$(1.31 \pm 0.28)10^{1}$	$(3.50 \pm 10.1)10^{1}$	$(1.10 \pm 0.54)10^{1}$
52Cr	$(3.1 \pm 2.2)10^{2}$	$(3.4 \pm 2.8)10^{2}$	$(9.5 \pm 9.3)10^{2}$
55Mn	$(5.3 \pm 1.6)10^{4}$	$(7.8 \pm 4.6)10^{4}$	$(5.0 \pm 1.7)10^{4}$
56Fe	$(7.0 \pm 1.0)10^{4}$	$(5.9 \pm 1.4)10^{4}$	$(6.5 \pm 2.0)10^{4}$
59Co	$(1.15 \pm 0.32)10^{2}$	$(2.9 \pm 1.7)10^{2}$	$(1.48 \pm 0.52)10^{2}$
60Ni	$(4.8 \pm 1.2)10^{3}$	$(5.9 \pm 1.6)10^{3}$	$(3.7 \pm 1.4)10^{3}$
63Cu	$(2.95 \pm 0.86)10^{4}$	$(2.89 \pm 0.62)10^{4}$	$(2.70 \pm 0.58)10^{4}$
65Cu	$(2.8 \pm 1.0)10^{4}$	$(2.83 \pm 0.71)10^{4}$	$(2.63 \pm 0.71)10^{4}$
66Zn	$(3.0 \pm 1.1)10^{4}$	$(3.05 \pm 0.51)10^{4}$	$(2.61 \pm 0.56)10^{4}$
71Ga	$(3.8 \pm 1.2)10^{0}$	$(3.33 \pm 0.79)10^{0}$	$(3.17 \pm 0.79)10^{0}$
75As	$(3.9 \pm 1.2)10^{1}$	$(4.1 \pm 2.1)10^{1}$	$(3.79 \pm 0.68)10^{1}$
78Se	$(2.8 \pm 1.1)10^{2}$	$(2.6 \pm 1.5)10^{2}$	$(3.4 \pm 3.1)10^{2}$
88Sr	$(1.19 \pm 0.14)10^{4}$	$(1.18 \pm 0.27)10^{4}$	$(1.45 \pm 0.61)10^{4}$
89Y	$(5.2 \pm 1.0)10^{0}$	$(3.2 \pm 1.0)10^{0}$	$(4.1 \pm 1.1)10^{0}$
107Ag	$(4.3 \pm 2.8)10^{1}$	$(5.8 \pm 4.1)10^{1}$	$(5.6 \pm 4.9)10^{1}$
111Cd	$(1.68 \pm 0.93)10^{1}$	$(3.4 \pm 2.5)10^{1}$	$(1.46 \pm 0.87)10^{1}$
120Sn	$(5.7 \pm 6.7)10^{1}$	$(3.8 \pm 2.5)10^{1}$	$(5.4 \pm 5.2)10^{1}$
138Ba	$(5.7 \pm 2.8)10^{3}$	$(7.0 \pm 2.6)10^{3}$	$(7.9 \pm 3.9)10^{3}$
139La	$(5.8 \pm 2.9)10^{0}$	$(2.94 \pm 0.66)10^{0}$	$(3.6 \pm 1.1)10^{0}$
140Ce	$(9.8 \pm 5.0)10^{0}$	$(4.6 \pm 1.8)10^{0}$	$(5.9 \pm 1.6)10^{0}$
141Pr	$(1.10 \pm 0.54)10^{0}$	$(5.0 \pm 2.0)10^{-1}$	$(6.0 \pm 1.5)10^{-1}$
146Nd	$(5.4 \pm 2.6)10^{0}$	$(2.6 \pm 1.1)10^{0}$	$(2.94 \pm 0.74)10^{0}$
147Sm	$(1.18 \pm 0.50)10^{0}$	$(6.7 \pm 2.6)10^{-1}$	$(6.6 \pm 2.1)10^{-1}$
153Eu	$(2.11 \pm 0.97)10^{0}$	$(2.46 \pm 0.84)10^{0}$	$(2.7 \pm 1.2)10^{0}$
158Gd	$(1.17 \pm 0.50)10^{0}$	$(6.1 \pm 2.7)10^{-1}$	$(7.1 \pm 1.6)10^{-1}$
159Tb	$(5.5 \pm 3.2)10^{-1}$	$(2.6 \pm 3.5)10^{-1}$	$(6.8 \pm 2.6)10^{-1}$
163Dy	$(7.8 \pm 2.3)10^{-1}$	$(4.5 \pm 1.3)10^{-1}$	$(4.6 \pm 1.2)10^{-1}$
165Ho	$(4.4 \pm 2.6)10^{-1}$	$(2.2 \pm 3.0)10^{-1}$	$(5.6 \pm 2.3)10^{-1}$
166Er	$(3.23 \pm 0.80)10^{-1}$	$(2.12 \pm 0.62)10^{-1}$	$(2.01 \pm 0.43)10^{-1}$
169Tm	$(4.6 \pm 2.1)10^{-2}$	$(2.76 \pm 0.73)10^{-2}$	$(2.6 \pm 1.0)10^{-2}$
172Yb	$(3.3 \pm 1.0)10^{-1}$	$(1.91 \pm 0.67)10^{-1}$	$(2.05 \pm 0.62)10^{-1}$
175Lu	$(5.2 \pm 2.4)10^{-2}$	$(2.5 \pm 1.4)10^{-2}$	$(3.37 \pm 0.90)10^{-2}$
187Re	$(3.5 \pm 2.0)10^{-1}$	$(2.1 \pm 2.9)10^{-1}$	$(5.2 \pm 2.6)10^{-1}$
193Ir	$(6.0 \pm 2.9)10^{-2}$	$(6.2 \pm 5.9)10^{-2}$	$(7.0 \pm 4.3)10^{-2}$
206Pb	$(1.5 \pm 1.0)10^{2}$	$(1.3 \pm 1.4)10^{2}$	$(1.22 \pm 0.90)10^{2}$

207Pb	$(1.40 \pm 0.97)10^{2}$	$(1.2 \pm 1.4)10^{2}$	$(1.13 \pm 0.87)10^{2}$
208Pb	$(1.27 \pm 0.87)10^{2}$	$(1.1 \pm 1.2)10^{2}$	$(1.02 \pm 0.78)10^{2}$
232Th	$(1.36 \pm 0.58)10^{0}$	$(8.0 \pm 3.4)10^{-1}$	$(8.2 \pm 2.5)10^{-1}$
238U	$(1.20 \pm 0.76)10^{0}$	$(8.3 \pm 3.4)10^{-1}$	$(1.20 \pm 0.66)10^{0}$
Ca	$(1.32 \pm 0.17)10^{6}$	$(1.26 \pm 0.18)10^{6}$	$(1.08 \pm 0.20)10^{6}$
Fe	$(3.45 \pm 0.48)10^{4}$	$(2.98 \pm 0.60)10^{4}$	$(3.07 \pm 0.86)10^{4}$
Mg	$(1.63 \pm 0.16)10^{6}$	$(1.71 \pm 0.12)10^{6}$	$(1.31 \pm 0.24)10^{6}$
Na	$(2.12 \pm 0.78)10^{4}$	$(2.09 \pm 0.59)10^{4}$	$(1.76 \pm 0.63)10^{4}$
P	$(2.17 \pm 0.30)10^{6}$	$(2.41 \pm 0.19)10^{6}$	$(1.72 \pm 0.34)10^{6}$
S	$(1.63 \pm 0.21)10^{6}$	$(1.57 \pm 0.11)10^{6}$	$(1.24 \pm 0.24)10^{6}$
Si	$(1.64 \pm 0.54)10^{4}$	$(1.16 \pm 0.33)10^{4}$	$(1.26 \pm 0.57)10^{4}$
Al	$(5.7 \pm 1.8)10^{3}$	$(4.4 \pm 2.0)10^{3}$	$(4.5 \pm 1.2)10^{3}$
	Romana		
	Raw	**Roasted**	**Paste**
45Sc	$(7.3 \pm 4.4)10^{0}$	$(6.8 \pm 2.4)10^{0}$	$(4.6 \pm 2.4)10^{0}$
51V	$(1.54 \pm 0.38)10^{1}$	$(1.33 \pm 0.76)10^{1}$	$(8.0 \pm 4.1)10^{0}$
52Cr	$(4.2 \pm 2.5)10^{2}$	$(3.8 \pm 2.2)10^{2}$	$(3.7 \pm 5.1)10^{2}$
55Mn	$(1.13 \pm 0.15)10^{0}$	$(8.3 \pm 2.0)10^{4}$	$(8.4 \pm 4.2)10^{4}$
56Fe	$(9.5 \pm 1.2)10^{4}$	$(9.7 \pm 1.6)10^{4}$	$(6.7 \pm 3.1)10^{4}$
59Co	$(3.7 \pm 1.7)10^{2}$	$(2.73 \pm 0.98)10^{2}$	$(1.69 \pm 0.94)10^{2}$
60Ni	$(1.42 \pm 0.65)10^{3}$	$(1.37 \pm 0.85)10^{3}$	$(1.11 \pm 0.61)10^{3}$
63Cu	$(4.04 \pm 0.59)10^{4}$	$(3.62 \pm 0.96)10^{4}$	$(2.7 \pm 1.3)10^{4}$
65Cu	$(4.07 \pm 0.58)10^{4}$	$(3.65 \pm 0.97)10^{4}$	$(2.6 \pm 1.3)10^{4}$
66Zn	$(3.71 \pm 0.61)10^{4}$	$(4.4 \pm 1.7)10^{4}$	$(2.8 \pm 1.3)10^{4}$
71Ga	$(5.2 \pm 1.3)10^{0}$	$(3.62 \pm 0.90)10^{0}$	$(2.9 \pm 1.7)10^{0}$
75As	$(9.1 \pm 7.2)10^{1}$	$(7.4 \pm 3.4)10^{1}$	$(4.6 \pm 1.8)10^{1}$
78Se	$(2.9 \pm 1.3)10^{2}$	$(1.98 \pm 0.96)10^{2}$	$(1.17 \pm 0.48)10^{2}$
88Sr	$(7.7 \pm 2.6)10^{4}$	$(1.06 \pm 0.23)10^{5}$	$(5.9 \pm 2.9)10^{4}$
89Y	$(7.9 \pm 2.1)10^{0}$	$(6.6 \pm 2.1)10^{0}$	$(5.4 \pm 1.5)10^{0}$
107Ag	$(6.2 \pm 3.1)10^{1}$	$(3.7 \pm 2.3)10^{1}$	$(2.0 \pm 1.8)10^{1}$
111Cd	$(1.84 \pm 0.64)10^{1}$	$(1.92 \pm 0.79)10^{1}$	$(1.33 \pm 0.62)10^{1}$
120Sn	$(9.0 \pm 11.1)10^{1}$	$(6.3 \pm 3.0)10^{1}$	$(3.6 \pm 4.2)10^{1}$
138Ba	$(3.1 \pm 1.7)10^{4}$	$(3.8 \pm 1.9)10^{4}$	$(2.9 \pm 1.6)10^{4}$
139La	$(1.50 \pm 0.32)10^{1}$	$(1.9 \pm 3.2)10^{1}$	$(5.3 \pm 2.6)10^{0}$
140Ce	$(1.98 \pm 0.35)10^{1}$	$(1.20 \pm 0.57)10^{1}$	$(7.0 \pm 3.6)10^{0}$

141Pr	$(2.30 \pm 0.62)10^{0}$	$(1.46 \pm 0.69)10^{0}$	$(8.3 \pm 4.4)10^{-1}$
146Nd	$(9.6 \pm 1.8)10^{0}$	$(6.5 \pm 3.1)10^{0}$	$(3.8 \pm 2.0)10^{0}$
147Sm	$(2.06 \pm 0.74)10^{0}$	$(1.53 \pm 0.77)10^{0}$	$(8.8 \pm 4.8)10^{-1}$
153Eu	$(1.07 \pm 0.53)10^{1}$	$(1.24 \pm 0.53)10^{1}$	$(9.2 \pm 5.4)10^{0}$
158Gd	$(1.92 \pm 0.67)10^{0}$	$(1.30 \pm 0.56)10^{0}$	$(8.1 \pm 4.0)10^{-1}$
159Tb	$(8.09 \pm 8.09)10^{-1}$	$(5.7 \pm 3.3)10^{-1}$	$(8.8 \pm 9.6)10^{-1}$
163Dy	$(1.11 \pm 0.57)10^{0}$	$(8.1 \pm 3.1)10^{-1}$	$(5.6 \pm 2.8)10^{-1}$
165Ho	$(7.5 \pm 8.5)10^{-1}$	$(5.2 \pm 3.0)10^{-1}$	$(7.9 \pm 9.2)10^{-1}$
166Er	$(5.6 \pm 4.3)10^{-1}$	$(3.7 \pm 1.8)10^{-1}$	$(2.3 \pm 1.2)10^{-1}$
169Tm	$(1.9 \pm 4.1)10^{-1}$	$(8.18 \pm 0.11)10^{-2}$	$(3.1 \pm 2.0)10^{-2}$
172Yb	$(5.9 \pm 5.3)10^{-1}$	$(3.7 \pm 2.1)10^{-1}$	$(2.3 \pm 1.1)10^{-1}$
175Lu	$(1.8 \pm 4.0)10^{-1}$	$(8.51 \pm 0.13)10^{-2}$	$(3.4 \pm 2.3)10^{-2}$
187Re	$(7.1 \pm 9.4)10^{-1}$	$(4.3 \pm 3.5)10^{-1}$	$(7.1 \pm 8.7)10^{-1}$
193Ir	$(2.3 \pm 3.7)10^{-1}$	$(1.6 \pm 2.0)10^{-1}$	$(6.9 \pm 5.0)10^{-2}$
206Pb	$(9.6 \pm 6.3)10^{1}$	$(1.18 \pm 0.95)10^{2}$	$(1.10 \pm 0.84)10^{2}$
207Pb	$(9.2 \pm 6.1)10^{1}$	$(1.12 \pm 0.89)10^{2}$	$(1.01 \pm 0.78)10^{2}$
208Pb	$(8.2 \pm 5.5)10^{1}$	$(1.01 \pm 0.80)10^{2}$	$(9.2 \pm 7.1)10^{1}$
232Th	$(4.60 \pm 0.82)10^{0}$	$(2.9 \pm 1.9)10^{0}$	$(1.38 \pm 0.73)10^{0}$
238U	$(3.4 \pm 1.8)10^{0}$	$(3.8 \pm 3.6)10^{0}$	$(1.1 \pm 0.75)10^{0}$
Ca	$(1.34 \pm 0.18)10^{6}$	$(1.77 \pm 0.40)10^{6}$	$(1.50 \pm 0.22)10^{6}$
Fe	$(4.60 \pm 0.40)10^{4}$	$(5.04 \pm 0.82)10^{4}$	$(4.0 \pm 0.61)10^{4}$
Mg	$(1.79 \pm 0.12)10^{6}$	$(1.95 \pm 0.21)10^{6}$	$(1.57 \pm 0.18)10^{6}$
Na	$(1.44 \pm 0.98)10^{4}$	$(1.41 \pm 0.82)10^{4}$	$(2.23 \pm 0.48)10^{4}$
P	$(2.40 \pm 0.28)10^{6}$	$(2.55 \pm 0.33)10^{6}$	$(2.00 \pm 0.28)10^{6}$
S	$(1.76 \pm 0.12)10^{6}$	$(2.02 \pm 0.24)10^{6}$	$(1.61 \pm 0.18)10^{6}$
Si	$(1.85 \pm 0.70)10^{4}$	$(1.48 \pm 0.61)10^{4}$	$(1.11 \pm 0.42)10^{4}$
Al	$(5.9 \pm 1.3)10^{3}$	$(4.9 \pm 2.5)10^{3}$	$(4.0 \pm 2.0)10^{3}$

Table 4*: the concentration levels expressed as μg/kg of product together to the corresponding standard deviation*

The analytes can be ideally divided into three groups:

- majority elements (Ca, Mg, P, S), with concentration levels in the range of g/kg;

- trace elements (Fe, Na, Si, Al, Ni, Cu, Zn, Sr, Ba), with concentration levels in the range of ppm;
- micro-trace elements (V, Cr, Co, As, Se, Ag, Cd, La, Ce, Eu, Pb), with concentration levels in the range of ppb;
- ultra-trace elements (Sc, Mn, Ga, Y, Sn, Pr, Nd, Sm, Gd, Dy, Re, Ir, Th, U), with concentrations levels in the range of ppt.

Looking at the raw data, it is not possible to identify elements with an increasing or decreasing trend along the production chain (raw / roasted / paste), considering the great variability of the data collected. Similarly, differences in the concentration levels of single elements cannot be identified by a direct comparison of the concentration levels of the different cultivars.

4.2.2.1 Principal Component Analysis (PCA)

Since in principle, the absolute concentration level of the analytes could vary along the production chain in the order: raw > roasted > paste, the absolute concentration levels are not a good choice for describing the data. Data were therefore scaled for each analyte independently since each analyte could be used as a normalizing factor. (as described in section 1.1.3.1)

The final dataset has therefore size 119 x 2068 (119 being the number of samples and 2068 being the number of ratios of each analyte with respect to all the others) (^{159}Tb, ^{165}Ho, ^{187}Re and ^{193}Ir were eliminated as normalizing factors since some null values were present).

A first PCA carried out on the dataset, after autoscaling, showed that a slight differentiation of the samples according to the type of product is present notwithstanding the predominance of the information about the cultivar. In order to remove this source of confounding information, data were first centered with respect to the mean of each type of product (raw, roasted or paste), and then autoscaled (mean-centered and normalized to unit variance).

Figure 1 reports the score plot of the first two PCs that account for about 28% of the overall variance contained in the dataset (respectively PC_1=17%, PC_2=11%, PC_3=8%, PC_4=7%). Figure 1 reports two representations of the same score plot: one where the samples are labelled according to the different cultivar (figure 1a) and the other with a labelling related to the type of sample (figure 1b): the score plot reports a quite clear separation of the samples according to the cultivar along the first PC, with R samples at negative values along PC_1, P samples at positive values and M samples at intermediate levels. The same plot shows no differentiation of the samples according to the different type of sample investigated.

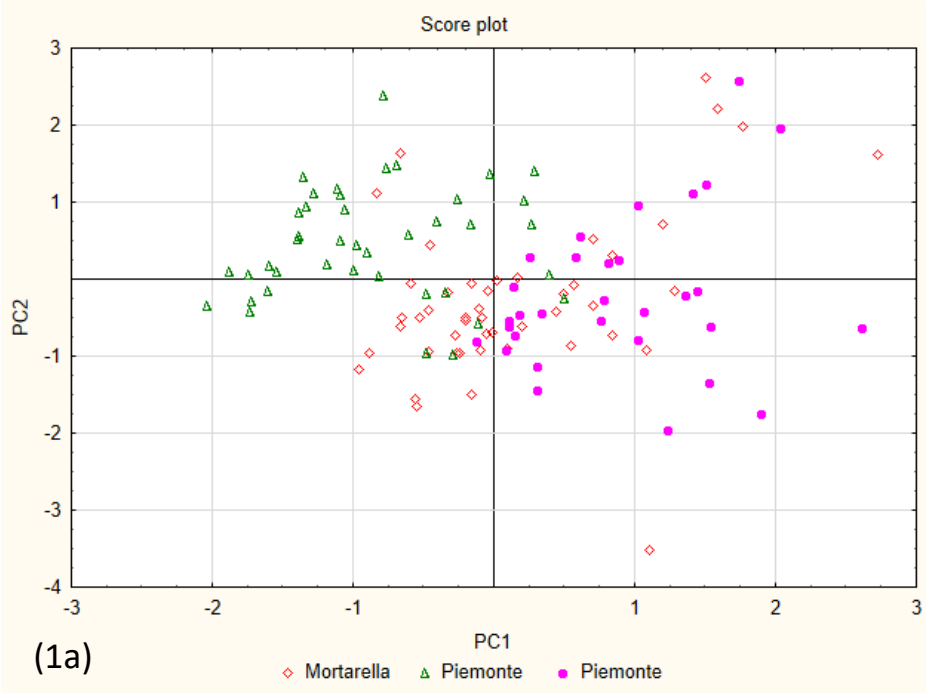

(1a)

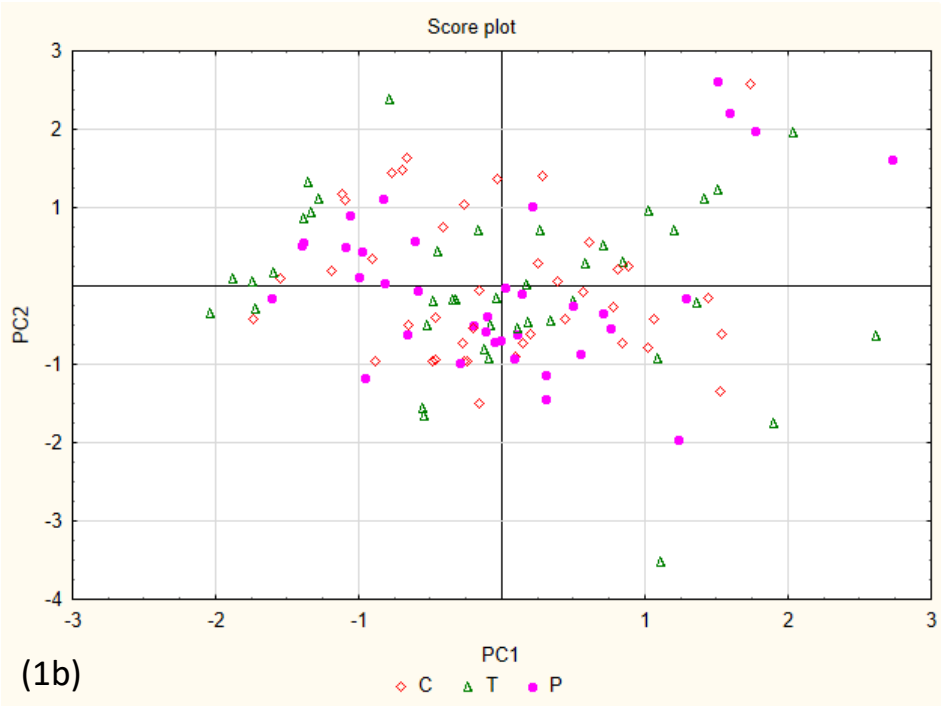

Figure 1*: results of PCA carried out on the overall dataset. Score plot of the first two PCs labelling the samples according to the cultivar (a) and to the type of product (b).*

4.2.2.2 Partial-Least-Squares Discriminant Analysis (PLS-DA)

Classification tools were then applied to identify the variables responsible for the differences between the cultivars, independently from the technological treatment that hazelnut samples underwent. To this purpose, PLS-DA was applied with an iterative variable selection procedure in backward elimination: at each iteration, the variables with the least classification ability are eliminated according to the minor error in cross-validation; the excluded variables are characterized by the smallest importance (55) and no more than 3% of the variables is eliminated at each iteration. Cross-validation was accomplished by a leave-more-out (LMO) procedure with 5 cancellation groups, eliminating at each cycle all the replications of the same sample in order to make the validation more genuine. Three PLS-DA models were obtained, each discriminating one class from the others. The final model was obtained by

merging the variables selected by the three independent models and contained 421 variables. The best performance was obtained with a final model containing five LVs (table 5), explaining 49% of the information about class belonging and 85% of the elemental profile.

	X		Y		X		Y	
	% Expl. Var. Fitting	% Expl. Var. CV	% Expl. Var. Fitting	% Expl. Var. CV	% Cum. Expl. Var. Fitting	% Cum. Expl. Var. CV	% Cum. Expl. Var. Fitting	% Cum. Expl. Var. CV
LV1	41.03	40.46	22.64	20.74	41.03	40.46	22.64	20.74
LV2	35.66	32.50	7.06	5.70	76.69	72.96	29.70	26.44
LV3	4.85	4.66	7.23	6.74	81.54	77.62	36.93	33.18
LV4	3.35	1.93	4.90	4.21	84.89	79.55	41.83	37.40
LV5	0.90	1.10	8.04	5.79	85.79	80.65	49.87	43.19
LV6	1.47	-0.78	2.48	3.40	87.26	79.87	52.35	46.59
LV7	2.00	-0.99	1.71	2.56	89.25	78.87	54.06	49.15
LV8	0.87	0.06	3.91	2.28	90.13	78.93	57.97	51.43
LV9	0.79	0.00	3.82	2.15	90.92	78.93	61.79	53.58
LV10	0.76	0.26	2.54	2.01	91.67	79.19	64.34	55.59

***Table 5**: Percentage of explained and cumulative explained variance for the first ten LVs calculated.*

Figure 2a shows the score plot of the first three LVs, the three classes being represented with different marks (M with full black circles, P with empty circles and R with full gray circles): the three classes appear well separated along the first three LVs calculated. LV_1 is mostly responsible for the differences between P samples (at negative scores) and the other two cultivars (at positive scores), while the differences between P and R on one side and M samples on the other side are mainly described by the second LV (P and R at negative or slightly positive scores and r samples at positive scores). The third one mainly separates P and M cultivars from R (P and M at positive scores and R at negative ones).

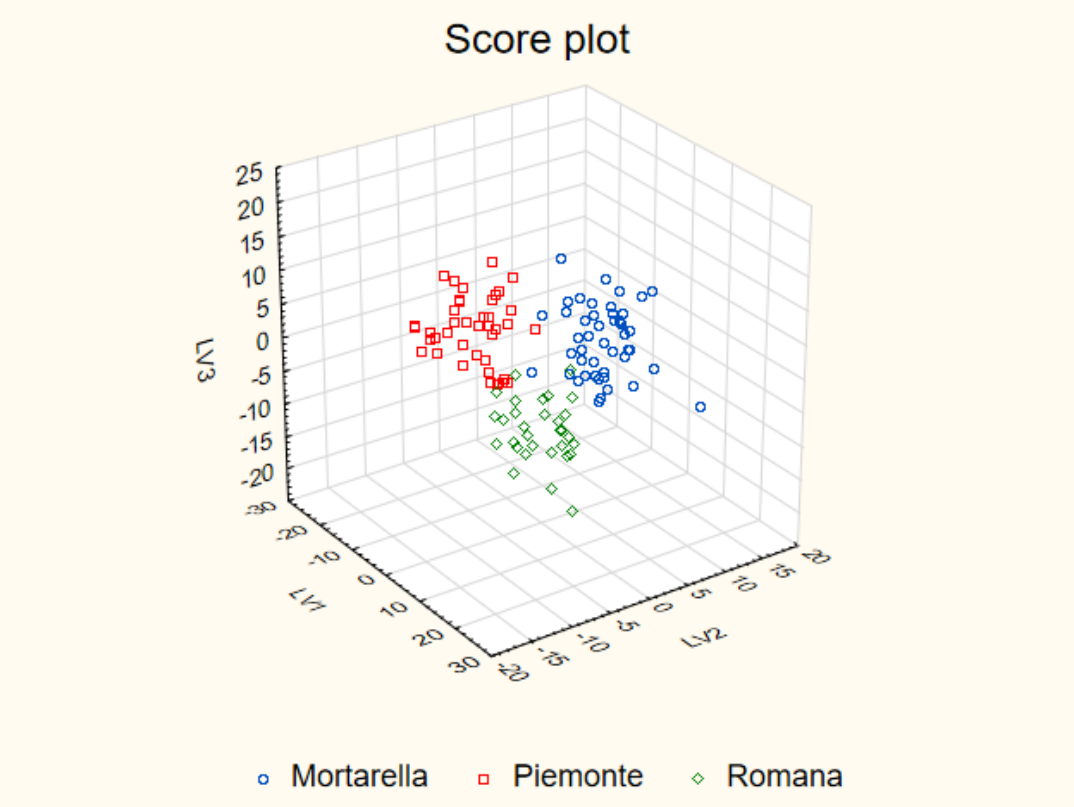

***Figure 2**: results of PLS-DA with variable selection. Score plot of the first three LVs calculated. Samples are labelled according to the cultivar.*

The classification performance in cross-validation was calculated for the final model by a leave-more-out procedure with 1000 iterations, eliminating at each iteration the 20% of the samples of each class, randomly selected. The final model shows a very good classification performance both in fitting and cross-validation, with an NER% of 100% in fitting and 96.95% in cross-validation and an accuracy of 100% in fitting and 96.72% in cross-validation.

The values calculated for sensitivity, precision and specificity (table 3) are very good both in fitting (precision, sensitivity and specificity always equal to 100%) and in cross-validation (precision always > 96.1%, sensitivity > 94.8% and specificity > 97.9%).

The information about the discriminating variables is contained in the regression coefficients: since three classes are present, three sets of regression coefficients can be calculated, one for each cultivar. To clarify the identification of the potential markers of authentication, a dendrogram was built on these coefficients (Ward method; distance calculated by the Pearson's correlation index) considering all the three classes (figure 3).

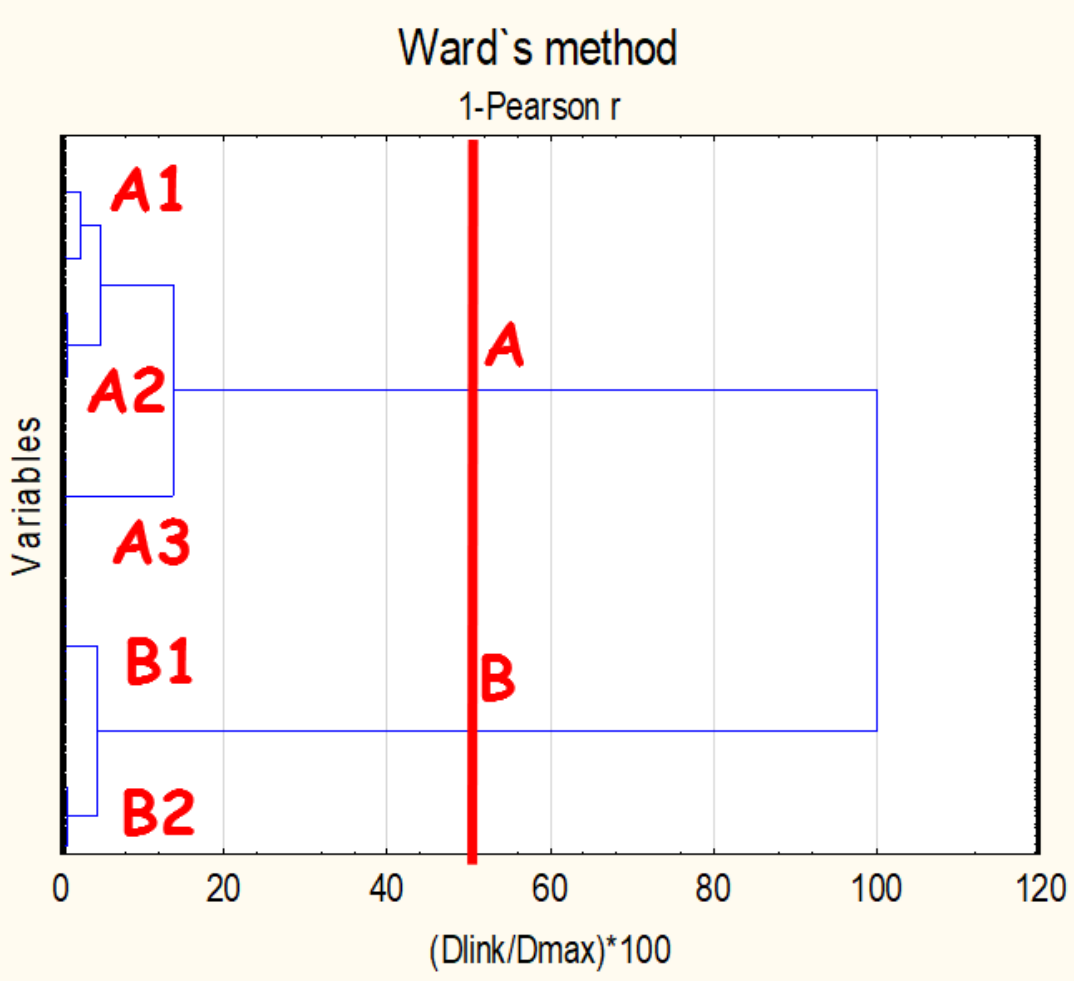

Figure 3: *Dendrogram of the regression coefficients (Ward method; Pearson's r-coefficient). The variables are on the y-axis and the distance% on the x-axis. The vertical cut applied in the dendrogram identifies two groups of variables, further separated in five total groups.*

This representation reports the variables on the y-axis and the distance at which the groups are merged together (scaled to the maximum distance) on the x-axis and it is useful to identify groups of variables with similar behavior. The dendrogram represents the variables along the y-axis, all separated (each one represents a different group); they are progressively merged in groups from left to right (where all the variables merge in a unique group). Groups can be identified by operating vertical cuts of the diagram and individuating the number of horizontal lines encountered. The dendrogram reported in figure 3, first identifies two main groups of variables (A and B) operating a cut at a distance level of 50%. These groups can be further separated into five sub-groups operating a cut at a distance level of 5%: three sub-groups of A (A1, A2 and A3) and two sub-groups of B (B1 and B2). Figure 4 reports the regression coefficients (Y-axis) calculated for each selected variable (x-axis) for each class (cultivar) independently: to make the discussion clearer, the entire representation was separated into different panels according to the group to which the variables belong in the dendrogram. In general, positive coefficients for a specific cultivar indicate variables (ratios) with a larger value for that cultivar, while negative coefficients show an opposite behavior.

Group A1 (Figure 4a) was separated in two panels for a clearer evaluation of the markers included in the group (x-axis): looking at the values of the coefficients for the three cultivars, it can be noticed that the markers belonging to this group allow to discriminate M from R samples (markers with large values for M samples and small values for R samples; P samples show intermediate values).

Group A2 (Figure 4b) contains markers that allow the differentiation between M samples and the other two (larger values for M samples and small in both P and R samples).

Group A3 (Figure 4c) contains markers differentiating P from M cultivars (includes variables with large values in P samples and small in M samples; R samples show intermediate values).

Group B1 (Figure 4 d) contains markers that discriminate M from the ther two cultivars but with an opposite behavior with respect to group A2: these variables show large values for P and R samples and small ones for M samples.

Group B2 (Fig 4 e) contains markers for the differences between R and M cultivars (includes variables with large values in R samples and small in M samples, P samples showing intermediate values). This group shows a behavior opposite to group A1.

Analyzing the variables present in the five groups, it is possible to say that:

- In Group A1, the most frequent elements are Ga, Al and Sc, in terms of ratios in which these elements are at the numerator. For what regards the normalizing factors, those most present in this group are Cr, Th, As and Co.
- Similarly, group A2 contains several ratios with a contribution (at the numerator) of Fe, Cu, Ag, Re and Mn. The most frequent normalizing factors are instead Pb, Ni, Gd, P, S and Dy.
- Group A3 shows a great contribution of Gd, Pb, Ni, Se and Ca (at the numerator), while the most frequent normalizing factors are Ba, La and Sr.
- Group B1 contains ratios with a large contribution of Cr, As and Ba, but also, at a smaller extent S, Gd, P and Eu. For what regards the normalizing factors, the most frequent are Cd, V and Na.
- Group B2 contains several rations with a contribution of Ba, Eu, Co and Sr, while the most present normalizing factors are Sc, Cu, Zn, Ga and Na.

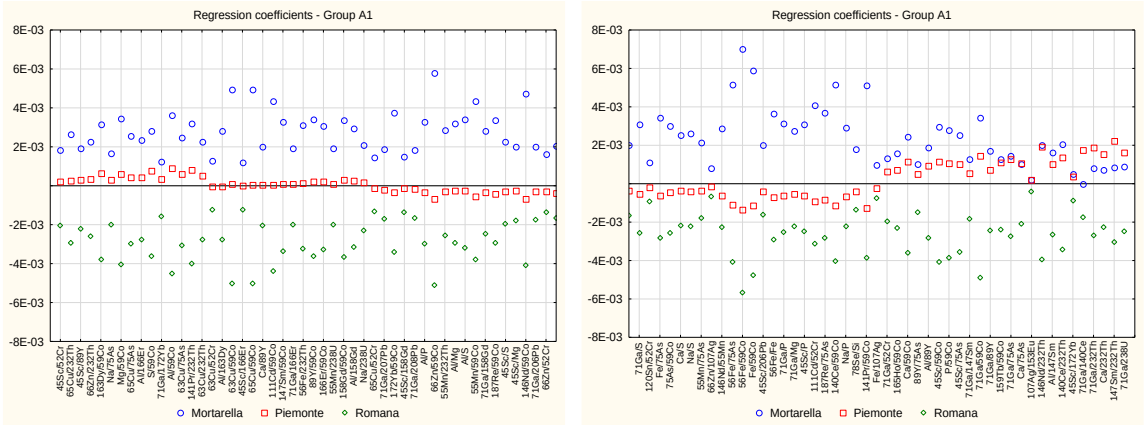

Figure 4a: *A1: Mortarelle vs Romane*

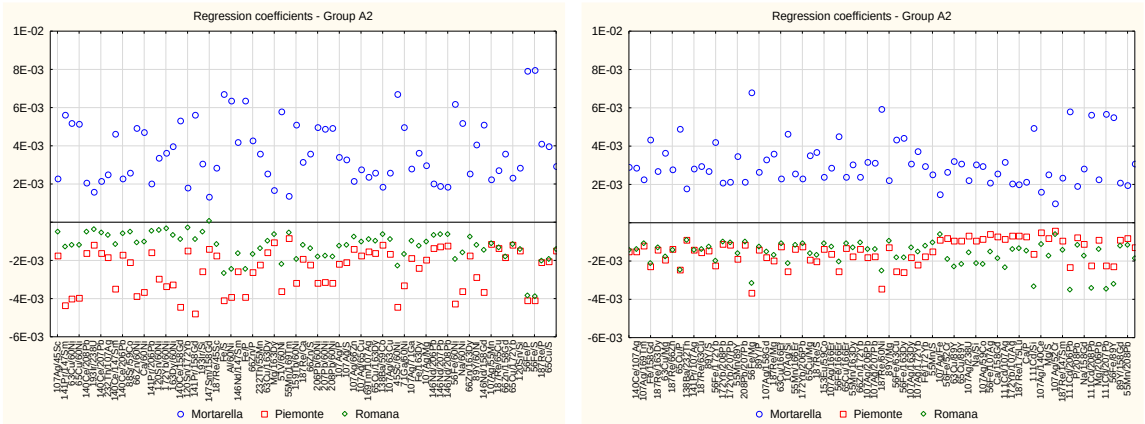

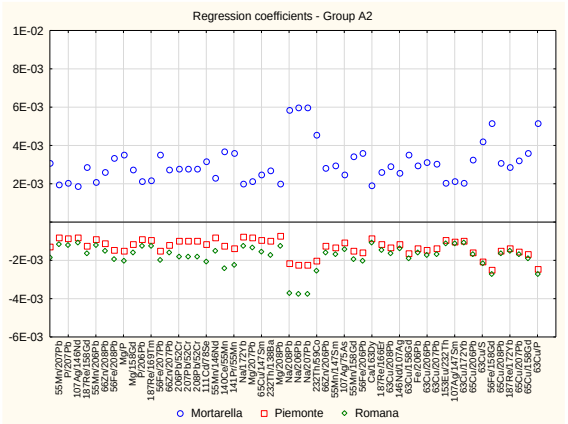

Figure 4b*: A2: Mortarelle vs Romane/Piemonte*

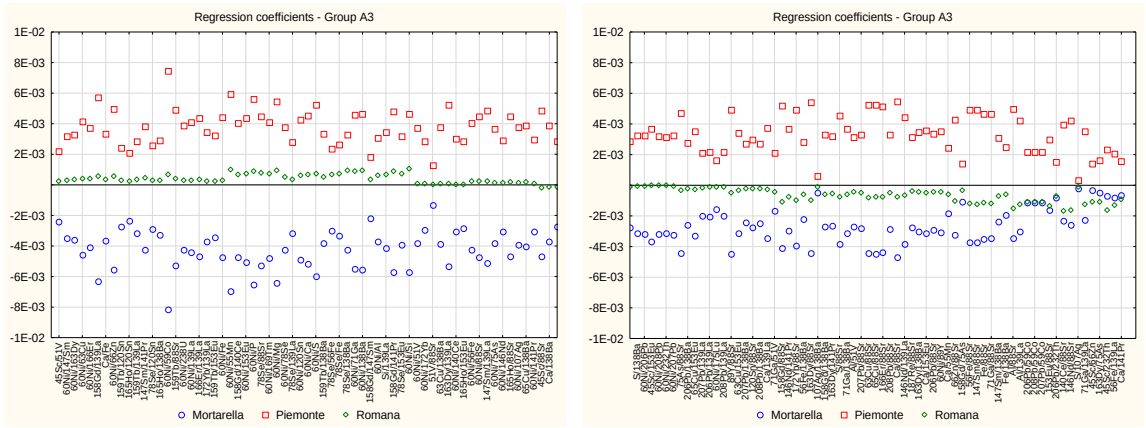

Figure 4c: *A3: Piemonte vs Mortarelle*

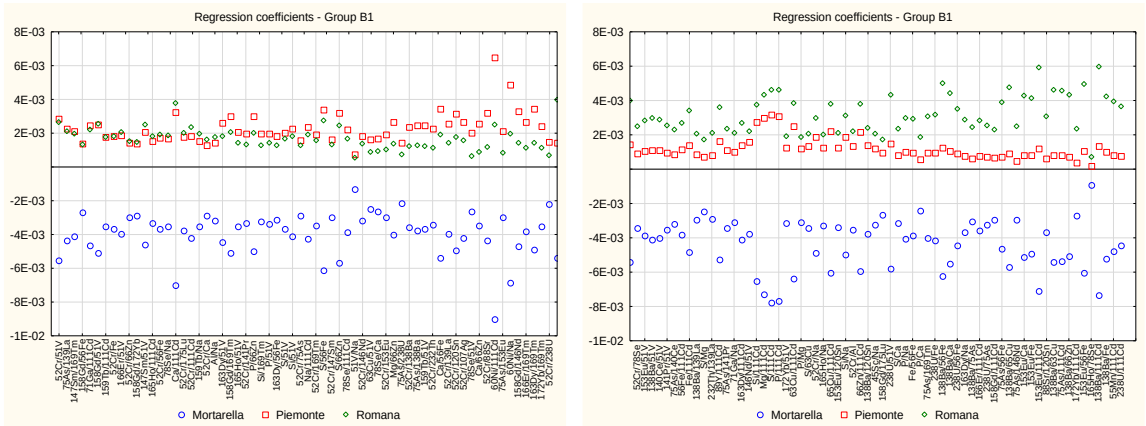

Figure 4d: *B1 Mortarelle vs Romane/Piemonte*

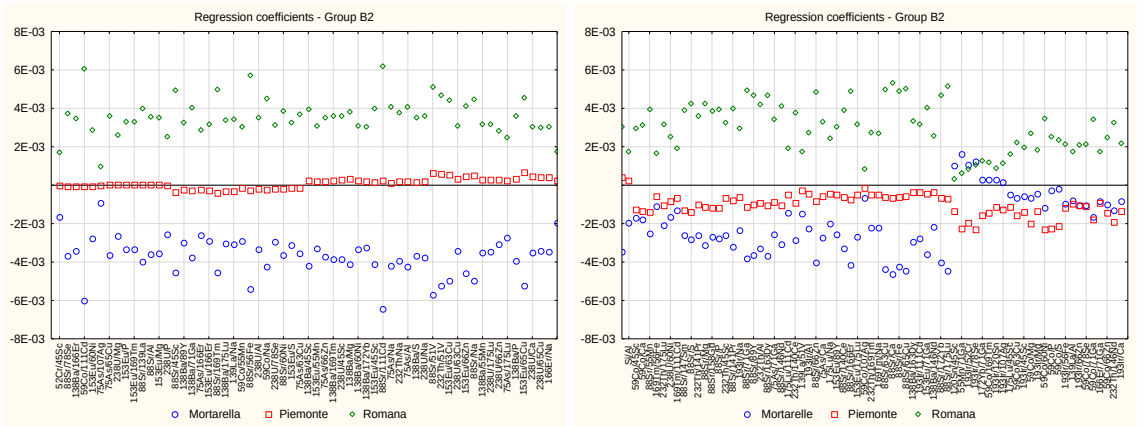

Figure 4e: *B2: Mortarelle vs Romane*

Figure 4(a, b, c, d, e): *Regression coefficients (reported on the y-axes) of each selected original variable (x-axes), labelled independently for each cultivar: regression coefficients were calculated on the final model containing three LVs. The overall representation is split in six panels corresponding to the groups identified in the dendrogram. Group A1 was split in two parts to make it more readable.*

4.2.3 Conclusion

Here, a model for the authentication of the hazelnut cultivar along the production chain of hazelnut paste was built, based on the elemental profile of the samples. The work involved three different cultivars: "Mortarella", "Tonda Gentile delle Langhe" and "Romana". The 119 available samples were mineralized by microwave assisted digestion and the elemental profile was determined by ICP-OES and ICP-MS.

Data were normalized for each element separately and then the data were centered with respect to each type of product independently (raw hazelnuts, toasted hazelnuts or paste).

The procedure based on the calculation of elemental ratios based on different normalizing factors proved to be a good choice, since the discriminating variables identified by PLS-DA include variables normalized by different normalizing factors with a quite different behavior as markers of authenticity, as highlighted by the analysis of the regression coefficients. In fact, the five groups of identified markers are characterized by both different elements and different normalizing factors. The results obtained show that authentication of hazelnuts along the production chain of hazelnuts paste, passing from raw to roasted fruits and then producing the corresponding paste, is possible with a good accuracy, based on the elemental profiling of both major elements and trace and ultra-trace elements.

4.3 Authentication of hazelnut cultivars by FTIR spectroscopy

The second study was carried out to investigate whether FTIR spectroscopy could be applied for a fast authentication of hazelnut cultivars. Infrared spectra were therefore collected on raw hazelnuts from three different cultivars ("Tonda gentile delle Langhe" from Piedmont, "Mortarella" from Campania and "Tonda gentile Romana" from Latium); the spectra were processed with different pre-treatment methods (baseline, first and second derivative, multiplicative scatter correction, standard normal variate) and coupled to different multivariate statistical methods in order to find the best classification model able to discriminate the samples according to their cultivar. PCA-LDA and PLS-DA, with and without the application of a variable selection algorithm, were employed to classify the hazelnut samples from different cultivars (18).

4.3.1 Materials and Methods

4.3.1.1 Samples 2.1

A total of 60 raw hazelnut samples from different geographical origins/cultivars were employed. The samples were from three different Italian regions and correspond to three different cultivars: "Tonda gentile delle Langhe" (TGL; from Piedmont), "Mortarella" (Campania) and "Tonda gentile Romana" (TGR, from Latium); the hazelnuts were shelled and preserved in a cold room before the analysis. For each cultivar taken into consideration, 5 different batches were available (each batch representing a different producer from the same geographical area): two samples from each batch were selected, the two halves of each sample were separated and three spectra in three different positions of each half were recorded. The average of each set of the three spectra was used for the statistical analysis, providing a total of 60 spectra (3 cultivars x 5 batches x 2 samples x 2 halves). The halves were directly put on the ATR crystal without any further sample pre-treatment (18).

4.3.1.2 Instrumentation and software

Fourier transform infrared spectral analysis of the hazelnut samples was carried out by ATR-FT-IR spectroscopy. All the spectra were recorded by an Agilent 4100 Exoscan FTIR portable spectrometer (Agilent Technologies, Santa Clara, CA, USA). The spectra were obtained in absorption mode over a wavelength range from 650 cm^{-1} to 4000 cm^{-1} at 32 scans per second, and a resolution of 4 cm^{-1}. The total analysis time is about 15 seconds. Background readings were collected prior to each sample spectrum collection. The background was subsequently subtracted from each spectrum before data treatment.

The spectra were processed by OPUS v.2.3 (Bruker Corporation, Billerica, MA, USA), statistical analysis and data pre-treatment were performed by The Unscrambler X 10.3 (Camo Inc., Oslo, Norway), Matlab 2014b (The MathWorks Inc., Natick, USA), Parvus (Prof Michele Forina, University of Genova, Italy) and the Classification Toolbox for Matlab from the Milano Chemometrics Group (38). Graphical representations were performed by Statistica v7.1 (Statsoft, Tulsa, OK, USA) (18).

4.3.1.3 Spectra pre-treatment

Each average spectrum was smoothed (moving average with step 3) to reduce the noise. Then, nine different pre-treatment algorithms were applied and compared:

- Offset baseline;
- Standard Normal Variate (SNV);
- First Derivative (D1), calculated by the Sawitzky-Golay algorithm (second degree polynomial order; smoothing with 5 left and 5 right side points);
- Second Derivative (D2), calculated by the Sawitzky-Golay algorithm (second degree polynomial order; smoothing with 5 left and 5 right side points);
- Multiplicative Scatter Correction (MSC);
- SNV followed by D1;

- MSC followed by D1;
- SNV followed by D2;
- MSC followed by D2.

Each of the nine treatments just described was applied, independently, after the smoothing, and coupled to different classification methods to identify the strategy (spectra pre-treatment / classification tool) with the best predictive ability (18).

4.3.1.4 Spectra pre-treatment theory

Nine different spectra pre-treatment methods were applied. Here, the theoretical aspects of some of them are presented.

Standard Normal Variate (SNV) is aimed to reduce baseline shifting or tilting due to non-specific scattering of radiation and variable spectral path length; this type of noise shows a larger effect at larger wavelengths. SNV correction is calculated, for each spectrum independently, by:

$$x'_{ij} = \frac{x_{ij} - \bar{x}_i}{s_i} \quad (1)$$

where x_{ij} is the absorbance measured at the *j*-th wavelength for the *i*-th sample, $\bar{x}_i$ is the average absorbance of the original *i*-th spectrum and s_i in the standard deviation of the absorbance of the *i*-th spectrum.

In *Multiplicative Scatter Correction (MSC),* the noise of each sample is estimated relatively to a reference sample, usually the average spectrum. MSC correction for each x_{ij} value is calculated as:

$$x'_{ij} = \frac{x_{ij} - a}{b} \quad (2)$$

where x_{ij} is the intensity of the *i*-th spectrum and the *j*-th wavelength, while *a* and *b* are estimated for each sample by ordinary least-squares regression of spectrum x_i versus the reference one (here, the average spectrum), over the available wavelengths.

First Derivative (D1) and Second Derivative (D2) are usually applied with two

different purposes: to remove horizontal baselines of varying levels (D1) and of varying levels and slopes (D2) (74) (i.e. acting as filters); to operate a deconvolution of the spectra to identify adjacent and convoluted peaks (74). Here, deconvolution is the main objective since IR spectra presented a horizontal baseline.

Combination of different pre-treatment procedures. SNV and MSC were combined with both D1 or D2 separately. As pointed out by Fearn (75,76), the order in which the two treatments (SNV or MSC and first or second derivative) are applied is relevant: here, after an initial smoothing procedure of each spectrum, D1 or D2 followed the treatment by MSC or SNV (18).

4.3.1.5 Classification models

Each of the nine pre-treatment methods was coupled to the following three classification tools:

- Principal Component Analysis followed by Linear Discriminant Analysis (PCA-LDA) carried out on the scores of the first 20 PCs calculated. The most discriminating PCs were selected by a variable selection procedure carried out by a stepwise algorithm in forward search, based on the best NER% in prediction. Cross-validation was accomplished by a leave-more-out procedure with 10 cancellation groups: at each iteration of the cross-validation procedure, one tenth of the samples was excluded from the calculation of the model and was used to evaluate its predictive ability. The samples taken out at each iteration were equally divided in the three classes.
- Partial Least Squares – Discriminant Analysis (PLS-DA). The choice of the number of LVs to be retained in the final model was accomplished by cross-validation with the same method adopted for PCA-LDA (the samples were divided in 10 cancellation groups) but in this case the procedure was repeated for 500 iterations randomly selecting at each iteration the samples included in each cancellation group. Once the number of LVs was identified, the

prediction ability of the final model was instead evaluated by cross-validation with a bootstrap procedure with 1000 iterations: at each iteration, 20% of the samples of each class was excluded from the training set and used to evaluate the predictive ability of the model.

- Backward elimination PLS-DA (BE-PLS-DA). PLS-DA was applied with variable selection by a stepwise algorithm in backward elimination: at each iteration, a variable (i.e. wavenumber) is eliminated according to the minimum error obtained in cross-validation, selecting the variable to be excluded according to the smallest importance (19) calculated by leave-more-out cross-validation with 10 cancellation groups. For each pre-treatment method applied, a final model containing a different number of original variables (wavenumbers) was obtained. To guarantee both limited calculation times during the selection of the best number of LVs to be included in the models, and the reliable evaluation of the predictive ability of the final models, two different cross-validation procedures were applied: a) the number of LVs in the final models was identified by cross-validation with a random selection of the samples to be included in the model (10 cancellation groups and 500 iterations); 2) the prediction ability of the final models was evaluated by cross-validation with a bootstrap procedure (1000 iterations; 20% of the samples of each class excluded from the training set for each iteration) (18).

The classification methods were applied to a restricted range of wavelengths containing only the significant signals, excluding wavelengths of the baseline. This led to the restricted range: 3660 – 2500 cm^{-1} and 1850-667 cm^{-1} (18).

4.3.2 Results and Discussion

4.3.2.1 IR spectra of hazelnuts

Figure 1 reports a sample spectrum recorded, showing the main bands as described in (61); the band assignments are reported in Table 1.

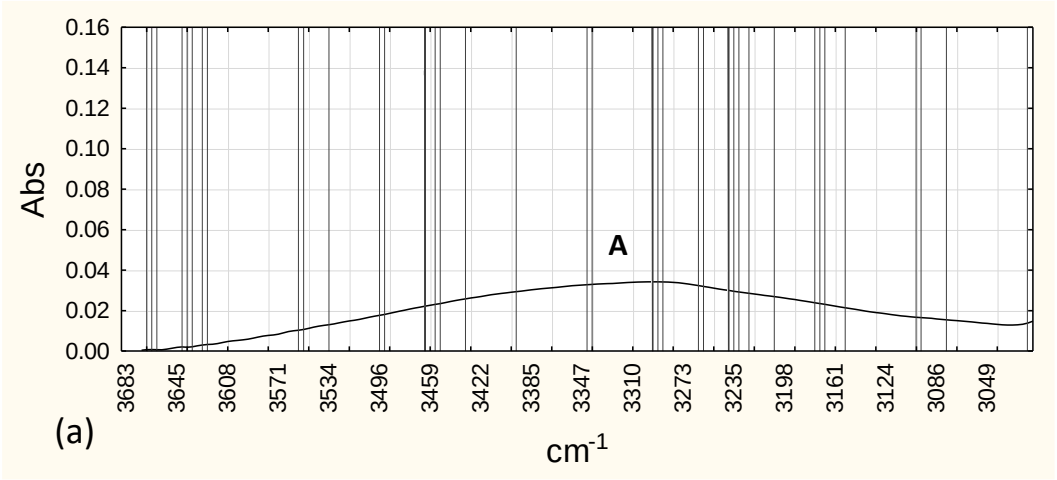

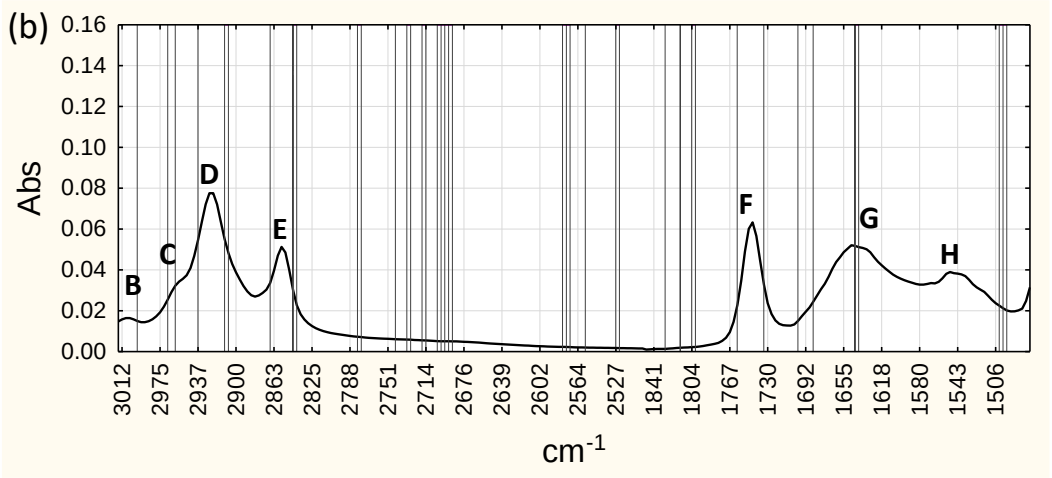

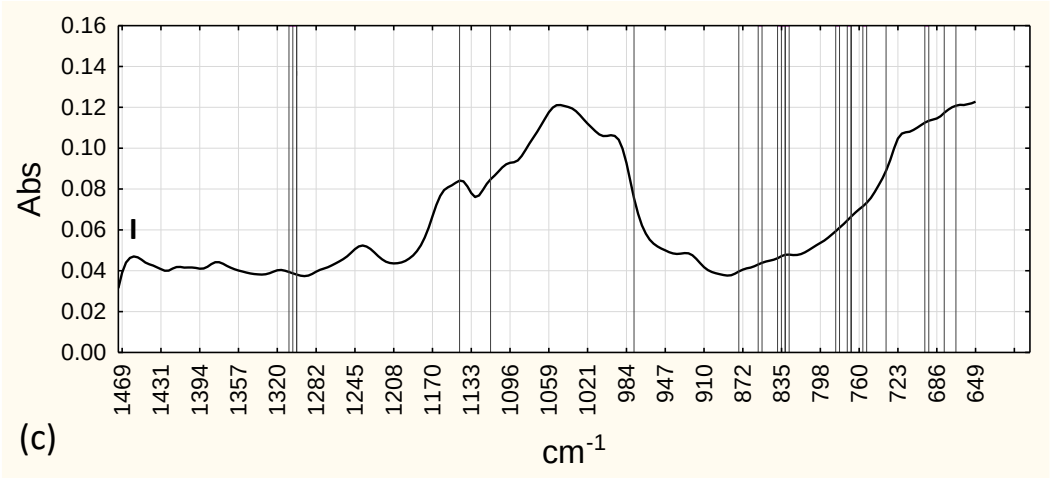

Figure 1: *Example of a recorded spectrum (only the regions used for statistical analysis are represented). The overall spectrum is separated in three spectral regions to make the representation clearer. Vertical lines represent the wavenumbers identified as significant by BE-PLS-DA. The letters represent the band assignments as reported in Table 1.*

A simple visual inspection of the spectra was not able to point out clear differences due to the different cultivar.

Table 1: Major bands assignments of hazelnuts IR spectra, as reported in (61).

Spectral region	**Band assignment**
3050-3645 cm^{-1}	O–H and N–H stretching due to polysaccharides and proteins (band A)
2993-3020 cm^{-1}	olefinic=CH stretching due to lipids (mainly unsaturated) (band B)
2948-2967 cm^{-1}	CH_3 asymmetric stretching, due mainly to lipids with the little contribution from proteins, carbohydrates, nucleic acids (band C)
2900-2940 cm^{-1}	CH_2 asymmetric stretching mainly due to lipids (mainly unsaturated) with the little contribution from proteins, carbohydrates, nucleic acids (band D)
2829-2877 cm^{-1}	CH_2 symmetric stretching mainly due to lipids (mainly unsaturated) with the little contribution from proteins, carbohydrates, nucleic acids (band E)
1714-1778 cm^{-1}	ester C=O stretching due to triglycerides and phospholipids (band F)
1599-1673 cm^{-1}	amide I (protein C=O stretching) (band G)
1510-1565 cm^{-1}	amide II (protein N–H bending and C–N stretching) (band H)

1442-1479 cm^{-1}	CH_2 bending due to lipids and proteins (band I)

Comparison of classification models

Table 2 reports the results obtained for the three classification procedures in terms of accuracy, NER% and ER%, both in calibration and cross-validation.

		Fitting			Cross-validation				
		Accuracy	**NER%**	**ER%**	**Accuracy**	**NER%**	**ER%**	**Number of PCs or LVs included in the model**	**PCs or variables included in the final model***
PCA-LDA	**Baseline**	96.23	95.83	4.17	80.81	79.93	20.07	17 PCs	PC7, PC2, PC3, PC13, PC4, PC8, PC17, PC5, PC1, PC20, PC11, PC14, PC10, PC19, PC12, PC18, PC9
	MSC	96.23	96.06	3.94	83.12	82.69	17.31	16 PCs	PC15, PC2, PC17, PC3, PC11, PC6, PC4, PC13, PC16, PC1, PC5, PC10, PC8, PC7, PC18, PC9
	SNV	86.79	86.40	13.60	60.38	59.47	40.53	7 PCs	PC4, PC12, PC15, PC11, PC2, PC17, PC19
	D1	**100**	**100**	**0.00**	**88.23**	**88.02**	**11.98**	**15 PCs**	**PC2, PC8, PC5, PC10, PC17, PC4, PC11, PC6, PC1, PC12, PC3, PC20, PC9, PC14, PC7**
	D2	92.45	91.90	8.10	84.00	83.27	16.73	6 PCs	PC5, PC1, PC2, PC4, PC6, PC8
	MSCD1	90.57	90.24	9.76	81.40	80.91	19.09	6 PCs	PC4, PC10, PC9, PC18, PC2, PC15
	MSCD2	94.34	93.98	6.02	80.82	80.20	19.80	7 PCs	PC6, PC3, PC4, PC1, PC7, PC5, PC20
	SNVD1	86.79	86.96	13.04	72.06	72.09	27.91	7 PCs	PC4, PC2, PC1, PC18, PC20, PC15, PC13
	SNVD2	94.34	94.21	5.79	81.63	81.16	18.84	9 PCs	PC6, PC3, PC4, PC1, PC18, PC20, PC19, PC12, PC5
PLS-DA	**Baseline**	100	100	0	88.87	88.52	11.48	15 LVs	
	MSC	100	100	0	86.74	86.44	13.56	14 LVs	
	SNV	100	100	0	87.53	87.35	12.65	20 LVs	
	D1	**100**	**100**	**0**	**89.05**	**88.86**	**11.14**	**11 LVs**	
	D2	100	100	0	84.70	84.57	15.43	6 LVs	
	MSCD1	100	100	0	87.92	87.62	12.38	15 LVs	
	MSCD2	100	100	0	85.65	85.53	14.47	7 LVs	
	SNVD1	100	100	0	88.86	88.64	11.36	13 LVs	
	SNVD2	100	100	0	85.90	85.75	14.25	6 LVs	
BE-PLS-DA	**Baseline**	100	100	0	92.82	92.54	7.46	12 LVs	166 original variables
	MSC	100	100	0	91.49	91.36	8.64	13 LVs	188 original variables
	SNV	100	100	0	93.57	93.41	6.59	14 LVs	202 original variables
	D1	100	100	0	95.79	95.66	4.34	13 LVs	85 original variables
	D2	100	100	0	93.72	93.70	6.30	5 LVs	266 original variables
	MSCD1	100	100	0	95.81	95.77	4.23	10 LVs	130 original variables

	MSCD2	**100**	**100**	**0**	**98.00**	**97.81**	**2.19**	**4 LVs**	**90 original variables**
	SNVD1	100	100	0	94.68	94.65	5.35	9 LVs	276 original variables
	SNVD2	**100**	**100**	**0**	**98.18**	**98.06**	**1.94**	**3 LVs**	**102 original variables**
*For PCA-LDA, the last column reports the PCs in the order they are included in the final model. For BE-PLS-DA, the last column reports the number of origina l variables retained as signification by the variable selection procedure.									

Table 2: *Results of the application of the different classification methods: Accuracy, NER%, ER% in fitting and in cross-validation. Results in bold represent the best models obtained for each classification method.*

Table 3 reports instead the results obtained for what regards class overlapping and purity: precision, sensitivity and specificity, both in calibration and cross-validation. All the results are reported as percentages. Table 3 reports only the results obtained for all the data pre-treatments for each classification method separately.

			Fitting			**Cross-validation**		
			TGL	**Mortarella**	**TGR**	**TGL**	**Mortarella**	**TGR**
PCA-LDA	**Baseline**	**Precision**	90	100	100	70.54	78.05	95.47
		Sensitivity	100	87.5	100	86.88	63.55	89.35
		Specificity	94.29	100	100	81.34	92.39	97.6
	MSC	**Precision**	100	93.75	95	80.01	81.55	87.63
		Sensitivity	94.44	93.75	100	89.09	73.01	85.97
		Specificity	100	97.3	97.06	88.62	92.86	93.17
	SNV	**Precision**	81.82	85.71	94.12	59.78	53.92	65.08
		Sensitivity	100	75	84.21	67.4	42.98	68.03
		Specificity	88.57	94.59	97.06	76.06	84.5	79.67
	D1	**Precision**	**100**	**100**	**100**	**88.97**	**83.22**	**91.83**
		Sensitivity	**100**	**100**	**100**	**93.17**	**82.85**	**88.03**
		Specificity	**100**	**100**	**100**	**94.00**	**92.81**	**95.65**

	D2	**Precision**	89.47	92.86	95	80.55	77.95	91.92
		Sensitivity	94.44	81.25	100	87.43	68.53	93.86
		Specificity	94.29	97.3	97.06	89.12	91.58	95.42
	MSCD1	**Precision**	94.74	86.67	89.47	93.19	70.23	78.97
		Sensitivity	100	81.25	89.47	95.52	68.88	78.35
		Specificity	97.14	94.59	94.12	96.35	87.47	88.44
	MSCD2	**Precision**	89.47	93.33	100	74.69	76.34	91.18
		Sensitivity	94.44	87.5	100	85.56	67.35	87.68
		Specificity	94.29	97.3	100	85.13	90.96	95.25
	SNVD1	**Precision**	80.95	87.5	93.75	75.02	69.69	70.39
		Sensitivity	94.44	87.5	78.95	88.55	68.22	59.49
		Specificity	88.57	94.59	97.06	84.61	87.37	86.02
	SNVD2	**Precision**	94.12	88.24	100	77.88	75.07	90.68
		Sensitivity	88.89	93.75	100	79.45	74.16	89.87
		Specificity	97.14	94.59	100	88.34	89.5	94.79
PLS-DA	**Baseline**	**Precision**	100	100	100	87.57	85.88	92.73
		Sensitivity	100	100	100	95.7	80.35	89.51
		Specificity	100	100	100	92.93	94.3	96.12
	MSC	**Precision**	100	100	100	87.76	83.89	87.97
		Sensitivity	100	100	100	92.49	79.16	87.68
		Specificity	100	100	100	93.4	93.43	93.27
	SNV	**Precision**	100	100	100	87.06	86.41	88.92
		Sensitivity	100	100	100	91.53	82.65	87.87
		Specificity	100	100	100	93.01	94.33	93.92
	D1	**Precision**	100	100	100	**89.35**	**82.69**	**94.52**
		Sensitivity	100	100	100	**91.18**	**84.74**	**90.67**
		Specificity	100	100	100	**94.37**	**92.3**	**97.1**
	D2	**Precision**	100	100	100	83.43	78.52	91.88
		Sensitivity	100	100	100	86.9	81.79	85.02
		Specificity	100	100	100	91.04	90.41	95.81
	MSCD1	**Precision**	100	100	100	85.26	85.53	92.74
		Sensitivity	100	100	100	92.96	80.52	89.4
		Specificity	100	100	100	91.75	94.1	96.08

	MSCD2	**Precision**	100	100	100	86.20	79.29	91.01
		Sensitivity	100	100	100	89.86	81.76	84.97
		Specificity	100	100	100	92.66	90.69	95.31
	SNVD1	**Precision**	100	100	100	86.79	86.63	92.9
		Sensitivity	100	100	100	92.72	82.99	90.21
		Specificity	100	100	100	92.78	94.4	96.17
	SNVD2	**Precision**	100	100	100	85.91	80.31	90.87
		Sensitivity	100	100	100	90.38	81.11	85.74
		Specificity	100	100	100	92.52	91.42	95.08
BE-PLS-DA	**Baseline**	**Precision**	100	100	100	91.80	90.83	95.52
		Sensitivity	100	100	100	97.65	86.43	93.55
		Specificity	100	100	100	95.43	96.25	97.58
	MSC	**Precision**	100	100	100	92.64	91.28	90.56
		Sensitivity	100	100	100	96.57	86.1	91.39
		Specificity	100	100	100	96.14	96.33	94.71
	SNV	**Precision**	100	100	100	93.65	94.73	92.58
		Sensitivity	100	100	100	95.88	89.98	94.36
		Specificity	100	100	100	96.62	97.86	95.78
	D1	**Precision**	100	100	100	94.31	93.06	99.48
		Sensitivity	100	100	100	95.35	93.92	97.7
		Specificity	100	100	100	97.04	97.06	99.71
	D2	**Precision**	100	100	100	92.56	92.59	95.9
		Sensitivity	100	100	100	97.56	91.7	91.86
		Specificity	100	100	100	96.05	96.77	97.79
	MSCD1	**Precision**	100	100	100	95.77	95.07	96.47
		Sensitivity	100	100	100	98.44	94.32	94.55
		Specificity	100	100	100	97.75	97.89	98.07
	MSCD2	**Precision**	**100**	**100**	**100**	**96.69**	**99.45**	**98.15**
		Sensitivity	**100**	**100**	**100**	**99.80**	**93.97**	**99.64**
		Specificity	**100**	**100**	**100**	**98.25**	**99.78**	**98.93**
	SNVD1	**Precision**	100	100	100	92.26	94.81	97.13
		Sensitivity	100	100	100	97.18	93.46	93.33
		Specificity	100	100	100	95.77	97.77	98.48

	SNVD2	**Precision**	**100**	**100**	**100**	**97.02**	**98.65**	**98.91**
		Sensitivity	**100**	**100**	**100**	**98.92**	**95.78**	**99.48**
		Specificity	**100**	**100**	**100**	**98.43**	**99.44**	**99.39**

Table 3*: Results of the application of the different classification methods: Precision, Sensitivity, Specificity in fitting and in cross-validation.*

For what regards PCA-LDA, the best results are obtained by calculating the first derivative of each spectrum: the final model contains 15 PCs (the order in which they are included in the model is reported in table 2) and guarantees the perfect classification of all the samples in calibration, but the accuracy decreases to about 88% in cross-validation. With D1 treatment, specificity is always greater than 92% for the three classes, while sensitivity shows values larger than 90% only for the first class and precision shows values larger than 90% only for the third class. The number of PCs included in the model is quite large; this is due in part to the applied method: since in PCA-LDA, LDA is applied to PCs, i.e. directions of maximum variance calculated in an unsupervised manner, the number of PCs to achieve good classification performances can be rather large if class belonging is not the only source of relevant information. Moreover, here, the natural variability of the hazelnut products needed a larger number of PCs to be taken into account properly. It must be pointed out that in this approach no selection of the original variables was operated: the overall spectrum was used to describe each sample, thus including also wavenumbers not directly related to classification, increasing the experimental error. The large number of PCs included reflects also in the not very good accuracy obtained in cross-validation: PCA-LDA provides good results but samples appear not very well separated in the three classes.

Similar results are obtained by PLS-DA where the best model performances are obtained after D1 treatment and the final model includes 11 LVs showing the perfect classification of all the samples in calibration, but an accuracy of about 89% in cross-validation. With D1 treatment, specificity is always greater than 92% for the three

classes, while sensitivity shows values larger than 90% for the first and third classes and precision shows values larger than 90% only for the third class. The number of LVs included in the model is large but smaller than the number of PCs in PCA-LDA: this is due to the fact that LVs are calculated in a supervised manner, usually providing a simpler model; however, the number of LVs is yet large due to both the natural variability of hazelnuts and the fact that no variable selection was applied, including therefore in the final model also wavenumbers not directly related to classification.

The best overall results are obtained by PLS-DA with variable selection: the best model performances are obtained in this case after a D2 treatment coupled to both MSC or SNV (in this last case the model is slightly better). The final model (SNV+D2) contains only three LVs and is calculated on 102 original variables (for a better description of the 102 variables identified as discriminating, refer to paragraph 4.3). This model allows the perfect classification of all the samples in calibration, while the accuracy is of about 98% in cross-validation. Specificity is always greater than 98% for all the classes, while sensitivity is always greater than 95% and precision is always greater than 97%. This model is really satisfactory for the purpose of discriminating the 3 types of samples. In this case, only 3 LVs are included in the final model and very good classification performances are obtained. This is mostly due to the variable selection procedure, able to eliminate from the model the original variables not related to classification and reduce therefore the experimental error accounted for by the final model. The number of retained variables accounts for this effect: out of the 629 original wavenumbers, just 102 were retained in the final model. This was selected as the best overall model both due to its very good classification performances and to its simplicity in terms of number of original variables/LVs included in the final model (18).

PLS-DA with variable selection

The best results were obtained by PLS-DA coupled to variable selection, after pre-treatment by SNV and D2. Figure 2 reports the score plot of the first three latent variables: the samples appear well grouped according to the different cultivars. The first LV mainly separates the TGL samples (at positive values) from the TGR samples (at negative values), while the second LV mainly separates Mortarella (at positive values) from the other two classes (at negative values).

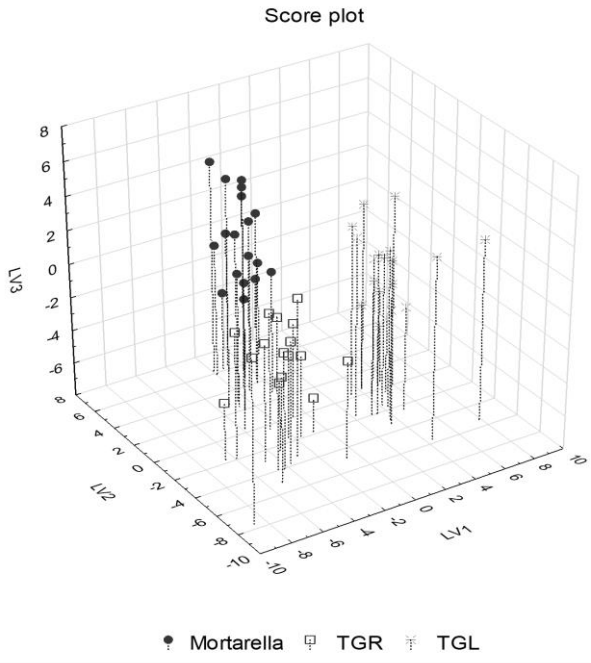

***Figure 2**: BE-PLS-DA results: score plot of the first three LVs calculated (the score plot represents the samples indicated with different markers according to the three different classes).*

Figure 3a-c reports instead the regression coefficients of the three classes, calculated on the basis of the first three LVs: for each class, positive regression coefficients indicate wavelengths that have a large signal for the corresponding class, while negative coefficients indicate regions with a small signal in the corresponding class. It must be pointed out however that the spectra were treated by SNV followed by the second derivative, therefore the discussion about the behavior of the different

spectral bands according to the different cultivars must take it into account. For a clearer interpretation, a sample spectrum is represented in figure 1; the figure reports as vertical lines the wavenumbers that were selected as significant by BE-PLS-DA. As it can be noticed by the joint analysis of figure 3 and figure 1, the large band centered at about 3340 cm^{-1} (band A) shows a great influence on the cultivar: this band represents the convolution of signals involving the N-H stretching of Amide A of proteins, with contributions from the O-H stretching from inter- and intra-molecular hydrogen bonds (34). The complex convolution of these modes reflects in the complex behavior of the second derivative that shows some regions within this band where the signal can discriminate between TGR and TGL samples (mainly at larger wavenumbers; larger signals for TGR and smaller for TGL) and other regions that discriminate between Mortarella and the other two classes (mainly at smaller wavenumbers within this band).

The band at 2959 cm^{-1} corresponds to the asymmetric stretching of CH_3 groups and is mainly related to lipids, that show a larger signal in TGL samples than in Mortarella.

The band at 1650 cm^{-1} corresponds to the amide I vibrations of structural proteins: this band shows a larger signal in TGL samples and a smaller signal in TGR samples.

For what regards the other signals identified as significant in the discrimination between the classes, they all belong to regions were a relevant absorption is recorded for the samples, however, these signals correspond in general to shoulders of the major bands, pointing out that the differences between the three investigated cultivars are quite slight and do not reside in major absorbment peaks (18).

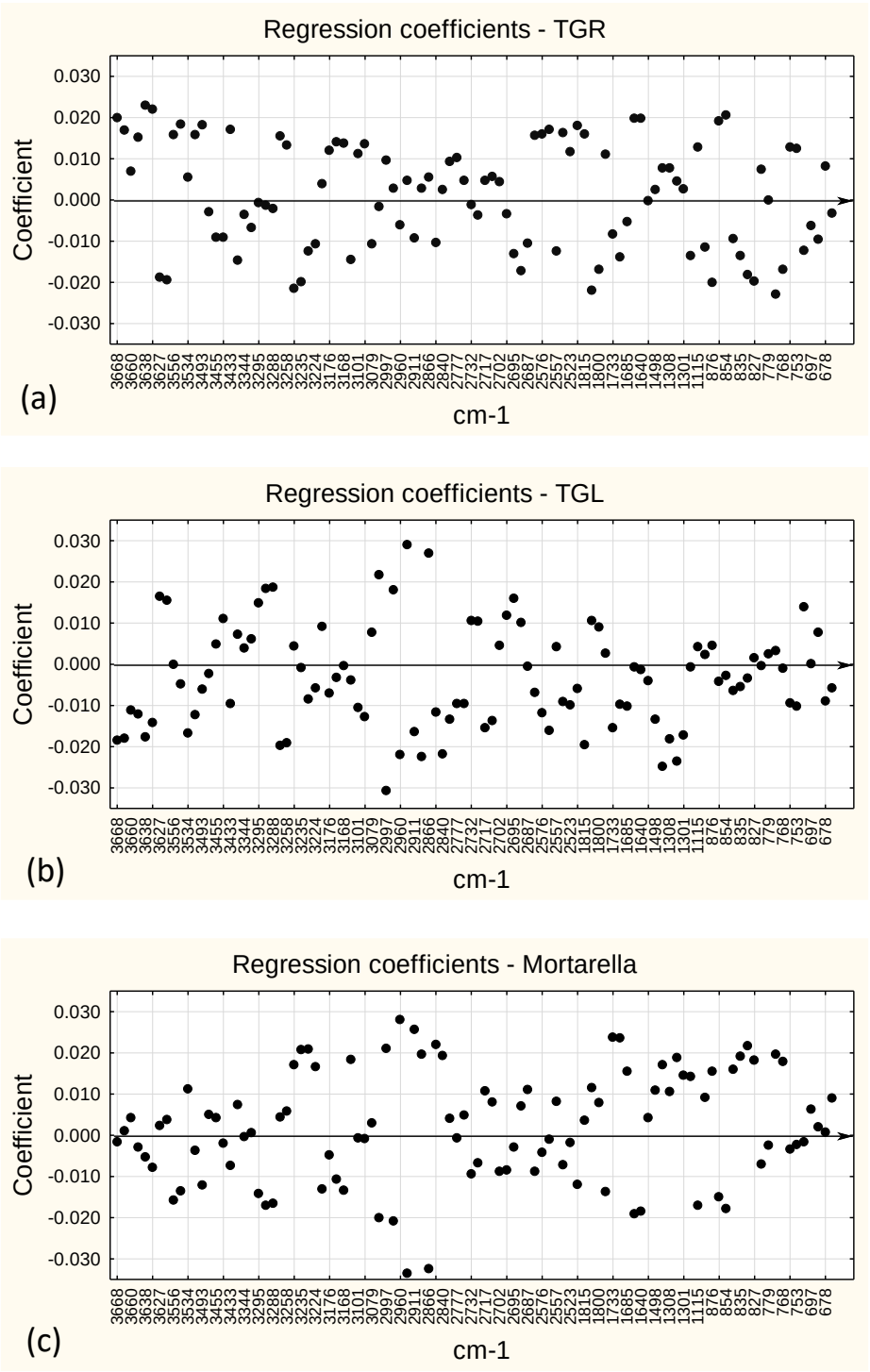

***Figure 3**: BE-PLS-DA results: regression coefficients of the 102 significant original variables separately for the three classes considered (a-c).*

4.3.3 Conclusions

FTIR spectroscopy was applied for the identification of the cultivar of raw hazelnuts. The infrared spectra collected on the raw hazelnuts from three cultivars (TGL, Mortarella and TGR), were processed by different pre-treatment algorithms coupled to three different classification methods (PCA-LDA, PLS-DA and BE-PLS-DA). The best classification performances were obtained by BE-PLS-DA after spectra pre-treatment by SNV, followed by the calculation of the second derivative. The final model includes 102 original wavelengths and provides the perfect classification of all the samples in calibration as well as very good performances in cross-validation. The applied cross-validation procedure (bootstrap with 1000 iterations; 20% of the samples of each class excluded from the training set for each iteration) allowed to obtain a robust evaluation of the prediction ability of the models notwithstanding the lack of a test set for an external prediction.

The analysis of the significant wavelenghts pointed out that differences among the cultivars reside in some major contributions, mainly due to lipids (for discriminating TGL from Mortarella) and proteins (for discriminating TGL from TGR). However, the good classification performances are also due to other signals that regard shoulders of the major bands.

The model built provides an important proof of concept of the ability of ATR-FT-IR spectroscopy coupled to multivariate statistical methods for the identification of the cultivar of raw hazelnuts. This application is of particular interest since hazelnuts from different origins are characterized by very different commercial values, with "Tonda Gentile delle Langhe" representing the product more suitable for confectionery. The applied methodology represents an important advance in the field of cultivar identification of raw hazelnuts for the food industry, showing high sensitivity, simplicity and above all not requiring any particular sample preparation; the analysis is very fast (about 30 seconds per sample, including the sample treatment); to the advantages of FT-IR spectroscopy, the possibility of on-site

measurements is an important added value, making this application particularly effective for industrial quality control.

To this purpose, in spite of seeming a quite complex data treatment, for a future application in on-line industrial quality controls, SNV and D2 calculation can be accomplished automatically in a few fractions of seconds by standard software packages or by home-made algorithms developed in Matlab or R environments. For what regards the variable selection procedure by BE-PLS-DA, once the model is calculated on the samples of the training set, the coefficients calculated for each selected original variable can be used to calculate the class belonging of any new sample in a very fast way. The application represents therefore an important proof of concept of the applicability of this approach in industrial quality control (18).

4.4 Bibliography

1. Oliveira I., Sousa A., Sa´ Morais J., Ferreira I.C.F.R., Bento A., Estevinho L., Pereira J.A. (2008) Chemical composition, and antioxidant and antimicrobial activities of three hazelnut (Corylus avellana L.) cultivars. Food and Chemical Toxicology. 46, 1801–1807.
2. Koksal A.I., Artik N., Simsek A., Gunes N. (2006) Nutrient composition of hazelnut (Corylus avellana L.) varieties cultivated in Turkey. Food Chemistry. 99, 509–515.
3. Alasalvar C., Shahidi F., Liyanapathirana C.M., Ohshima T. (2003) Turkish Tombul Hazelnut (Corylus avellana L.).1. Compositional Characteristics J. Agric. Food Chem. 51, 3790-3796.
4. Alasalvar C., Amaral J.S., Shahidi F. (2006) Functional lipid characteristics of Turkish Tombul hazelnut (Corylus avellana L.) Journal of Agricultural and Food Chemistry. 54 (26), pp. 10177-10183.
5. Perna S., Giacosa A., Bonitta G., Bologna C., Isu A., Guido D., Rondanelli M. (2016) Effects of Hazelnut Consumption on Blood Lipids and Body

Weight: A Systematic Review and Bayesian Meta-Analysis Nutrients 2016, 8, 747.

6. Alasalvar C., Bolling B.W. (2015) Review of nut phytochemicals, fat-soluble bioactives, antioxidant components and health effects. British Journal of Nutrition. 113 (S2), pp. S68-S78.
7. Granata M.U., Bracco F., Gratani L., Catoni R., Corana F., Mannucci B., Sartori F., Martino E. (2017) Fatty acid content profile and main constituents of Corylus avellana kernel in wild type and cultivars growing in Italy. Natural Product Research. 31(2), 204-209.
8. Orem A., Yucesan F.B., Orem C., Akcan B., Kural B.V., Alasalvar C., Shahidi F. (2013) Hazelnut-enriched diet improves cardiovascular risk biomarkers beyond a lipid-lowering effect in hypercholesterolemic subjects (2013) Journal of Clinical Lipidology. 7 (2), pp. 123-131.
9. Rezaei F., Bakhshi D., Ghazvini R.F., Majd D.J., Pourghayoumi M. (2014) Evaluation of fatty acid content and nutritional properties of selected native and imported hazelnut (Corylus avellana L.) varieties grown in Iran. Journal of Applied Botany and Food Quality. 87, 104–107.
10. Ozdemir F., Akinci I. (2004) Physical and nutritional properties of four major commercial Turkish hazelnut varieties. Journal of Food Engineering. 63, 341–347.
11. Taş N.G., Gökmen V. (2015) Bioactive compounds in different hazelnut varieties and their skins. Journal of Food Composition and Analysis. 43, 203-208.
12. Food and Agriculture Organization of the United Nations (FAO). (2013). FAO Statistics Division. Retrieved April 3, 2015 from http://faostat3.fao.org/download/Q/QC/E.
13. Ciemniewska-Zytkiewicz H., Verardo V., Pasini F., Brys J., Koczon P., Caboni M.F. (2015) Determination of lipid and phenolic fraction in two

hazelnut (Corylus avellana L.) cultivars grown in Poland. Food Chemistry. 168, 615–622.

14. Caligiani A.C., Coisson J.D., Travaglia F., Acquotti D., Palla G., Palla L., Arlorio M. (2014) Application of ^{1}H NMR for the characterisation and authentication of "Tonda Gentile Trilobata" hazelnuts from Piedmont (Italy). Food Chem. 148, 77−85.
15. Oddone M., Aceto M., Baldizzone M., Musso D., Osella D. (2009) Authentication and Traceability Study of Hazelnuts from Piedmont. Italy. J. Agric. Food Chem. 57 (9), 3404–3408.
16. Garrone W., Vacchetti M. (1994) La qualità delle nocciole in rapporto alle esigenze dell'industria dolciaria utilizzatrice. Acta Horticulturae. 351, 641-647.
17. Granata M.U., Bracco F., Gratani L., Catoni R., Corana F., Mannucci B., Sartori F., Martino E. (2017) Fatty acid content profile and main constituents of Corylus avellana kernel in wild type and cultivars growing in Italy. Natural Product Research. 31(2), 204-209.
18. Manfredi M., Robotti E., Quasso F., Mazzucco E., Calabrese G., Marengo E. (2017) Fast classification of hazelnut cultivars through portable infrared spectroscopy and chemometrics. Spectrochim Acta A Mol Biomol Spectrosc. 189:427-435.
19. Alasalvar C., Pelvan E., Amarowicz R. (2010) Effects of roasting on taste-active compounds of Turkish hazelnut varieties (Corylus avellana L.). J. Agric. Food Chem. 2010, 58, 8674−8679.
20. Marzocchi S., Pasini F., Verardo V., Ciemniewska-Żytkiewicz H., Caboni M.F., Romani S. (2017) Effects of different roasting conditions on physical-chemical properties of Polish hazelnuts (Corylus avellana L. var. Kataloński), LWT - Food Science and Technology. 77: 440-448.

21. Stuetz W., Schlörmann W., Glei M. (2017) B-vitamins, carotenoids and α-/γ-tocopherol in raw and roasted nuts, Food Chemistry. 221: 222-227.
22. Amaral J.S., Casal S., Seabra R.M., Oliveira B.P.P. (2006) Effects of roasting on hazelnut lipids. J. Agric. Food Chem. 54, 1315−1321.
23. Alasalvar C., Pelvan E., Topal B. (2010) Effects of roasting on oil and fatty acid composition of Turkish hazelnut varieties (Corylus avellana L.). Int. J. Food Sci. Nutr. 61, 630−642.
24. Siciliano I., Dal Bello B., Zeppa G., Spadaro D., Gullino M.L. (2017) Static Hot Air and Infrared Rays Roasting are Efficient Methods for Aflatoxin Decontamination on Hazelnuts. Toxins. 9(2): E72.
25. Kahyaoglu T., Kaya S. (2006) Determination of optimum processing conditions for hot-air roasting of hulled sesame seeds using response surface methodology. J Sci Food Agric. 86: 1452–1459.
26. Menozzi D., Halawany-Darson R., Mora C., Giraud G. (2015) Motives towards traceable food choice: A comparison between French and Italian consumers. Food Control. 49: 40-48 .
27. Baffi C., Trincherini P.R. (2016) Food traceability using the Sr-87/Sr-86 isotopic ratio mass spectrometry. European Food research and Technology. 242(9), 1411-1439.
28. Drivelos S.A., Higgins K., Kalivas J.H., Haroutounian S.A., Georgiou C.A. (2014) Data fusion for food authentication. Combining rare earth elements and trace metals to discriminate ‘‘Fava Santorinis’’ from other yellow split peas using chemometric tools. Food Chemistry. 165: 316–322.
29. Brunner M., Katona R., Stefanka Z., Prohaska T. (2010) Determination of the geographical origin of processed spice using multielement and isotopic pattern on the example of Szegedi paprika. European Food research and Technology. 231(4), 623-634.

30. Bontempo L., Camin F., Manzocco L., Nicolini G., Wehrens R., Ziller L., Larcher R. (2011) Traceability along the production chain of Italian tomato products on the basis of stable isotopes and mineral composition. Rapid Communications in Mass Spectrometry. 25(7): 899-909.
31. Furia E., Naccarato A., Sindona G., Stabile G., Tagarelli A. (2011) Multielement Fingerprinting as a Tool in Origin Authentication of PGI Food Products: Tropea Red Onion. J. Agricultural Food Chem. 59(15): 8450-8457.
32. Benabdelkamel H., Di Donna L., Mazzotti F., Naccarato A., Sindona G., Tagarelli A., Taverna D. (2012) Authenticity of PGI "Clementine of Calabria" by Multielement Fingerprint. J. Agricultural Food Chem. 60(14) 3717-3726.
33. Li C., Dong H., Luo D.H., Xian Y.P., Fu X. (2016) Recent Developments in Application of Stable Isotope and Multi-element Analysis on Geographical Origin Traceability of Cereal Grains. Food Analytical Methods. 9(6): 1512-1519.
34. Baroni M.V., Podio N.S., Badini R.G., Inga M., Ostera H.A., Cagnoni M., Gautier E.A., Garcia P.P., Hoogewerff J., Wunderlin D.A. (2015) Linking Soil, Water, and Honey Composition To Assess the Geographical Origin of Argentinean Honey by Multielemental and Isotopic Analyses. J. Agricultural Food Chem. 63(18): 4638-4645.
35. Hu S.L., Xue J., Lin Y., Yu J.P., Zhou J.G. (2014) Determination of rare earth elements in Navel oranges from different geographical regions of China by Inductively Coupled Plasma – Mass Spectrometry. Analytical Letters. 47(8): 1400-1408.
36. Di Bella G., Lo Turco V., Potorti A.G., Bua G.D., Fede M.R., Dugo G. (2015) Geographical discrimination of Italian honey by multi-element analysis with a chemometric approach. J. Food Composition and Analysis. 44: 25-35.

37. Gonzalvez A., Armenta S., de la Guardia M. (2009) Trace-element composition and stable-isotope ratio for discrimination of foods with Protected Designation of Origin. TRAC-Trends in Analytical Chemistry. 28(11): 1295-1311.
38. D'Archivio A.A., Giannitto A., Incani A., Nisi S. (2014) Analysis of the mineral composition of Italian saffron by ICP-MS and classification of geographical origin. Food Chem. 157: 485-489.
39. Llorent-Martinez E.J., Ortega-Barrales P., Fernandez-de Cordova M.L., Dominguez-Vidal A., Ruiz-Medina A. (2011) Investigation by ICP-MS of trace element levels in vegetable edible oils produced in Spain. Food Chem. 127(3): 1257-1262.
40. Portarena S., Baldacchini C., Brugnoli E. (2017) Geographical discrimination of extra-virgin olive oils from the Italian coasts by combining stable isotope data and carotenoid content within a multivariate analysis. Food Chem. 215: 1-6.
41. Maietti A., Tedeschi P., Stagno C., Bordiga M., Travaglia F., Locatelli M., Arlorio M., Brandolini V. (2012) Analytical Traceability of Melon (Cucumis Melo Var Reticulatus): Proximate Composition, Bioactive Compounds, and Antioxidant Capacity in Relation to Cultivar, Plant Physiology State, and Seasonal Variability. Journal of Food Science. 77(6), C646-C652.
42. Janská V., Piknová L., Kuchta T. (2011) Relative quantification of walnuts and hazelnuts in bakery products using real-time polymerase chain reaction. European Food Research and Technology. 232(6), 1057-1060.
43. Lopez-Calleja I.M., Cruz S.D.L., Pegels N., Gonzalez I., Garcia T., Martin R. (2013) High resolution TaqMan real-time PCR approach to detect hazelnut DNA encoding for ITS rDNA in foods. Food Chemistry. 141(3), 1872-1880.

44. Costa J., Mafra I., Kuchta T., Oliveira M.B.P.P. (2012) Single-tube nested real-time PCR as a new highly sensitive approach to trace hazelnut. Journal of Agricultural and Food Chemistry. 60(33), 8103-8110.
45. Locatelli M., Coïsson J.D., Travaglia F., Cereti E., Garino C., D'Andrea M., Martelli A., Arlorio M. (2011) Chemotype and genotype chemometrical evaluation applied to authentication and traceability of "tonda Gentile Trilobata" hazelnuts from Piedmont (Italy). Food Chemistry. 129(4), 1865-1873.
46. Mosetti R., Radicetti E., Monarca D., Cecchini M., Massantini R. (2015) Near infrared spectroscopy is suitable for the classification of hazelnuts according to Protected Designation of Origin. Journal of the Science of Food and Agriculture. 95(13), 2619-2625.
47. Cordero C., Liberto E., Bicchi C., Rubiolo P., Schieberle P., Reichenbach S.E., Tao Q. (2010) Profiling food volatiles by comprehensive two-dimensional gas chromatography coupled with mass spectrometry: Advanced fingerprinting approaches for comparative analysis of the volatile fraction of roasted hazelnuts (Corylus avellana L.) from different origins. Journal of Chromatography A. 1217(37), 5848-5858.
48. Ciarmiello L.F., Mazzeo M.F., Minasi P., Peluso A., De Luca A., Piccirillo P., Siciliano R.A., Carbone V. (2014) Analysis of Different European Hazelnut (Corylus avellana L.) Cultivars: Authentication, Phenotypic Features, and Phenolic Profiles. J. Agricultural Food Chem. 62(26): 6236-6246.
49. Locatelli M., Coisson J.D., Travaglia F., Cereti E., Garino C., D'Andrea M., Martelli A., Arlorio M. (2011) Chemotype and genotype chemometrical evaluation applied to authentication and traceability of "Tonda Gentile Trilobata" hazelnuts from Piedmont (Italy). Food Chem. 129(4): 1865-1873.

50. Klockmann S., Reiner E., Bachmann R., Hackl T., Fischer M. (2016) Food Fingerprinting: Metabolomic Approaches for Geographical Origin Discrimination of Hazelnuts (Corylus avellana) by UPLC-QTOF-MS. J. Agricultural Food Chem. 64(48): 9253-9262.
51. Oddone M., Aceto M., Baldizzone M., Musso D., Osella D. (2009) Authentication and Traceability Study of Hazelnuts from Piedmont, Italy. J. Agricultural Food Chem. 57(9): 3404-3408.
52. Aceto M., Robotti E., Oddone M., Baldizzone M., Bonifacino G., Bezzo G., Di Stefano R., Gosetti F., Mazzucco E., Manfredi M., Marengo E. (2013) A traceability study on the Moscato wine chain. Food Chemistry. 138(2-3), 1914-1922.
53. Ballabio D., Todeschini R. Multivariate classification for qualitative analysis. in Sun, D. (Edt.) Infrared Spectroscopy in Food Quality and Analytical Control. (2009) Academic Press. London. pp. 83–104.
54. Ozaki Y., McClure W., Christy A. (2006) Near-infrared Spectroscopy in Food Science and Technology. John Wiley & Sons. Hoboken.
55. Nicolaï B.M., Beullens K., Bobelyn E., Peirs A., Saeys W., Theron K.I. et al. (2007) Nondestructive measurement of fruit and vegetable quality by means of NIR spectroscopy: A review. Postharvest Biol Technol. 46, 99–118.
56. Camina J.M., Pellerano R.G., Marchevsky E.J. (2012) Geographical and botanical classification of honeys and apicultural products by chemometric methods. A review. Curr Anal Chem. 8, 408–425.
57. Gok S., Severcan M., Goormaghtigh E., Kandemir I., Severcan F. (2015) Differentiation of Anatolian honey samples from different botanical origins by ATR-FTIR spectroscopy using multivariate analysis. Food Chem. 170, 234-240.

58. Anjos O., Campos M.G., Ruiz P.C., Antunes P. (2015) Application of FTIR-ATR spectroscopy to the quantification of sugar in honey. Food Chem. 169, 218-223.
59. Ci Y.X., Gao T.Y., Feng J., Guo Z.Q. (1999) Fourier transform infrared spectroscopic characterization of human breast tissue: implications for breast cancer diagnosis. Appl. Spectrosc. 53(3), 312-315.
60. Moscetti R., Haff R.P., Saranwong S., Monarca D., Cecchini M., Massantini R. (2014) Nondestructive detection of insect infested chestnuts based on NIR spectroscopy. Postharvest Biol Technol. 87, 88–94.
61. Dogan A., Siyakus G., Severcan F. (2007) FTIR spectroscopic characterization of irradiated hazelnut (Corylus avellana L.). Food Chem. 100, 1106–1114.
62. Amaral J.S., Cunha S.C., Santos A., Alves M.R., Seabra R.M., Oliveira B.P.P. (2006) Influence of cultivar and environmental conditions on the triacylglycerol profile of hazelnut (Corylus avellana L.). J. Agricult. Food Chem. 54(2), 449-456.
63. Gurdeniz G., Ozen B. (2009) Detection of adulteration of extra-virgin olive oil by chemometric analysis of mid-infrared spectral data. Food Chem. 116, 519–525.
64. Maia M., Barros A.I.A., Nunes F.M. (2013) A novel, direct, reagent-free method for the detection of beeswax adulteration by single-reflection attenuated total reflectance mid-infrared spectroscopy. Talanta. 107, 74–80.
65. Oussama A., Elabadi F., Platikanov S., Kzaiber F., Tauler R. (2012) Detection of olive oil adulteration using FT-IR spectroscopy and PLS with variable importance of projection (VIP) scores. J. Am. Oil Chem. Soc. 89, 1807–1812.

66. Zhang Q., Liu C., Sun Z., Hu X., Shen Q., Wu J. (2012)Authentication of edible vegetable oils adulterated with used frying oil by Fourier Transform Infrared Spectroscopy. Food Chem. 132, 1607–1613.
67. Cozzolino D. (2012) Recent Trends on the Use of Infrared Spectroscopy to Trace and Authenticate Natural and Agricultural Food Products. Appl. Spectrosc. Rev. 47, 518–530.
68. Bevilacqua M., Bucci R., Magrì A.D., Magrì A.L., Marini F. (2012) Tracing the origin of extra virgin olive oils by infrared spectroscopy and chemometrics: A case study. Anal. Chim. Acta. 717, 39–51.
69. Lerma-García M.J., Ramis-Ramos G., Herrero-Martínez J.M., Simó-Alfonso E.F. (2010) Authentication of extra virgin olive oils by Fourier-transform infrared spectroscopy. Food Chem. 118, 78–83.
70. Moscetti R., Radicetti E., Monarca D., Cecchini M., Massantini R. (2015) Near infrared spectroscopy is suitable for the classification of hazelnuts according to Protected Designation of Origin. J Sci Food Agric. 95, 2619–2625.
71. Ciemniewska-Żytkiewicz H., Bryś J., Sujka K., Koczoń P. (2015) Assessment of the Hazelnuts Roasting Process by Pressure Differential Scanning Calorimetry and MID-FT-IR Spectroscopy. Food Anal. Methods. 8, 2465–2473.
72. Vanatta L.E., Coleman D.E. (1997) Calculation of detection limits for a single-laboratory ion chromatographic method to determine parts-per-trillion ions in ultrapure water. Journal of Chromatography A. 770 (1-2): 105-114.
73. Coleman D., Auses J., Grams N. (1997) Regulation - From an industry perspective or relationships between detection limits, quantitation limits, and significant digits. Chemometrics and Intelligent Laboratory Systems. 37 (1): 71-80.

74. Fearn T. (1999) A look at some standard pretreatments for spectra, NIR News. 10 (3).
75. Fearn T., Riccioli C., Garrido-Varo A., Guerrero-Ginel J.E. (2009) On the geometry of SNV and MSC, Chemom. Intell. Lab. Syst. 96 22–26.
76. Fearn T. (2008) The interaction between standard normal variate and derivatives, NIR News. 19 (7).

CHAPTER 5

5.1 Conclusions

The studies carried out within this PhD thesis project allowed to highlight the importance of elemental profiling, coupled to multivariate statistical tools, as an analytical approach to face modern problems in the field of applied and life sciences from two different points of view: the use of elemental profiling to evaluate the variation of heavy metals concentrations in urine samples during a chelation therapy; the use of the same profiling technique for food authentication, to promote the value of food products.

The first part of this Ph.D. thesis was therefore focused to study the effectiveness of chelating therapy and deepen the knowledge about what cations may or may not be excreted during the therapy, exploiting a patient diagnosed with chronic fatigue syndrome as case study. Urine samples were systematically collected before and after the chelation therapy and the results confirmed the efficacy of the therapy in the elimination of the heavy metals accumulated in the body. In fact, several elements showed an excretion peak in the 12 hours after the EDTA administration, while for others the elimination continued for 36 hours after the treatment, showing a pattern defined as "basal excretion". It was interesting to note the large excretion of Rb and Ti, whose toxic effects have been scarcely investigated. Therefore, it is worth to further investigate, in order to clarify the origin of their presence in the patient's body and their potential patho-physiological effects. Since it resulted that also beneficial microelements are massively eliminated, I confirmed that it is mandatory to introduce adequate dietary supplements in the time interval between two EDTA administrations.

The mechanisms of action of the chelation therapy were further investigated by a proteomic approach, monitoring the effects and pathways involved during the

chelating therapy, through shotgun proteomics of plasma samples, before and after the chelating therapy. Our results showed a significant modulation of the proteins related to redox balance in cells and to the elimination of ROS in plasma. Moreover, for the first time, we shed light on the mechanism of how chelation can reduce major cardiovascular events. In fact, although the effect of EDTA on cardiovascular diseases has already been studied by several projects and consortiums, its effect on the broad plasma proteome was never considered. The results obtained with the shotgun proteomic approach allowed us to identify the down regulation of proteins related to lipoprotein processes (i.e. APOC3, APOC2 and RET4), which are associated to high cardiovascular risk.

The purpose of the second part of the PhD study was instead to define a system to ensure the authentication of food products by exploiting rare earth (REEs) and other elements as indicators. These analytes were determined by ICP-MS and ICP-OES, using hazelnuts as the case study. This study involving the production chain of hazelnut paste: from raw fruits, to roasted hazelnuts, down to the final paste of three different hazelnut cultivars ("Tonda Gentile delle Langhe, TGL", "Romana, TGR" and "Mortarella"). PLS-DA with variable selection was applied to identify a model able to distinguish the three cultivars, independently on the type of technological transformation, and to search for elemental markers of authenticity. The model performances were very good both in fitting and cross-validation with accuracy always greater than 96.9%.

The results obtained show that authentication of hazelnuts along the production chain of hazelnuts paste, passing from raw to roasted fruits and then producing the corresponding paste, is possible with a good accuracy, based on the elemental profiling of both major elements and trace and ultra-trace elements. To the authors knowledge, this is the first authentication study involving the production chain of this product.

Authentication of hazelnuts was also carried out by a parallel approach exploiting FTIR spectroscopy using a portable FTIR spectrometer.

The multivariate classification methods, namely principal component analysis (PCA) followed by linear discriminant analysis (LDA) and partial least square discriminant analysis (PLS-DA), with or without variable selection, were applied to process the infrared spectra collected on the raw hazelnuts from three cultivars (TGL, TGR and Mortarella).

These methods allowed a very good discrimination among the groups, with PLS-DA coupled to variable selection providing the best results. The analysis showed that the differences between the cultivars reside in some important contributions, mainly due to lipids (to discriminate Mortarella's TGL) and proteins (to discriminate TGL of TGR).

The applied methodology represents an important advance in the field of cultivar identification of raw hazelnuts for the food industry, showing high sensitivity, simplicity, the possibility of on-site measurements and above all not requiring any particular sample preparation and the analysis is very fast (about 30 s per sample, including the sample treatment).

DECLARATION AND AUTHORISATION TO ANTIPLAGIARISM DETECTION

The undersigned Quasso Fabio student of Chemistry&Biology Ph.D course (XXIX Cicle)

declares:

- to be aware that the University has adopted a web-based service to detect plagiarism through a software system called “Turnitin”,
- his/her Ph.D. thesis was submitted to Turnitin scan and reasonably it resulted an original document, which correctly cites the literature

acknowledges:

- his/her Ph.D. thesis can be verified by his/her Ph.D. tutor and/or Ph.D Coordinator in order to confirm its originality.

Date: 15/11/2017 Signature: 

LIST OF PUBLICATIONS

- Manfredi M, Robotti E, Quasso F, Mazzucco E, Calabrese G, Marengo E (2017) Fast classification of hazelnut cultivars through portable infrared spectroscopy and chemometrics. Spectrochim Acta A Mol Biomol Spectrosc. 189:427-435.

- Robotti E, Quasso F, Mazzucco E, Manfredi M, Gosetti F, Isidoro C, Marengo E. Determination of elemental urine excretion profile during the monitoring of a chelating therapy by ICP-MS and multivariate data analysis: a case study". (2018) BioMetals (submitted).

- Manfredi M, Conte E, Quasso F, Barberis E, Robotti E, Gosetti F, Marengo E. Functional and Proteomic Alterations of Low-abundant Plasma Proteins after Chelation Therapy. (2018) Marker Disease (submitted).

ACKNOWLEDGEMENTS

Ringrazio il Prof. Emilio Marengo per avermi offerto l'opportunità di seguire questo percorso di formazione, per i consigli e gli stimoli nel proseguire questo lavoro. Un grazie soprattutto per gli incoraggiamenti che ha saputo riservarmi sia nell'esperienza lavorativa che personale.

Un ringraziamento di cuore alla Prof.ssa Elisa Robotti per avermi supportato e sopportato in questi anni. Per il suo pronto intervento, la sua cortesia, i suoi preziosi consigli e la sua sincera amicizia.

Ringrazio la THOT (Associazione per il sostegno alla Ricerca Scientifica ONLUS, Torino, Italia) che ha sostenuto l'attività di ricerca contenuta in questa tesi di dottorato.

Ringrazio gli amici Marcello, Elettra ed Eleonora per il tempo che mi avete dedicato, per la saggezza e il supporto che avete saputo offrirmi in questi quattro anni: Grazie di cuore.

Ringrazio gli "altri compagni di viaggio" Eleonora, Bianca, Fabio, Beppe, Arianna, Elisa e Mattia per aver condiviso con me questa esperienza.

Ringrazio Simone, John, Valentina, Alberto, Giorgia, Elena, Ilaria, Beatrice per l'allegria e la spensieratezza dispensate quotidianamente.

Ringrazio gli amici Carlo, Valerio, Federica, Ildo, Maria Elena, Alberto, Barbara, Canan, Umberto, Cristian e Emilio per essermi stati vicini, avermi sostenuto e sopportato.

Ringrazio la mia famiglia per il sostegno di questi anni. Vi sono grato per aver compreso, accettato e condiviso le mie scelte.

E infine a quella parte di me che in questi anni non si è arresa ed ha continuato a lottare.